ANDRÉ MIEDE & IVO PLETIKOSIĆ

A CLASSIC THESIS STYLE

[April 16, 2024 at 12:34 – classicthesis v4.6]

A CLASSIC THESIS STYLE

ANDRÉ MIEDE & IVO PLETIKOSIĆ

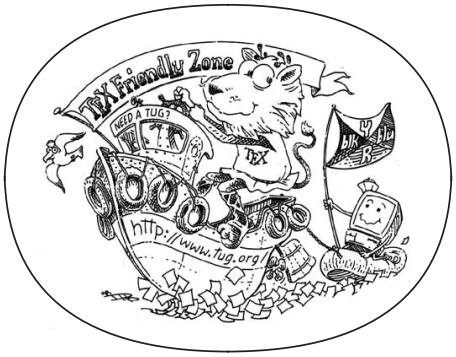

An Homage to The Elements of Typographic Style

June 2018 – classicthesis v4.6

Ohana means family.
Family means nobody gets left behind, or forgotten.

— Lilo & Stitch

Dedicated to the loving memory of Rudolf Miede.
1939 – 2005

ABSTRACT

Short summary of the contents in English. . . a great guide by Kent Beck how to write good abstracts can be found here:

https://plg.uwaterloo.ca/~migod/research/beckOOPSLA.html

RESUMEN

Kurze Zusammenfassung des Inhaltes in deutscher Sprache. . .

PUBLICATIONS

This is just an early – and currently ugly – test!

This might come in handy for PhD theses: some ideas and figures have appeared previously in the following publications:

Attention: This requires a separate run of `bibtex` for your `refsection`, e. g., `ClassicThesis1-blx` for this file. You might also use `biber` as the backend for `biblatex`. See also `http://tex.stackexchange.com/questions/128196/problem-with-refsection`.

We have seen that computer programming is an art,
because it applies accumulated knowledge to the world,
because it requires skill and ingenuity, and especially
because it produces objects of beauty.

— knuth:1974 [knuth:1974]

ACKNOWLEDGMENTS

Put your acknowledgments here.

Many thanks to everybody who already sent me a postcard!

Regarding the typography and other help, many thanks go to Marco Kuhlmann, Philipp Lehman, Lothar Schlesier, Jim Young, Lorenzo Pantieri and Enrico Gregorio[1], Jörg Sommer, Joachim Köstler, Daniel Gottschlag, Denis Aydin, Paride Legovini, Steffen Prochnow, Nicolas Repp, Hinrich Harms, Roland Winkler, Jörg Weber, Henri Menke, Claus Lahiri, Clemens Niederberger, Stefano Bragaglia, Jörn Hees, Scott Lowe, Dave Howcroft, José M. Alcaide, David Carlisle, Ulrike Fischer, Hugues de Lassus, Csaba Hajdu, Dave Howcroft, and the whole LaTeX-community for support, ideas and some great software.

Regarding LyX: The LyX port was intially done by *Nicholas Mariette* in March 2009 and continued by *Ivo Pletikosić* in 2011. Thank you very much for your work and for the contributions to the original style.

1 Members of GuIT (Gruppo Italiano Utilizzatori di TeX e LaTeX)

CONTENTS

LIST OF FIGURES

LIST OF TABLES

LISTINGS

ACRONYMS

Part I

INTRODUCTION

INTRODUCTION

The Standard Model (SM) of particle physics is the theory that describes and unifies three of the four fundamental interactions in Nature: electromagnetism, the weak nuclear force or interaction, and the strong force, also named Quantum Chromodyamics or QCD. The particle content of the SM is structured in three generations of ... In turn, these particles can be left- or right-handed (...) In Nature fermions of both chiralities exist, except for right-handed neutrinos which have never been observed. One possible reason for this is that neutrinos are only affected by the weak and gravitational interactions. However, their mass being extremely small (...) we can only detect them through the former (...) But the weak interaction only interacts with left-handed fermions (...). These particles complete the matter content of the theory. On the other hand, the three fundamental interactions are mediated by gauge bosons. The weak interaction is mediated by the massive W and Z bosons, electromagnetism by massless photons, and the strong interaction by massless gluons.

The theory of the Standard Model is founded on the framework of Quantum Field theory. (Special relativity + QM... is a description of particles and interactions founded on the concept of gauge symmetry (...) Renormalization (...))

The Standard Model was developed for decades, its definite formulation in the (...) During the decades it has proved extremely successful in passing experimental tests. (Discovery of the top and bottom quarks, W boson, Higgs boson after decades...)

Despite the astonishing success of the SM, we now it cannot be the whole story. To begin with, it does not explain one of the four fundamental interactions of Nature, gravity. On the other hand, there's no candidate particle in the SM for dark matter, which we know accounts for about 20% of the matter in the Universe. In addition to this, there are other theoretical puzzles, like the hierarchy problem of the Higgs mass, triviality of the Higgs coupling, the flavor puzzle or the strong CP problem, to quote a few. All this points to the fact that the SM is an effective theory that describes extremely well the Universe at the energy scales probed by modern day colliders, but that there must be some new physics lurking at high energy. Search for New Physics (NP) is the holy grail of modern day particle physics.

One way to search for NP is to perform precission tests of the SM. This involves making theoretical predictions to a high accuracy, and comparing them to high precission experiments. This allows to disentangle subtle NP effects that may affect processes accesible to nowadays colliders. In this respect, low-energy QCD is a rich arena to

look for NP effects (B-anomalies, flavor changing neutral currents, B meson rare decays...).

The framework usually employed to study Quantum Field Theory (QFT) is perturbation theory. It consists in expanding expectation values in the coupling of the theory, which must be smaller than 1 in order for the series to be convergent. However, in QFT the couplings run with the energy. In the case of electromagnetism, the coupling (the electron electric charge) decreases with energy. However, there may be cases in which a coupling is small at high energies, but that grows and becomes greater than 1 at low energies. This is the case of Yang-Mills theories, which are QFT whose gauge symmetry group is SU(N) for some value of N. QCD is a Yang-Mills theory with $N = 3$ coupled to matter. Indeed, at low-energies, the strong coupling grows logarithmically and perturbation theory no longer provides a reliable description of the dynamics. The only other known first-principles method to study QFTs is Lattice Field Theory. It consists in discreticing space-time into a grid or lattice and Wick rotating to the Euclidean. This allows to treat the theory as a statistichal physics system, computing integrals and expectation values numerically. This apporach allows to make reliable predictions of non-perturbative phenomena such as low-energy QCD, and thus is of utmost relevance for precission tests of the SM and search of NP. In particular, some NP related problems are expected to involve non-perturbative processes, and in this respect Lattice Field Theory provides an excellent tool for its understanding.

In this thesis we are interested in the definition and setting of a mixed action approach for the study of charm physics with Lattice QCD. This mixed action uses (...) The motivation is that it is expected that this setup allows to properly control the systematic effects associated to the charm quark mass when regularizing QCD in a lattice of finite spacing a. This is of great importance for studying charm physics at the non-perturbative level. The setting of this mixed action involves precise calculations in the light (up and down) and strange quark sector, which is what we focus on in this work. In particular, one needs to tune the parameters of the mixed action to have the same physical quark masses in the sea and valence sectors of the theory. Since the sea we will use employ only two degenerate up/down and a strange flavor, a matching in the light/strange sector is needed. Furthermore, in Lattice Field Theory any physical quantity is computed in units of the lattice spacing a. Thus in order to make predictions, one needs to find the value of a in physical units. This task is called scale setting, and is one of the main focus of this thesis. In addition to this, we will determine the physical value of the up/down and strange quark masses, which can only be determined from the lattice approach (...)

The thesis is structured as follows. In Chapter (...)

INTRODUCCIÓN

Blabla

Part II

FOUNDATIONS

1 QCD ON THE LATTICE

1.1 MOTIVATION

The theory that describes the strong interactions between quarks and gluons is called Quantum Chromodynamics, or QCD.

QCD has many remarkable properties. Among others, it is an asymptotically free theory, which means that at high energies (or short distances) the fundamental particles interact very weakly and can be treated as free. On the other hand, this implies the phenomenon of confinement at low energies (or large distances), phenomenon by which no color charged particles can be observed in Nature at these energy scales, but only color singlets. These are composite particles called mesons and baryons, which are made of quarks and gluons. Furthermore, at low energies the coupling constant grows logarithmically and perturbation theory fails to make reliable predictions. Another important feature of QCD is spontaneous chiral symmetry breaking, which is responsible for the light mass of pions, among other phenomena.

QCD is a non-abelian theory associated to the SU($N_c = 3$) Lie group. SU(3) rotations are described by unitary 3×3 matrices $\Omega(x)$ with $\det(\Omega(x)) = 1$. This is a non-abelian group since its elements do not commute under multiplication. The elements of the group can be written as

$$\Omega(x) = e^{i\alpha^{(a)}(x)T^{(a)}}, \tag{1.1}$$

where summation over $a = 1, ..., N_c^2 - 1 = 8$ is implicit and $T^{(a)}$ are the 8 generators of the SU(3) Lie group. Quarks are described by elements of the group in the fundamental representation, and gluons in the adjoint, both of them carrying the QCD charge: color.

Quarks are described by the fermionic fields ψ, $\bar{\psi}$. They carry a Dirac spinor index $\alpha = 1, 2, 3, 4$, a flavor index $i = 1, ..., N_f$ and a color index $c = 1, 2, 3$,

$$\psi^i(x)_{\alpha c}. \tag{1.2}$$

In Nature, $N_f = 6$ and each flavor of quark has a different mass m_i. Under SU(3) quarks transform as

$$\psi(x) \to \Omega(x)\psi(x), \quad \bar{\psi}(x) \to \bar{\psi}(x)\Omega^\dagger(x). \tag{1.3}$$

Gluons are described by the gauge fields $A_\mu(x)$, which are 3×3 hermitian and traceless matrices belonging to the Lie algebra su(3).

Gluons, being gauge bosons, carry a Lorentz index $\mu = 0, 1, 2, 3$ and two color indices $c, d = 1, 2, 3$,

$$A_\mu(x)_{cd}. \tag{1.4}$$

Since $A_\mu(x)$ are in the Lie algebra su(3) we can decompose it into

$$A_\mu(x) = \sum_{a=1}^{8} A_\mu^{(a)}(x) T^{(a)}, \tag{1.5}$$

$A_\mu^{(a)}(x)$ being real-valued fields.

Omitting color and spinor indices, the continuum QCD action takes the form

$$S_{\text{QCD}} = \sum_{i=1}^{N_f} \int d^4x \; \bar{\psi}^i(x) \left(\gamma_\mu D_\mu(x) + m_i \right) \psi^i(x) \tag{1.6}$$

$$+ \frac{1}{2g_0^2} \text{tr} \left(F_{\mu\nu}(x) F_{\mu\nu}(x) \right), \tag{1.7}$$

where the covariant derivative is given by

$$D_\mu(x) = \partial_\mu + iA_\mu(x) = \partial_\mu + iA_\mu^{(a)} T^{(a)}(x), \tag{1.8}$$

and the strength tensor

$$F_{\mu\nu}(x) = -i \left[D_\mu(x), D_\nu(x) \right] \tag{1.9}$$

$$= \partial_\mu A_\nu(x) - \partial_\nu A_\mu(x) + i \left[A_\mu(x), A_\nu(x) \right] \tag{1.10}$$

$$= \left(\partial_\mu A_\nu^{(a)}(x) - \partial_\nu A_\mu^{(a)}(x) \right) T^{(a)} - f_{abc} A_\mu^{(b)}(x) A_\nu^{(c)}(x) T^{(a)} \tag{1.11}$$

$$\equiv F_{\mu\nu}^{(a)} T^{(a)}, \tag{1.12}$$

with f_{abc} the structure constants of the SU(3) group, which are anti-symmetric and given by

$$\left[T^{(b)}, T^{(c)} \right] = i f_{bca} T^{(a)}. \tag{1.13}$$

This allows to write the gauge action as

$$\frac{1}{4g_0^2} \int d^4x \; F_{\mu\nu}^{(a)}(x) F_{\mu\nu}^{(a)}(x). \tag{1.14}$$

In order for the QCD action to be invariant under SU(3) rotations, the gauge fields must transform as

$$A_\mu(x) \to \Omega(x) A_\mu(x) \Omega^\dagger(x) + i \left(\partial_\mu \Omega(x) \right) \Omega^\dagger(x), \tag{1.15}$$

and so they are in the adjoint representation. From this we obtain the transformation relations

$$D_\mu(x) \to \Omega(x) D_\mu(x) \Omega^\dagger(x), \tag{1.16}$$

$$F_{\mu\nu}(x) \to \Omega(x) F_{\mu\nu}(x) \Omega^\dagger(x). \tag{1.17}$$

As mentioned above, at low energies or large distances QCD cannot be studied using perturbation theory. The only other known first-principles method to perform theoretical predictions is Lattice Field Theory, or Lattice QCD when applied to the study of Quantum Chromodynamics. This method is based on the discretization of spacetime into a hypercubic box or lattice

$$\Lambda = \{n_0, n_1, n_2, n_3 | n_0 = 0, ..., T/a - 1; n_i = 0, ..., L/a - 1; i = 1, 2, 3\}, \tag{1.18}$$

where a is the lattice spacing between two adjacent sites, and L, T are the spatial and temporal lattice extents (in physical units) respectively. The discretization of spacetime and introduction of a finite lattice spacing a provides a natural energy cutoff for momenta $\sim a^{-1}$, removing UV divergences. On the other hand, the finite volume lattice ensures the absence of IR divergences. This means that the lattice formulation can be seen as a way to regularize any particular Quantum Field Theory. However, this also implies the presence of finite volume and discretization effects, which should be removed from the results. To do this, after having computed the physical observables in the lattice setup, one must perform a continuum extrapolation to obtain results at $a \to 0$ and simulate large enough volumes in order to be able to neglect the effects associated with finite volume. If the theory is renormalizable, physical quantities will remain finite in the continuum limit.

Having discretized spacetime, fields are placed at the lattice sites $n \in \Lambda$. Fermions thus look like

$$\psi(n), \bar{\psi}(n), \quad n \in \Lambda. \tag{1.19}$$

For the gauge fields, it will be helpful to use the definition of a parallel transporter in SU(N). An N-component unit vector v is parallel transported along a curve parameterized by $z_\mu(t)$ from point $z_\mu(a) = x$ to $z_\mu(b) = y$ as

$$v(b) = P(y, x)v(a), \tag{1.20}$$

$$P(y, x) = e^{i \int_x^y A_\mu(z) dz_\mu}, \tag{1.21}$$

with A_μ the SU(N) gauge fields. This means that a fermion in the fundamental representation picks up a phase of $P(y, x)$ when going from x to y. This parallel transporter is called a gauge link and its discrete version will be the variable to be used in the lattice for the gauge fields. It transforms in the fundamental representation of SU(N),

$$P(x, y) \to \Omega(x) P(x, y) \Omega^\dagger(y). \tag{1.22}$$

Having defined the fields in the lattice, one needs to discretize the QCD action, formulating it in a finite box Λ in terms of said fields in

such a way that in the continuum limit $a \to 0$ the continuum QCD action is recovered. We discuss this in the following sections.

The Chapter is structured as follows. In Sec. 1.2 we show the Wilson formulation of the gauge action in the lattice, in terms of the link variables. In Sec. 1.3 we show different ways of discretizing the fermion action. In Sec. 1.3.1 we discuss the problem of doublers that appear with a naive fermion discretization and its relation with formulating chiral symmetry in the lattice, briefly commenting on Ginsparg-Wilson fermions. In Sec. 1.3.2 we show the solution to the doublers problem proposed by Wilson, which implies adding a term which explicitly breaks chiral symmetry. This term gives a heavy mass to the doublers that grows with the inverse of the lattice spacing a, and thus they decouple in the continuum. In Sec. 1.3.3 we discuss a modification of Wilson fermions which adds a chirally rotated mass term. This regularization poses some advantages which will be of importance for our study. In Sec. 1.4 we review some concepts of the path integral formalism and how expectation values are computed numerically in the lattice. In Sec. 1.5 we review some concepts of renormalizability and the continuum limit in the lattice. In Sec. 1.6 we discuss the Symanzik improvement program, which allows to reduce cutoff effects associated to the lattice action and fields, helping in the task of performing the continuum limit. Finally, in Sec. 1.7 the procedure to set the scale in the lattice is discussed. This is necessary in order to extract lattice predictions in physical units.

1.2 PURE GAUGE SU(3) IN THE LATTICE

In the lattice, gluon fields can be defined by the link variables $U_\mu(x) \in$ SU(3) that act as a discrete version of the gauge transporters connecting points x and $x + \hat{\mu}$, with $\hat{\mu} = \{a\hat{x}_0, a\hat{x}_1, a\hat{x}_2, a\hat{x}_3\}$

$$U_\mu(x) = \exp\left(iaA_\mu(x)\right). \tag{1.23}$$

The gauge fields transform as

$$U_\mu(x) \to \Omega(x)U_\mu(x)\Omega^\dagger(x+\hat{\mu}), \tag{1.24}$$

These fields live on the links of the lattice that connect sites x and $x + \hat{\mu}$.

A common discretization of the gluonic action is the Wilson gauge action **[Wilson:1974sk]**, which is expressed in terms of the link variables $U_\mu(x)$

$$S_G = \frac{1}{g_0^2}\sum_x\sum_{\mu,\nu}\text{Re}\ \ \text{tr}\left(1 - U_{\mu\nu}(x)\right), \tag{1.25}$$

where $U_{\mu\nu}(x)$ is the plaquette centered on the lattice site x

$$U_{\mu\nu}(x) = U_\mu(x)U_\nu(x+\hat{\mu})U_\mu^\dagger(x+\hat{\nu})U_\nu^\dagger(x), \tag{1.26}$$

and we have used

$$U_\mu^\dagger(x) = U_{-\mu}(x+\hat{\mu}). \tag{1.27}$$

Using the Baker-Campbell-Hausdorff formula iteratively

$$\exp(A)\exp(B) = \exp\left(A + B + \frac{1}{2}[A,B] + ...\right), \tag{1.28}$$

and using eq. (1.23) we get

$$S_G = a^4 \frac{\beta}{3} \sum_x \sum_{\mu,\nu} \mathrm{tr}\left(F_{\mu\nu}^2(x)\right) + \mathcal{O}(a^2), \tag{1.29}$$

where we introduced the inverse coupling

$$\beta = \frac{6}{g_0^2}. \tag{1.30}$$

Taking the continuum limit $a^4 \sum_x \to \int d^4x$ we recover the continuum Yang-Mills action.

Eq. (1.29) shows that the effects related to the discretization of space-time are of order $\mathcal{O}(a^2)$ for the Wilson gauge action. The discretization of the SU(3) pure Yang-Mills action is not unique, and different choices result in different cutoff effects.

The $\mathcal{O}(a^2)$ cutoff effects present in the Wilson regularization of the gauge action can be further reduced by adding additional terms that respect the symmetries of the theory following the Symanzik improvement program. One such choice is the Lüscher-Weisz action [], which we discuss in Sec. 1.6.

1.3 INTRODUCING FERMIONS IN THE LATTICE

After discretizing the SU(3) gauge action, we still need to find a suitable discrete version of the fermion action in eq. (1.6) to fully formulate QCD on the lattice. It will be shown that theoretical challenges arise with the naive fermion discretization and how these can be addressed with alternative formulations.

1.3.1 *Naive fermions*

To discretize the continuum fermionic action in the absence of gauge fields, considering only one flavor with mass m,

$$S_F = \int d^4x \bar{\psi}(x)\left(\gamma_\mu \partial_\mu + m\right)\psi(x), \tag{1.31}$$

the derivative ∂_μ needs to take a discrete form, which can be done easily by

$$\partial_\mu \psi(x) \to \hat{\partial}_\mu \psi(x) = \frac{1}{2a}\left(\psi(x+\hat{\mu}) - \psi(x-\hat{\mu})\right). \tag{1.32}$$

To respect gauge symmetry in our action, we must promote the derivative $\hat{\partial}_\mu$ to a covariant one, as in the continuum case. To achieve this, we note that terms like

$$\bar{\psi}(x)\psi(x+\hat{\mu}), \tag{1.33}$$

which arise from $\bar{\psi}(x)\hat{\partial}_\mu\psi(x)$ are not gauge invariant

$$\bar{\psi}(x)\psi(x+\hat{\mu}) \to \bar{\psi}(x)\Omega^\dagger(x)\Omega(x+\hat{\mu})\psi(x+\hat{\mu}). \tag{1.34}$$

The solution is again to introduce the link variable or parallel transporter $U_\mu(x)$ from site x to $x+\hat{\mu}$ defined in eq. (1.23) which transforms as in eq. (1.24). This way, the discretized fermion action reads

$$S_\mathrm{F} = a^4 \sum_x \bar{\psi}(x) \left(\gamma_\mu \frac{U_\mu(x)\psi(x+\hat{\mu}) - U_\mu^\dagger(x-\hat{\mu})\psi(x-\hat{\mu})}{2a} + m\psi(x) \right). \tag{1.35}$$

From this the massive Dirac operator D can be defined such that

$$S_\mathrm{F} = \int d^4x \bar{\psi}(x) D \psi(x). \tag{1.36}$$

The lattice fermion action used here suffers from the problem of doublers, which are unwanted poles that appear in the Kallen-Lehman representation of the fermion propagator $\langle\psi(x)\bar{\psi}(y)\rangle$. These doublers appear due to the presence of two zeros of the Dirac operator in the First Brillouin Zone (FBZ) in each lattice direction, all with the same vacuum energy. Thus, for d dimensions, there are 2^d one particle states with the same ground state energy. The problem of the doublers is related to chiral symmetry and its implementation in the lattice.

Chiral symmetry in continuum QCD can be expressed as

$$\{D, \gamma_5\} = 0, \tag{1.37}$$

with D the Dirac operator. There's a theorem by Nielsen and Ninomiya [] that states that one cannot implement chiral symmetry in this way in the lattice without the appearance of doublers. In this lattice formulation of chiral symmetry, there must be an equal number of right movers and left movers. In particular, this means having just one pole is not possible. Ginsparg and Wilson [] proposed a suitable version of chiral symmetry for the lattice as

$$\{D, \gamma_5\} = aD\gamma_5 D, \tag{1.38}$$

such that in the continuum eq. (1.37) is recovered. With this definition of chiral symmetry in the lattice, it is possible to construct Dirac operators that satisfy eq. (1.38) and are free of doublers. An example of such an operator is the overlap operator [].

If one is not interested in studying physics related to chiral symmetry, another choice is to build a Dirac operator that explicitly breaks chiral symmetry but removes the doublers. Wilson fermions and Wilson twisted mass fermions are examples of such a choice, which we will now study.

1.3.2 *Wilson fermions*

Wilson proposed [**Wilson:1974sk**] adding an extra term to the naive fermionic action in eq. (1.35) to eliminate doublers. This term vanishes in the continuum limit, but at finite lattice spacing it gives an additional mass to the doublers. This mass becomes infinitely heavy in the continuum limit, and thus the doublers decouple from the theory. The Wilson fermion action reads

$$S_{\mathrm{W}} = a^4 \sum_x \bar{\psi}(x) \frac{1}{2} \left(\gamma_\mu \left(\nabla_\mu + \nabla_\mu^* \right) + 2m - a \nabla_\mu \nabla_\mu^* \right) \psi(x), \quad (1.39)$$

where we have defined the forward and backward discrete covariant derivatives as

$$\nabla_\mu \psi(x) = \frac{U_\mu(x)\psi(x+\hat{\mu}) - \psi(x)}{a}, \quad (1.40)$$

$$\nabla_\mu^* \psi(x) = \frac{\psi(x) - U_\mu^\dagger(x-\hat{\mu})\psi(x-\hat{\mu})}{a}. \quad (1.41)$$

From the Wilson fermion action (1.39) the Wilson Dirac operator reads

$$D = D_{\mathrm{W}} + m = \frac{1}{2} \left(\gamma_\mu \left(\nabla_\mu + \nabla_\mu^* \right) - a \nabla_\mu \nabla_\mu^* \right) + m, \quad (1.42)$$

where we have introduced the massless Wilson Dirac operator D_{W}, and the action can be written as

$$S_{\mathrm{W}} = a^4 \sum_x \bar{\psi}(x) \left(D_{\mathrm{W}} + m \right) \psi(x). \quad (1.43)$$

For N_f flavors, an additional sum over a flavor index $i = 1, \ldots, N_f$ is required, and m is promoted to a diagonal matrix in flavor space, whose diagonal elements are m_i. The fermion mass m_i is commonly expressed in terms of the κ parameter

$$\kappa_i = \frac{1}{2am_i + 8}. \quad (1.44)$$

The Wilson term $a \nabla_\mu \nabla_\mu^*$ in the Wilson Dirac operator manifestly breaks chiral symmetry, even in the $m_i = 0$ limit, and this symmetry is only restored in the continuum limit. Consequently, the quark mass receives additive renormalization contributions,

$$m_i^{\mathrm{R}} = Z_m \left(m_i - m_{\mathrm{cr}} \right), \quad (1.45)$$

since it is not protected against renormalization by the axial symmetry.

The Wilson fermion action has $\mathcal{O}(a)$ cutoff effects, which again can be systematically reduced by using the Symanzik improvement program detailed in Sec. 1.6.

1.3.3 *Wilson twisted mass fermions*

Wilson twisted mass (tm) fermions [] introduce an imaginary mass term to the Wilson Dirac operator in eq. (1.42) of the form

$$i\bar{\psi}(x)\boldsymbol{\mu}\gamma_5\psi(x), \tag{1.46}$$

with the twisted quark mass matrix in flavor space with four flavors of quarks (as will be our case of interest) given by

$$\boldsymbol{\mu} = \mathrm{diag}\left(\mu_u, -\mu_d, -\mu_s, \mu_c\right). \tag{1.47}$$

More generally, the Wilson tm Dirac operator reads

$$D = D_{\mathrm{W}} + \boldsymbol{m} + i\boldsymbol{\mu}\gamma_5. \tag{1.48}$$

By rotating the fields

$$\psi \;\rightarrow\; \psi' = e^{-i\frac{\pi}{2}\gamma_5\frac{T}{2}}\psi, \quad \bar{\psi} \;\rightarrow\; \bar{\psi}' = \bar{\psi}e^{-i\frac{\pi}{2}\gamma_5\frac{T}{2}}, \tag{1.49}$$

$$T = \mathrm{diag}(\eta_u, \eta_d, \eta_s, \eta_c), \tag{1.50}$$

with $\alpha_i \equiv \frac{\pi}{2}\eta_i$ the so called twist angles, defined by

$$\cot\alpha_i = \frac{m_i^{\mathrm{R}}}{\mu_i^{\mathrm{R}}}, \tag{1.51}$$

one retrieves the usual physical (standard) formulation with real fermionic mass

$$M_i^2 = m_i^2 + \mu_i^2, \tag{1.52}$$

and a chirally rotated Wilson term. The rotated fields $\phi', \bar{\psi}'$ define the so called physical basis, while the unrotated ones $\psi, \bar{\psi}$ define the twisted basis.

In practice we will be working with Wilson tm fermions at full twist

$$\eta_u = \eta_c = -\eta_s = -\eta_d = 1, \tag{1.53}$$

which can be obtained by setting the renormalized standard masses m_i^{R} to zero. The procedure to achieve this is explained in Sec. 3.5.

Considering for simplicity the light sector of mass-degenerate u and d quarks, at full twist the symmetry group $SU(2)_V \times SU(2)_A$ is broken into

$$SU(2)_V \times SU(2)_A \rightarrow [U(1)_A]_1 \times [U(1)_A]_2 \times [U(1)_V]_3, \tag{1.54}$$

with

$$[U(1)_A]_a = \begin{cases} \psi(x) \rightarrow e^{i\alpha_A^a\gamma_5\frac{\tau^a}{2}}\psi(x) & a = 1,2 \\ \bar{\psi}(x) \rightarrow \bar{\psi}(x)e^{i\alpha_A^a\gamma_5\frac{\tau^a}{2}} & a = 1,2 \end{cases}, \tag{1.55}$$

and

$$[U(1)_V]_3 = \begin{cases} \psi(x) \to e^{i\alpha_A^3 \frac{\tau^3}{2}} \psi(x) \\ \bar{\psi}(x) \to \bar{\psi}(x) e^{-i\alpha_A^3 \frac{\tau^3}{2}} \end{cases} . \tag{1.56}$$

This means that at full twist axial symmetries are not completely broken, and thus the twisted mass is protected against additive renormalization,

$$\mu_i^R = Z_\mu(g_0^2, a\mu)\mu_i. \tag{1.57}$$

An important role in our setup is played by the Ward-Takahashi identities (WTI). They will be used to tune the Wilson twisted mass parameters to ensure full twist and to determine the quark masses in the Wilson regularization. Furthermore, they allow to identify the renormalization constant of the twist masses Z_μ. For the non-singlet case ($i \neq j$) the WTI for the axial and vector currents, in the continuum limit and in the twisted basis, are as follows (see Appendix **??** for the definition of the currents)

$$\partial_\mu V_\mu^{ij} = (m_i - m_j)S^{ij} + i(\eta_i\mu_i - \eta_j\mu_j)P^{ij}, \tag{1.58}$$

$$\partial_\mu A_\mu^{ij} = (m_i + m_j)P^{ij} + i(\eta_i\mu_i + \eta_j\mu_j)S^{ij}. \tag{1.59}$$

Note that at zero twist angle $\eta_u = \eta_d = \eta_s = \eta_c = 0$ the twisted and physical basis are the same, and the standard WTIs are recovered. However, at full twist the renormalized standard masses m_i^R vanish, which in turn means that the current masses m_i in eqs. (1.58) also vanish (up to cutoff effects). Moreover, the exact flavor symmetry of massless Wilson fermions implies the existence of a point-split vector current $\tilde{V}_\mu^{ij}$ on the lattice such that the vector WTI holds exactly on the lattice. In the twisted basis, this current takes the form

$$\tilde{V}_\mu^{ij} = \frac{1}{2}\left[\bar{\psi}^i(x)(\gamma_\mu - 1)U_\mu(x)\psi^j(x+\hat{\mu}) + \bar{\psi}^i(x+\hat{\mu})(\gamma_\mu + 1)U_\mu^\dagger(x)\psi^j(x)\right]. \tag{1.60}$$

The conservation of this WTI on the lattice for $\tilde{V}_\mu^{ij}$ means that the point-split vector current renormalizes trivially with

$$Z_{\tilde{V}} = 1. \tag{1.61}$$

Looking at eq. (1.58) this means that for all flavors

$$Z_\mu = Z_P^{-1}. \tag{1.62}$$

1.4 PATH INTEGRAL REGULARIZATION

Having formulated the QCD action in the lattice, we need to see how physical quantities are computed. To do so, we review some

aspects of the path integral formulation in Euclidean spacetime. In this formalism, physical quantities are expressed as expectation values of operators

$$\langle \mathcal{O}(x_1, ..., x_n) \rangle = \frac{1}{\mathcal{Z}} \int \mathcal{D}[\psi, \bar{\psi}, U] \mathcal{O}(x_1, ..., x_n) e^{-S[\psi, \bar{\psi}, U]}, \tag{1.63}$$

$$\mathcal{Z} = \int \mathcal{D}[\psi, \bar{\psi}, U] e^{-S[\psi, \bar{\psi}, U]}. \tag{1.64}$$

This is equivalent to expectation values in statistical mechanics with a Boltzmann factor of $e^{-S[\psi, \bar{\psi}, U]}$. The action can be decomposed into its gluon and fermion components $S[\psi, \bar{\psi}, U] = S_{\mathrm{G}}[U] + S_{\mathrm{F}}[\psi, \bar{\psi}]$, and fermion variables can be integrated out as

$$\langle \mathcal{O}(x_1, ..., x_n) \rangle = \frac{1}{\mathcal{Z}} \int \mathcal{D}[U] e^{-S_{\mathrm{G}}[U]} \mathcal{Z}_{\mathrm{F}} \times \tag{1.65}$$

$$\left[\frac{1}{\mathcal{Z}_{\mathrm{F}}} \int \mathcal{D}[\psi, \bar{\psi}] \mathcal{O}(x_1, ..., x_n) e^{-S_{\mathrm{F}}[\psi, \bar{\psi}]} \right] \tag{1.66}$$

$$= \frac{1}{\mathcal{Z}} \int \mathcal{D}[U] e^{-S_{\mathrm{G}}[U]} \mathcal{Z}_{\mathrm{F}} \left\langle \mathcal{O}(x_1, ..., x_n) \right\rangle_{\mathrm{F}}, \tag{1.67}$$

$$\mathcal{Z}_{\mathrm{F}} = \int \mathcal{D}[\psi, \bar{\psi}] e^{-S_{\mathrm{F}}[\psi, \bar{\psi}]} = \Pi_{i=1}^{N_f} \det(D), \tag{1.68}$$

This fermionic determinant can be expressed as an effective action as

$$\langle \mathcal{O}(x_1, ..., x_n) \rangle = \frac{1}{\mathcal{Z}} \int \mathcal{D}[U] e^{-S_{\mathrm{G}}[U] - S_{\mathrm{eff}}[U]} \left\langle \mathcal{O}(x_1, ..., x_n) \right\rangle_{\mathrm{F}}, \tag{1.69}$$

$$\mathcal{Z} = \int \mathcal{D}[U] e^{-S_{\mathrm{G}}[U] - S_{\mathrm{eff}}[U]}, \tag{1.70}$$

$$S_{\mathrm{eff}}[U] = -\sum_{i=1}^{N_f} \log \det(D). \tag{1.71}$$

In order to compute meson observables we will use meson interpolators, which are composite fermionic observables that share the same quantum numbers as the desired meson state. A generic meson interpolator has the form

$$O_A^{ij}(x) = \bar{\psi}^i(x) \Gamma_A \psi^j(x), \tag{1.72}$$

with Γ_A a Gamma matrix. This way, a meson two-point function reads

$$\left\langle O_A^{ij}(x_1) O_B^{ji}(x_2) \right\rangle = \frac{1}{\mathcal{Z}} \int \mathcal{D}[U] e^{-S_{\mathrm{G}}[U] - S_{\mathrm{eff}}[U]} \times \tag{1.73}$$

$$\left\langle \bar{\psi}^i(x_1) \Gamma_A \psi^j(x_1) \psi^i(x_2) \Gamma_B \bar{\psi}^j(x_2) \right\rangle_{\mathrm{F}} \tag{1.74}$$

$$= -\frac{1}{\mathcal{Z}} \int \mathcal{D}[U] e^{-S_{\mathrm{G}}[U] - S_{\mathrm{eff}}[U]} \times \tag{1.75}$$

$$\mathrm{tr} \left(\Gamma_A D_i^{-1}(x_1, x_2) \Gamma_B D_j^{-1}(x_2, x_1) \right), \tag{1.76}$$

where the trace is over spin indices and D_i the massive Dirac operator for flavor i. In order to perform this integral numerically, using

the connection with statistical mechanics, a finite set of N_{cnfg} gauge configurations is generated with Boltzmann distribution $e^{-S_G[U]-S_{\text{eff}}[U]}$ following a Markov process (see Appendices B, D). Then, measurements of the quantity

$$P = -\text{tr}\left(\Gamma D_i^{-1}(x_1, x_2)\Gamma D_j^{-1}(x_2, x_1)\right), \tag{1.77}$$

are taken in each of these configurations, and the expectation value is computed as

$$\langle P\rangle = \frac{1}{N_{\text{cnfg}}}\sum_i^{N_{\text{cnfg}}} P_i + \mathcal{O}\left(\frac{1}{\sqrt{N_{\text{cnfg}}}}\right). \tag{1.78}$$

1.5 CONTINUUM LIMIT

The lattice regularization provides a natural energy cutoff a^{-1}, ensuring that any loop integral is finite in perturbation theory. In perturbative renormalization, it is necessary to take the cutoff to infinity, which in the lattice means taking the lattice spacing to $a \to 0$. If the theory is renormalizable, any physical quantity (e.g. a mass m_{phys}) in units of the lattice spacing must vanish in the continuum limit

$$m_{\text{phys}} a \to 0, \tag{1.79}$$

since this means that m_{phys} remains finite in this limit.

Physical quantities are dependent on the couplings of the theory, $m_{\text{phys}}(g_0)$, and accordingly change with them. In turn, one can study how the couplings of the theory change in the lattice as one approaches the continuum limit by decreasing a. To do so and for simplicity, we assume a single coupling g_0, and write the most general local effective action at lattice spacing a_1

$$S(a_1) = g_0(a_1)\sum_i O_i, \tag{1.80}$$

where O_i are all possible local operators respecting the lattice symmetries. When the lattice spacing is reduced to $a_2 < a_1$, all the short-range extra degrees of freedom can be integrated out and reabsorbed into a redefinition of the coupling, such that the new action has the same generic form but with different couplings

$$g_0(a_1) \to R(g_0(a_1)) = g_0(a_2). \tag{1.81}$$

R here stands for the renormalization group (RG) transformation that defines the change in the couplings when varying the lattice spacing.

Since physical quantities change with the couplings, they also do with the lattice spacing, and we want to ensure eq. (1.79) to ensure renormalizability. It can be observed then that renormalizability corresponds to fixed points g_0^* of the RG transformation

$$R(g_0^*) = g_0^*. \tag{1.82}$$

In the context of SU(N) Yang-Mills theory, perturbation theory shows that at a fixed value of the renormalized coupling g_R the bare coupling runs with the lattice spacing as

$$a\frac{\partial g_0}{\partial a} \equiv \beta(g_0) = -\beta_0 g_0^3 - \beta_1 g_0^5 + ..., \tag{1.83}$$

where $\beta_{0,1}$ are universal coefficients (do not depend on the renormalization scheme) and positive for $N = 3$, as in the case of QCD. This shows that $g_0 = 0$ is a fixed point of the RG transformations and thus corresponds to the continuum limit. As the fixed point is in the weak coupling regime, this perturbative argument is expected to be valid. Therefore the continuum limit corresponds to

$$g_0 \to 0, \tag{1.84}$$

or in terms of the inverse coupling β

$$\beta \to \infty. \tag{1.85}$$

In practice, one cannot numerically simulate at infinite inverse coupling β. Therefore, physical observables are computed at several finite values of β. This introduces $\mathcal{O}(a^n)$ cutoff effects in the results, with some power n. To obtain results in the continuum, one parameterizes these cutoff effects with some function of the lattice spacing and extrapolates to $a \to 0$. However, this task is far from trivial []. To help in the continuum limit extrapolation, one can systematically reduce lattice artifacts, e.g. from $\mathcal{O}(a)$ to $\mathcal{O}(a^2)$ following the Symanzik improvement program.

1.6 SYMANZIK IMPROVEMENT PROGRAM

Symanzik improvement requires improving both the action of the theory and the lattice interpolators that enter the different correlators.

In order to improve a lattice action, one can describe the target continuum action in terms of an effective action

$$S_{\text{eff}} = \int d^4x \sum_k c_k \mathcal{L}_k(x) a^{k-4}. \tag{1.86}$$

Here $\mathcal{L}_0(x)$ is the discretized lattice Lagrangian unimproved, and the higher-dimension terms $\mathcal{L}_k$(x) are all possible Lagrangians built from fermion and gluon field operators that preserve the symmetries of the regularized theory, i.e. the lattice theory, with mass dimension $4 + k$, and c_k are numerical coefficients.

In the case of Lattice QCD, we saw that in the Wilson gauge action in eq. (1.29) lattice artifacts appear at $\mathcal{O}(a^2)$, and therefore no $\mathcal{O}(a)$ improvement is required. However, these $\mathcal{O}(a^2)$ effects can be further reduced by adding all possible dimension $4 + k = 6$ operators that preserve the underlying symmetries of the gauge action. These

dimension-6 operators are all three possible ways of writing a closed path in a rectangular lattice with 6 gauge links: planar, twisted and L-shaped rectangles. The action then reads

$$S_G = \frac{\beta}{3}\sum_{\mu\nu}\left[c_0\sum_p \mathrm{Re}\left(\mathrm{tr}\left(1-U_{\mu\nu}(p)\right)\right) + \sum_{i=1}^{3} c_i \sum_r \mathrm{Re}\left(\mathrm{tr}\left(1-U^{(i)}(r)\right)\right)\right], \tag{1.87}$$

with $U^{(i)}$ said dimension-6 operators. Tuning the coefficients c_i properly leads to $\mathcal{O}(a^2)$ improvement. In our study, the CLS ensembles we employ (see Sec. 3.2) use the so called Lüscher-Weisz gauge action [], with these coefficients computed at tree-level

$$c_0 = \frac{5}{3}, \quad c_1 = -\frac{1}{12}, \quad c_2 = c_3 = 0. \tag{1.88}$$

Thus, in the Lüscher-Weisz gauge action the only dimension-6 operators that survive are planar rectangles $U^{(1)}$.

We also need to improve the fermion action. Wilson fermions have $\mathcal{O}(a)$ cutoff effects. In order to improve the Wilson fermion action to $\mathcal{O}(a^2)$ we need to look for all possible operators with dimension $4+k=5$ that preserve the lattice symmetries. These are

$$\mathcal{L}^{(1)}_{k=1} = i\bar{\psi}\sigma_{\mu\nu}F_{\mu\nu}\psi, \tag{1.89}$$
$$\mathcal{L}^{(2)}_{k=1} = \boldsymbol{m}\mathrm{tr}\left(F_{\mu\nu}(x)F_{\mu\nu}(x)\right), \tag{1.90}$$
$$\mathcal{L}^{(3)}_{k=1} = \boldsymbol{m}^2\bar{\psi}\psi, \tag{1.91}$$

with

$$\sigma_{\mu\nu} = \frac{\left[\gamma_\mu,\gamma_\nu\right]}{2i}, \tag{1.92}$$
$$\hat{F}_{\mu\nu}(x) = \frac{-i}{8a^2}\left(Q_{\mu\nu}(x) - Q_{\nu\mu}(x)\right), \tag{1.93}$$
$$Q_{\mu\nu} = U_{\mu\nu}(x) + U_{\nu,-\mu}(x) + U_{-\mu,-\nu}(x) + U_{-\nu,\mu}(x). \tag{1.94}$$

$\mathcal{L}^{(1),(2)}_{k=1}$ are already present (up to numerical factors) in the original Wilson fermion action and can therefore be reabsorbed in those terms. The $\mathcal{O}(a)$ improved Wilson Dirac operator appearing in the improved fermion action reads

$$D_\mathrm{W} + \boldsymbol{m} + c_\mathrm{sw}a\frac{1}{2}\sum_{\mu<\nu}\sigma_{\mu\nu}\hat{F}_{\mu\nu}, \tag{1.95}$$

with c_sw the Sheikholeslami-Wohlert coefficient determined non-perturbatively in [].

Improving the lattice action ensures improvement of on-shell quantities such as meson masses. However, if one is interested in matrix elements mediated by some current $\mathcal{J}_\mu$, it is also necessary to improve the lattice interpolators that enter into the definition of those currents.

In analogy with the improvement of the action, a local operator O is expressed in the Symanzik effective theory as

$$O_{\text{eff}}(x) = \sum_k a^k O_k(x). \tag{1.96}$$

Again, O_k are gauge invariant local operators with the right mass dimensions. Following this, a generic n-point function reads

$$\langle \Phi \rangle = \langle \Phi_0 \rangle - a \int d^4y \, \langle \Phi_0 \mathcal{L}_1(y) \rangle + a \langle \Phi_1 \rangle + ..., \tag{1.97}$$

with

$$\langle \Phi_0 \rangle = \langle O_0(x_1)...O_0(x_n) \rangle \,, \tag{1.98}$$

$$\langle \Phi_1 \rangle = \sum_{i=1}^{n} \langle O_0(x_1)...O_1(x_i)...O_0(x_n) \rangle \,, \tag{1.99}$$

and vacuum expectation values taken in the continuum. The generic form of the O_k operators is a sum over all possible operators Ψ_k with the right mass dimension and that are local and gauge invariant,

$$O_k = \sum_i c_i \Psi_k, \tag{1.100}$$

with c_i some non-perturbatively determined coefficients required to suppress $\mathcal{O}(a^k)$ cutoff effects in the correlation functions. In Sec 2 we discuss the details of operator improvement for the case of standard Wilson fermions for the observables of interest.

The $\mathcal{O}(a)$ improved Wilson tm fermion action is analogous to the Wilson case, with the improved Dirac operator given by

$$D_{\text{W}} + \boldsymbol{m} + i\gamma_5 \boldsymbol{\mu} + c_{\text{sw}} a \frac{1}{2} \sum_{\mu<\nu} \sigma_{\mu\nu} \hat{F}_{\mu\nu}. \tag{1.101}$$

The advantage of Wilson tm fermions is that at full twist (vanishing renormalized standard quark mass) one achieves automatic $\mathcal{O}(a)$ improvement []. This means that physical quantities are automatically improved without the need of any improvement coefficients for lattice operators. The following argument is based on the original work [] to which we refer for a complete proof.

At full twist, the Wilson tm Dirac operator reads

$$D_{\text{W}} + i\boldsymbol{\mu}\gamma_5. \tag{1.102}$$

Working in the twisted basis, this action in the continuum is invariant under a discrete chiral symmetry

$$\mathcal{R}_5^{1,2} = \begin{cases} \psi(x) \to i\gamma_5 \tau^{1,2} \psi(x) \\ \bar{\psi}(x) \to \bar{\psi}(x) i\gamma_5 \tau^{1,2} \end{cases}, \tag{1.103}$$

while $\mathcal{L}^{(1)}_{k=1}$ in eq. (1.92) is not

$$\mathcal{L}^{(1)}_{k=1} \to -\mathcal{L}^{(1)}_{k=1}. \tag{1.104}$$

This is key for automatic $\mathcal{O}(a)$ improvement. For correlation functions like eq. (1.97), we have that operators may be even or odd under $\mathcal{R}_5$, $\langle\Phi_0\rangle$ and $\langle\Phi_1\rangle$ having opposite $\mathcal{R}_5$-chirality

$$\langle\Phi_0\rangle \to \pm\langle\Phi_0\rangle\,, \quad \langle\Phi_1\rangle \to \mp\langle\Phi_1\rangle\,. \tag{1.105}$$

This means that for even $\langle\Phi_0\rangle$

$$\langle\Phi_0\rangle = \langle\Phi_0\rangle\,, \quad \left\langle\Phi_0\mathcal{L}^{(1)}_{k=1}\right\rangle = -\left\langle\Phi_0\mathcal{L}^{(1)}_{k=1}\right\rangle = 0, \tag{1.106}$$

$$\langle\Phi_1\rangle = -\langle\Phi_1\rangle = 0, \tag{1.107}$$

and thus even operators are automatically $\mathcal{O}(a)$ improved. On the other hand, for odd operators what we have is

$$\langle\Phi_0\rangle = -\langle\Phi_0\rangle = 0, \quad \left\langle\Phi_0\mathcal{L}^{(1)}_{k=1}\right\rangle = \left\langle\Phi_0\mathcal{L}^{(1)}_{k=1}\right\rangle, \tag{1.108}$$

$$\langle\Phi_1\rangle = \langle\Phi_1\rangle\,, \tag{1.109}$$

and thus they vanish in the continuum. Summing up, the only tuning required for Wilson tm fermions to achieve $\mathcal{O}(a)$ improvement is to set the bare quark mass m to its critical value m_{cr} in order to obtain full twist.

In our particular case, we will be working with a mixed action setup employing standard Wilson quarks in the sea and fully twisted Wilson tm quarks in the valence (see Sec 3). This means valence observables still get residual $\mathcal{O}(a)$ cutoff effects from the sea sector, and thus improvement is still needed. However, these effects are expected to be $\mathcal{O}(g_0^4)$ in perturbation theory.

Finally, we also need to improve the bare gauge coupling, which at $\mathcal{O}(a)$ reads

$$\tilde{g}_0^2 = g_0^2\left(1 + ab_g \text{tr}\left(M_q\right)\right), \tag{1.110}$$

with b_g the improvement coefficient, whose value at one-loop is given in [].

1.7 SCALE SETTING

In the lattice, all physical observables are computed in units of the lattice spacing a. Thus, in order to make any prediction, it is necessary to determine a in physical units. This task is called scale setting. It involves the precise determination of a reference observable, called the scale, in physical units, to which any other observable is compared in order to extract the value of the latter in physical units. As an

example, we could use the proton mass m_{proton} as a reference scale, and calculate the ratio of it to a given mass m_i

$$R_i = \frac{m_i}{m_{\text{proton}}}. \tag{1.111}$$

After computing the continuum limit of R_i, we can extract the physical mass m_i as

$$m_i^{\text{ph}} = R_i(a = 0) \times m_{\text{proton}}^{\text{exp}}. \tag{1.112}$$

Here, the proton mass is used as a reference scale, and comparing any lattice observable to it allows to extract the latter in physical units, once the continuum limit is performed. This procedure is equivalent to finding the value of the lattice spacing in physical units, since it can be extracted as

$$a = \frac{(am_{\text{proton}})^{latt}}{m_{\text{proton}}^{\text{exp}}}. \tag{1.113}$$

From eq. (1.112) it is clear that when aiming for precise lattice calculations of any physical observable like m_i, a reliable and precise scale setting is of the utmost importance. In this example this means being able to determine m_{proton} with high accuracy in the lattice in order to compute the ratios R_i, controlling the continuum limit of R_i and having a high precision in $m_{\text{proton}}^{\text{exp}}$.

Instead of using a phenomenological scale like m_{proton}, another choice is to use intermediate scales, like the gradient flow scale t_0 introduced in Sec. 2.6. This quantity can be computed with very high precision in the lattice while it cannot be measured experimentally. To obtain its physical value, one constructs a dimensionless quantity $(\sqrt{t_0}\Lambda)^{\text{latt}}$ with some phenomenological quantity Λ in the lattice. After performing the continuum limit, the physical value of t_0 can be extracted as

$$\sqrt{t_0^{\text{ph}}} = \frac{\left(\sqrt{t_0}\Lambda\right)^{\text{latt}}\Big|_{a=0}}{\Lambda^{\text{exp}}}. \tag{1.114}$$

Once the physical value of t_0 is found, it can be used as an intermediate scale against which any other quantity Λ' in the lattice can be compared in order to extract the latter in physical units. For this purpose, one performs a continuum extrapolation of $\sqrt{t_0}\Lambda'$ and obtains the physical value of Λ' as

$$\Lambda^{'\,\text{ph}} = \frac{\left(\sqrt{t_0}\Lambda'\right)^{\text{latt}}\Big|_{a=0}}{\sqrt{t_0^{\text{ph}}}}. \tag{1.115}$$

This quantity is already a prediction of the lattice.

2 ON THE EXTRACTION OF PHYSICAL OBSERVABLES

2.1 INTRODUCTION

In this Chapter we discuss the technical details on the extraction of physical observables from the lattice. In Sec. 2.2 we define the two-point functions required for extracting the physical observables needed in the analysis of the scale setting and the light and strange quark masses: in Sec. 2.3 we discuss how to extract meson masses while Sec. 2.4 covers the extraction of decay constants, their improvement and renormalization. In Sec. 2.5 we define the PCAC quark masses which will be used to tune Wilson tm quarks at full twist and to extract the physical quark masses. In Sec. 2.6 we discuss the gradient flow scale t_0 which we will use as the reference scale for the scale setting. Finally, in Sec. 2.7 we discuss the model averaging technology which we employ in order to find the ground state signals from all these lattice observables.

2.2 CORRELATION FUNCTIONS

For the extraction of the physical observables of interest for this work we need two-point functions involving the pseudoscalar and axial currents, defined as

$$P^{ij}(x) = \bar{\psi}^i(x)\gamma_5\psi^j(x), \tag{2.1}$$

$$A_\mu^{ij}(x) = \bar{\psi}^i(x)\gamma_\mu\gamma_5\psi^j(x), \tag{2.2}$$

where i, j are flavor indices. The Wilson term in the Wilson and Wilson tm fermion action breaks chiral symmetry explicitly. As a result, the Noether currents of the theory are no longer protected against renormalization. This means that both the pseudoscalar and axial currents get renormalized as

$$P^{ij,\mathrm{R}} = Z_P(g_0^2, a\mu)\left(1 + a\tilde{b}_P m_{ij} + a\bar{b}_P \mathrm{tr}\left(M_q\right)\right) P^{ij}, \tag{2.3}$$

$$A_\mu^{ij,\mathrm{R}} = Z_A(g_0^2)\left(1 + a\tilde{b}_A m_{ij} + a\bar{b}_A \mathrm{tr}\left(M_q\right)\right) A_\mu^{ij}, \tag{2.4}$$

where the b-counterterms are improvement coefficients for the renormalization constants. The renormalization constants are shown in Table **??**, while the improvement coefficients are in Table **??**. For our purposes, we will only need the differences $\tilde{b}_A - \tilde{b}_P$, $\bar{b}_A - \bar{b}_P$ and $\tilde{b}_A$, the latter given in perturbation theory by []

$$\tilde{b}_A = 1 + 0.0472 g_0^2 + \mathcal{O}(g_0^4). \tag{2.5}$$

β	Z_A	Z_P
3.40	0.75642(72)	0.35121(56)
3.46	0.76169(93)	0.34941(44)
3.55	0.76979(43)	0.34767(55)
3.70	0.78378(47)	0.34732(63)
3.85	0.79667(47)	0.35014(73)

Table 2.1: Renormalization constants Z_A and Z_P for different values of β. Z_A, which does not depend on the energy scale but only on the bare coupling g_0^2, is calculated non-perturbatively in [] using the chirally rotated Schrödinger functional, the "l-convention" and subtraction of the one-loop cutoff effects. Z_P is calculated non-perturbatively at the scale $\mu_{\text{had}} = 233(8)$ MeV in []

β	$\tilde{b}_A - \tilde{b}_P$	$\bar{b}_A - \bar{b}_P$	$\tilde{b}_A$
3.40	-0.324(17)	$\mathcal{O}(g_0^4)$	1.2684
3.46	-0.265(14)	$\mathcal{O}(g_0^4)$	1.2638
3.55	-0.196(14)	$\mathcal{O}(g_0^4)$	1.2571
3.70	-0.119(14)	$\mathcal{O}(g_0^4)$	1.2467
3.85	-0.073(12)	$\mathcal{O}(g_0^4)$	1.2371

Table 2.2: Summary of improvement coefficients at CLS β values. $\tilde{b}_A - \tilde{b}_P$ is taken from LCP-1 results in [], while $\bar{b}_A - \bar{b}_P$ are computed in perturbation theory. $\tilde{b}_A$ is computed perturbatively in [] and given by eq. (2.5)

To achieve $\mathcal{O}(a)$ improvement in the Wilson regularization, we need to improve the axial current as part of the Symanzik improvement program as follows

$$A_\mu^{ij}(x) \to A_\mu^{ij}(x) + ac_A\tilde{\partial}_{x_0}P^{ij}(x), \tag{2.6}$$

where we defined the symmetric time derivative

$$\tilde{\partial}_{x_0} = \frac{\partial_{x_0} - \partial_{x_0}^*}{2}, \tag{2.7}$$

$$\partial_x f(x) = \frac{f(x+a) - f(x)}{a}, \tag{2.8}$$

$$\partial_x^* f(x) = \frac{f(x) - f(x-a)}{a}. \tag{2.9}$$

The improvement coefficient c_A is given non-perturbatively by []

$$c_A(g_0^2) = -0.006033 g_0^2 \left[1 + \exp\left(9.2056 - \frac{13.9847}{g_0^2}\right)\right]. \tag{2.10}$$

The two-point functions that we will focus on, projected to zero-momentum are given by

$$C_P^{ij}(x_0, y_0) = \frac{a^6}{L^3}\sum_{\vec{x},\vec{y}}\left\langle P^{ij}(x)P^{ji}(y)\right\rangle, \tag{2.11}$$

$$C_A^{ij}(x_0, y_0) = \frac{a^6}{L^3}\sum_{\vec{x},\vec{y}}\left\langle A_0^{ij}(x)P^{ji}(y)\right\rangle. \tag{2.12}$$

The measurements of the two-point functions (see Appendix C) are taken at fixed source times $y_0 = a, T-a$ and evaluated at all sink times x_0. Whenever we omit the source position y_0 in the following means that the average

$$C_X(x_0) = \frac{C_X(x_0, y_0 = a) \pm C_X(T - x_0, y_0 = T - a)}{2}, \tag{2.13}$$

is taken to increase statistics, with the $+$ sign for the $X = P$ case and $-$ sign for the $X = A$ case.

The spectral decomposition of the two-point functions C_X allows to extract relevant hadronic observables such as the meson masses and decay constants. In what follows we restrict to the case of the pion, but the same applies to any other flavor content. Using the Transfer Matrix formalism

$$\langle O(x)O(y)\rangle = \mathcal{Z}^{-1}\left\langle\phi_f\right| e^{-(T-x_0)\hat{H}}\hat{O}(\vec{x})e^{-(x_0-y_0)\hat{H}}\hat{O}(\vec{y})e^{-y_0\hat{H}}\left|\phi_i\right\rangle, \tag{2.14}$$

and inserting a complete set of states $|\vec{p}, n\rangle$

$$1 = \frac{1}{2E_n(\vec{p})L^3}\sum_{\vec{p},n}|\vec{p}, n\rangle\langle\vec{p}, n|, \tag{2.15}$$

we can write a two-point function as

$$\langle O(x)O(y)\rangle = \mathcal{Z}^{-1}\frac{1}{L^9}\sum_{n,m,l}\sum_{\vec{p},\vec{q},\vec{s}}\frac{1}{2^3 E_n(\vec{p})E_m(\vec{q})E_l(\vec{s})} \tag{2.16}$$

$$\times \left\langle \phi_f|\vec{q},m\right\rangle e^{-(T-x_0)E_m(\vec{q})}\times \tag{2.17}$$

$$\left\langle \vec{q},m\right| \hat{O}(\vec{x}) \left|\vec{p},n\right\rangle e^{-(x_0-y_0)E_n(\vec{p})} \tag{2.18}$$

$$\times \left\langle \vec{p},n\right| \hat{O}(\vec{y}) \left|\vec{s},l\right\rangle e^{-y_0 E_s(\vec{l})} \left\langle \vec{s},l|\phi_i\right\rangle . \tag{2.19}$$

The partition function reads

$$\mathcal{Z} = \left\langle \phi_f\right| e^{-T\hat{H}} \left|\phi_i\right\rangle = \frac{1}{L^3}\sum_{\vec{p},n}\frac{1}{2E_n(\vec{p})} \left\langle \phi_f|\vec{p},n\right\rangle e^{-TE_n(\vec{p})} \left\langle \vec{p},n|\phi_i\right\rangle \tag{2.20}$$

$$\to \left\langle \phi_f|0\right\rangle e^{-TE_0} \left\langle 0|\phi_i\right\rangle , \tag{2.21}$$

with

$$|0\rangle\langle 0| \equiv \frac{1}{2E_0 L^3}\left|\vec{0},0\right\rangle\left\langle \vec{0},0\right|. \tag{2.22}$$

We have assumed that the boundary states $\left|\phi_{i,f}\right\rangle$ share the same quantum numbers of the vacuum state $|0\rangle$. This is true when using open boundary conditions (OBC) in time, which will be the case for most of the ensembles under study (see Table E.1).

From the spectral decomposition of the two-point function, the exponentials with arguments $T - x_0$ and y_0 are contributions from the boundary states. We will label the quantum states as $\left|\vec{0},\alpha,n\right\rangle$, with n labeling the energy level and α the other quantum numbers, and using the fact that we are projecting to zero momentum $\vec{p} = \vec{0}$ we employ the shorthand notation

$$|\alpha,n\rangle\langle\alpha,n| \equiv \frac{1}{2E_n^\alpha L^3}\left|\vec{0},\alpha,n\right\rangle\left\langle \vec{0},\alpha,n\right|. \tag{2.23}$$

With all this, the two-point function can be written then as

$$\langle O(x)O(y)\rangle = \sum_{\alpha,\beta,\gamma}\sum_{n,m,l}\frac{\langle\Omega|\beta,m\rangle}{\langle\Omega|0,0\rangle}e^{-(T-x_0)E_m^\beta}\times \tag{2.24}$$

$$\left\langle \beta,m\right| \hat{O}(\vec{x}) \left|\alpha,n\right\rangle e^{-(x_0-y_0)E_n^\alpha} \tag{2.25}$$

$$\times \left\langle \alpha,n\right| \hat{O}(\vec{y}) \left|\gamma,l\right\rangle e^{-y_0 E_s^\gamma}\frac{\langle\gamma,l|\Omega\rangle}{\langle 0,0|\Omega\rangle}, \tag{2.26}$$

where we absorbed the e^{-TE_0} term coming from the partition function into the energy levels

$$E_n^\alpha \to E_n^\alpha - E_0, \tag{2.27}$$

such that $E_0^0 = 0$.

For sufficiently large source-sink separation $x_0 - y_0 \to \infty$, only the pion state $|\pi, 0\rangle$ propagates between $O(x)$ and $O(y)$. On the other hand, we made the assumption that the boundary states only overlap with the vacuum, so we are left with

$$\langle O(x)O(y)\rangle = \sum_{m,l} \frac{\langle\Omega|0,m\rangle}{\langle\Omega|0,0\rangle} e^{-(T-x_0)E^0_m} \langle 0,m|\,\hat{O}(\vec{x})\,|\pi,0\rangle\, e^{-(x_0-y_0)m_\pi} \tag{2.28}$$

$$\times \langle\pi,0|\,\hat{O}(\vec{y})\,|0,l\rangle\, e^{-y_0 E^0_l} \frac{\langle 0,l|\Omega\rangle}{\langle 0,0|\Omega\rangle}. \tag{2.29}$$

Finally, far away from the boundaries $T - x_0, y_0 \to \infty$ the first relevant contribution from the boundaries is the one with energy E^0_1

$$\langle O(x)O(y)\rangle = \langle 0,0|\,\hat{O}(\vec{x})\,|\pi,0\rangle\, e^{-(x_0-y_0)m_\pi} \langle\pi,0|\,\hat{O}(\vec{y})\,|0,0\rangle \tag{2.30}$$

$$\times \left[1 + \eta_x e^{-(T-x_0)E^0_1} + \eta_y e^{-y_0 E^0_1} + \ldots\right], \tag{2.31}$$

with

$$\eta_x = \frac{\langle\Omega|0,1\rangle \langle 0,1|\,O(x)\,|\pi,0\rangle}{\langle\Omega|0,0\rangle \langle 0,0|\,O(x)\,|\pi,0\rangle}, \tag{2.32}$$

$$\eta_y = \frac{\langle\Omega|0,1\rangle \langle\pi,0|\,O(y)\,|0,1\rangle}{\langle\Omega|0,0\rangle \langle\pi,0|\,O(y)\,|0,0\rangle}. \tag{2.33}$$

So far we have assumed OBC in time. In the case with periodic boundary conditions (PBC), the pseudoscalar and axial correlators are periodic in time and identical (up to a relative minus sign for the axial) in x_0 and $T - x_0$. Considering only the ground state contribution we can write them as

$$C_X(x_0, y_0) = a_X \left(e^{-m_\pi(x_0-y_0)} \pm e^{-m_\pi(T-x_0+y_0)}\right), \tag{2.34}$$

where the $+$ sign corresponds to the pseudoscalar correlator $X = P$ and the $-$ sign for the axial $X = A$, $a_P = |\langle 0,0|\,P^{ud}\,|\pi,0\rangle|^2$ and $a_A = \langle 0,0|\,A^{ud}_0\,|\pi,0\rangle \langle 0,0|\,P^{ud}\,|\pi,0\rangle$.

2.3 MESON MASSES

Meson masses can be extracted from the pseudoscalar two-point function $C_P(x_0)$ in eq. (2.11) with the effective mass, defined as

$$am_{\text{eff}}(x_0) = \log\left(\frac{C_P(x_0)}{C_P(x_0 + a)}\right). \tag{2.35}$$

For sufficiently large source-sink separation $x_0 \gg 1$ this effective mass $m_{\text{eff}}(x_0)$ tends to a plateau as can be seen from the spectral decomposition of the two-point function.

In the case of PBC, to extract the pion mass one can alternatively build the quantity

$$\frac{C_P(x_0)}{C_P(x_0+a)} = \frac{\cosh(m_\pi(x_0 - y_0 - T/2))}{\cosh(m_\pi(x_0 - y_0 + a - T/2))}, \tag{2.36}$$

and fit am_π.

The pion mass for a given ensemble is shown in Fig. **??**.

2.4 DECAY CONSTANTS

Meson decay constants are given by the vacuum-to-meson matrix elements. The matrix element we are interested in is the vacuum-to-pion mediated by the axial current

$$\langle 0,0|\, A_0^{ud}\, |\pi,0\rangle = f_\pi \sqrt{\frac{m_\pi}{2L^3}}, \tag{2.37}$$

where f_π is the bare pion decay constant. To extract this matrix element, we must remove the matrix element $\langle 0,0|\, P^{ud}\, |\pi,0\rangle$ from the axial two-point function $C_A(x_0)$ in eq. (2.11). To achieve this, we compute the ratio

$$R(x_0) = \sqrt{\frac{|C_A(x_0, y_0 = a) C_A(x_0, y_0 = T - a)|}{L^3 C_P(x_0 = T - a, y_0 = a)}}, \tag{2.38}$$

from which we extract then the decay constant as

$$f_\pi(x_0) = \sqrt{\frac{2}{L^3 m_\pi}} R(x_0). \tag{2.39}$$

In the PBC case, in order to isolate the matrix element $\langle 0,0|\, A_0^{ud}\, |\pi,0\rangle$ we fit the axial and pseudoscalar correlators in eq. (2.34) to extract the fit parameters $a_{P,A}$. This allows to compute the decay constant as

$$f_\pi = \frac{2}{L^3 m_\pi} \frac{a_A}{\sqrt{a_P}}. \tag{2.40}$$

In said fit, m_π is not a fit parameter but an external input after having determined it using eq. (2.36).

Following eq. (2.3), the pion decay constant in the Wilson regularization renormalizes as

$$f_\pi = Z_A(g_0^2) \left[1 + a\bar{b}_A \mathrm{tr}\left(M_q\right) + a\tilde{b}_A m_{ud}\right] f_\pi. \tag{2.41}$$

We assumed improvement of the axial current according to eq. (2.6).

In the Wilson tm regularization at full twist, the chiral rotation in eq. (1.49) rotates the axial to the vector current when going from the physical to the twisted basis

$$A_\mu^{ij} \to i V_\mu^{ij}, \tag{2.42}$$

which means that one can compute the decay constant from the vector current in the twisted basis following

$$\langle 0,0|\, V_0^{ud}\, |\pi,0\rangle = -if_\pi \sqrt{\frac{m_\pi}{2L^3}}. \tag{2.43}$$

The advantage of this is that the vector current is protected against renormalization (see eq. (1.61)) and thus so is f_π when extracted in this way. Furthermore, in the twisted basis we can use the PCVC Ward identity

$$\left\langle \left(\partial_0^* V_0^{ij}(x)\right) O^{ji}(y)\right\rangle = i\left(\eta_q\mu_q - \eta_{q'}\mu_{q'}\right)\left\langle P^{ij}(x)O^{ji}(y)\right\rangle, \tag{2.44}$$

where O is any interpolator chosen such that $\left\langle P^{ij}(x)O^{ji}(y)\right\rangle$ does not vanish, in order to write the decay constant as

$$f_\pi = \sqrt{\frac{2L^3}{m_\pi^3}}\left(|\mu_u| + |\mu_d|\right)\left|\langle 0,0|\, P^{ud}\, |\pi,0\rangle\right|. \tag{2.45}$$

Different choices of the interpolator O will lead to different values of the decay constants due to cutoff effects. We choose to use the pseudoscalar density P^{ij} since it enhances the signal. To extract the matrix element $\langle 0,0|\, P^{ud}\, |\pi,0\rangle$, analogously to the Wilson case we can estimate it by the plateau value of the ratio

$$R(x_0) = \sqrt{\frac{C_P(x_0, y_0 = a)C_P(x_0, y_0 = T-a)}{C_P(x_0 = T-a, y_0 = a)}}. \tag{2.46}$$

For PBC, using again the PCVC relation, the decay constant reads

$$f_\pi = \sqrt{\frac{2L^3}{m_\pi^3}}\sqrt{a_P}. \tag{2.47}$$

The ratios defined in this section for the extraction of decay constants are shown for the case of one particular ensemble in Fig. **??**.

2.5 QUARK MASSES

For the quark masses we use the Partially Conserved Axial Current (PCAC) Ward-Takahashi identity

$$\left\langle \left(\partial_\mu A_\mu^{ij}(x)\right) O^{ji}(y)\right\rangle = 2m_{ij}\left\langle P^{ij}(x)O^{ji}(y)\right\rangle, \tag{2.48}$$

where O is any interpolator chosen such that $\left\langle P^{ij}(x)O^{ji}(y)\right\rangle$ does not vanish, and m_{ij} is the so called PCAC quark mass, where the flavor indices indicate combinations of the individual quark masses

$$m_{ij} = \frac{m_i + m_j}{2}. \tag{2.49}$$

The subtracted quark mass $m_i - m_{\rm cr}$ must agree, up to cutoff effects, with the PCAC quark mass after renormalization, so by using the latter we do not need to know a priori the additive mass renormalization. As in the decay constants case, we take $O^{ij} = P^{ij}$ since we find the signal to be enhanced. Thus, the PCAC quark masses read

$$m_{ij}(x_0) = \frac{\tilde{\partial}_{x_0} C_A^{ij}(x_0)}{2C_P(x_0)}. \tag{2.50}$$

As seen above, the axial current needs to be improved, and the numerator becomes

$$\tilde{\partial}_{x_0} C_A^{ij}(x_0) + a c_A \partial_{x_0} \partial^*_{x_0} C_P^{ij}(x_0) \tag{2.51}$$

with the discrete second derivative given by

$$\partial_x \partial^*_x f(x) = \frac{f(x+a) + f(x-a) - 2f(x)}{a^2} + \mathcal{O}(a^2). \tag{2.52}$$

This improvement is not needed in the Wilson tm regularization at full twist thanks to automatic $\mathcal{O}(a)$ improvement (see Sec. 1.6).

From eq. (2.3) we see that the PCAC quark mass renormalizes as

$$m_{ij}^{\rm R} = \left[1 + a\left(\bar{b}_A - \bar{b}_P\right) \mathrm{tr}\left(M_q\right) + a\left(\tilde{b}_A - \tilde{b}_P\right) m_{ij}\right] m_{ij}. \tag{2.53}$$

In the Wilson regularization, physical quark masses are determined from the PCAC masses, while in the Wilson tm regularization at full twist, the latter vanish and the former are given by the renormalized twisted masses in eq. (1.57).

In Fig. **??** we show the dependence of the PCAC quark mass for one given ensemble.

2.6 GRADIENT FLOW

For the scale setting, we will use the gradient flow scale t_0 as an intermediate scale. The gradient flow is a method of smearing the gauge fields $U_\mu(x)$ [**flow**]. It involves evolving the gauge fields along a new dimension called flow time t using the flow equation

$$\partial_t V_t(x,\mu) = -g_0^2 \left[\partial_{x,\mu} S_W(V_t)\right] V_t(x,\mu), \tag{2.54}$$

$$V_{t=0}(x,\mu) = U_\mu(x), \tag{2.55}$$

with V_t the flowed gauge fields.

For positive flow time $t > 0$, gauge observables such as the energy density are finite and need not to be renormalized. The energy density can be defined as

$$E(x,t) = a^4 \sum_{\mu,\nu} \mathrm{tr}\left(\hat{F}_{\mu\nu}(x)\hat{F}_{\mu\nu}(x)\right), \tag{2.56}$$

using eq. (**??**) for the definition of $\hat{F}_{\mu\nu}$ but replacing the flowed fields V_t for the original gauge links U_μ. After averaging over the 4-dimensional volume

$$E(t) = \langle E(x,t) \rangle_x \,, \tag{2.57}$$

we are left with an average energy density that depends only on the flow time. This average is computed using the model averaging technique detailed in sec. 2.7. The quantity $t^2E(t)$ can be precisely calculated in the lattice, making it a suitable choice for setting the scale (see Sec. 4). To this end, the scale t_0 is defined as the flow time which satisfies

$$t^2E(t)|_{t=t_0} \equiv 0.3. \tag{2.58}$$

Fig. **??** shows the extraction of t_0/a^2 for one particular ensemble.

2.7 GROUND STATE SIGNALS AND MODEL AVERAGE

So far, we have expressed all physical observables under study as functions of the euclidean time x_0. As discussed in Sec. 2.2, these quantities are affected by boundary effects and excited states. In order to extract the ground state contribution of each observable, it is necessary to go to large source-sink separations and ensure sufficient distance from the boundaries. However, it is not clear how to decide when these conditions are met. In the community there are different approaches to adress this issue []. Our choice is to employ model averaging techniques as proposed in [].

The idea is to investigate multiple fit functions and/or several fit ranges and assign an Information Criterion IC to each choice, which allows to compute a weight

$$W_i \propto \exp\left(-\frac{1}{2}\mathrm{IC}_i\right), \tag{2.59}$$

for each choice i of the "model", which refers to a specific fit function and fit range. Then one can compute a weighted average for a fit parameter p that is common to all models as

$$\langle p \rangle_{\mathrm{MA}} = \sum_i p_i W_i, \tag{2.60}$$

(where p_i is the fit parameter result for model i) and add a systematic uncertainty related to the model variation as

$$\sigma^2_{\mathrm{syst}}[p] = \langle p^2 \rangle_{\mathrm{MA}} - \langle p \rangle^2_{\mathrm{MA}} \,. \tag{2.61}$$

For fitting we use a least-squares method that seeks to minimize a χ^2 function by finding the extremal values of the fit parameters (for

details see Appendix F). As proposed in [] we use the Takeuchi's Information Criterion (TIC)

$$\mathrm{TIC} = \chi^2 - 2\left\langle \chi^2 \right\rangle, \tag{2.62}$$

where $\left\langle \chi^2 \right\rangle$ is a measure of the expected value of the χ^2, for a precise definition see []. This IC is well-behaved for cases where fully correlated fits cannot be performed (see Appendix F for details), which is our case when fitting observables along the euclidean time direction. For a fully correlated fit, $\left\langle \chi^2 \right\rangle = \mathrm{dof}$, and thus the TIC reduces to the proposal in []

$$\mathrm{TIC} = \chi^2 - 2n_{\mathrm{param}} - 2n_{\mathrm{cut}}, \tag{2.63}$$

with n_{param} the number of parameters of the fit and n_{cut} the number of points left out of the fit. We see that this Information Criterion penalizes models with large number of parameters and big cuts in data, provided the minimization of the χ^2 succeeds.

In practice, for the extraction of the ground state signals of lattice observables, the data is fitted to a constant plus two exponential signals for the OBC ensembles

$$f(x_0) = A + Be^{-Cx_0} + De^{-E(T-x_0)}, \tag{2.64}$$

or for PBC ensembles

$$f(x_0) = A + Be^{-Cx_0} + Be^{-C(T-x_0)}, \tag{2.65}$$

and we investigate the effects of varying the fit range. The result for the fit parameter A corresponds to the ground state signal. An illustration of the method for the extraction of the ground state signal in the pion effective mass in Fig. **??** is shown in Fig. **??**, where we selected only a subset of the fit ranges explored for visualization purposes.

This model averaging technique will also be used for the chiral and continuum extrapolations needed to set the scale and determine the physical quark masses, but there we will also consider the variation of the fit functions and not only cutting data (variation of the fit range), see Secs. 4 and 5.

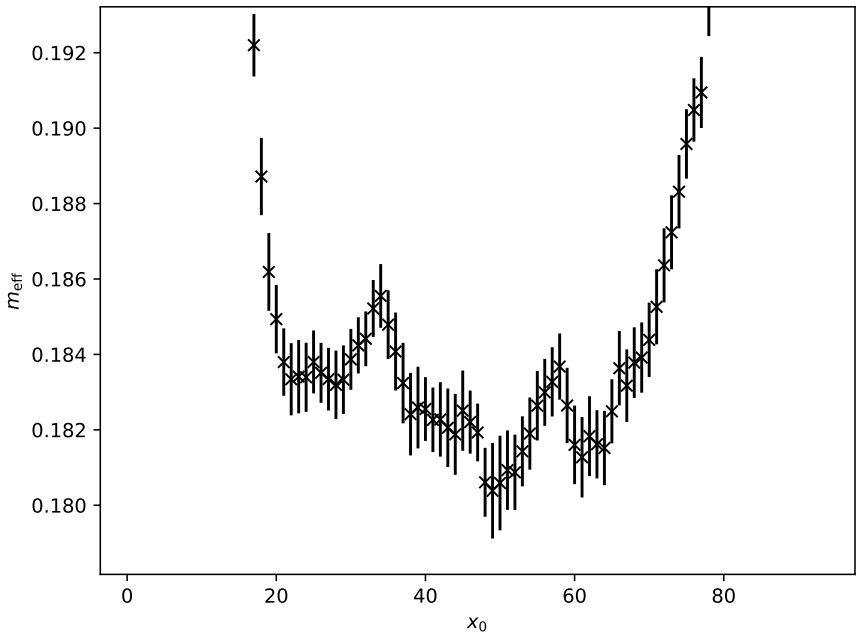

(a)

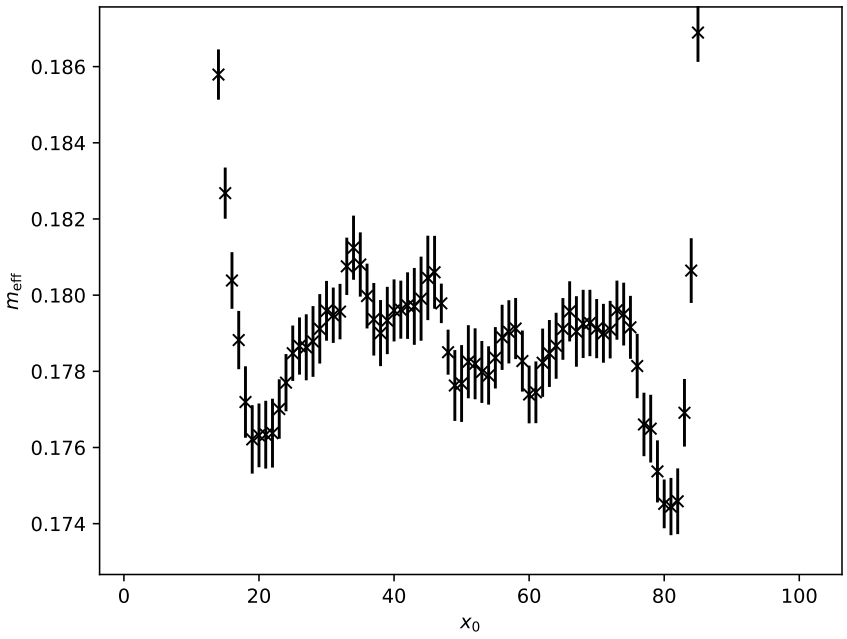

(b)

Figure 2.1: (a): pion effective mass m_{eff} in eq. (2.35) for ensemble H101 in the Wilson regularization. (b): the same but for the mixed action regularization for one point in our valence parameters grid, see Sec. 3.

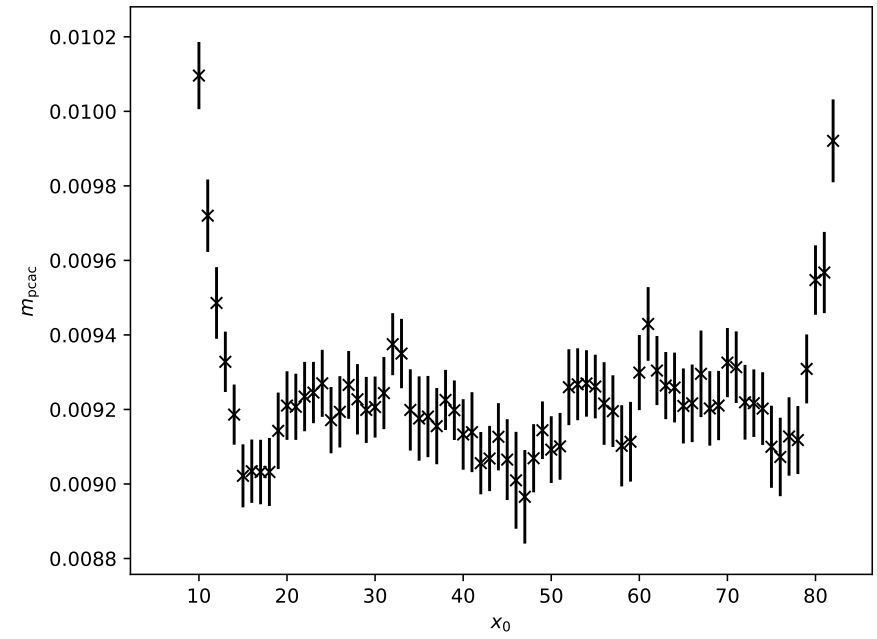

(a)

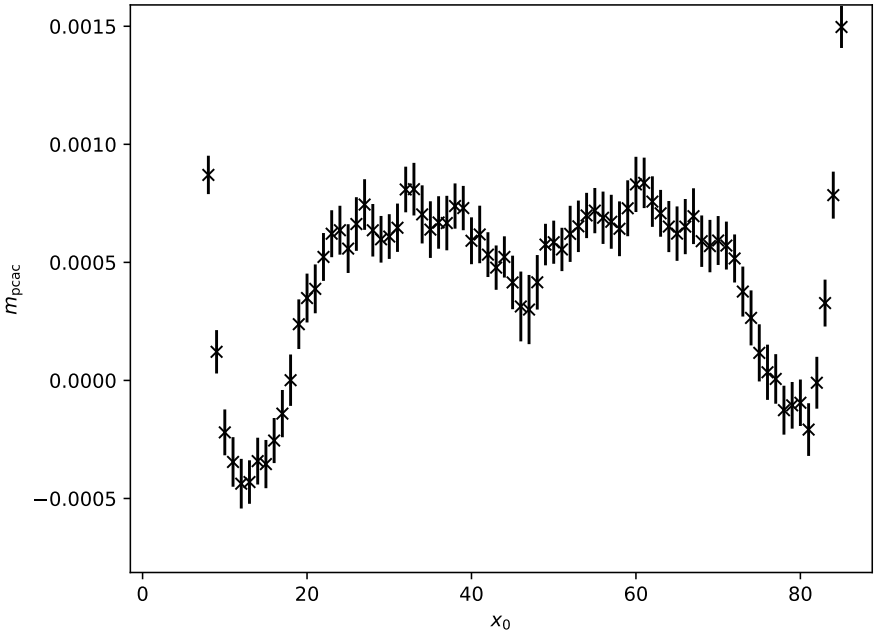

(b)

Figure 2.2: (a): up-down PCAC quark mass in eq. (2.48) for ensemble H101 in the Wilson regularization. (b): the same but for the mixed action regularization for one point in our valence parameters grid, see Sec. 3.

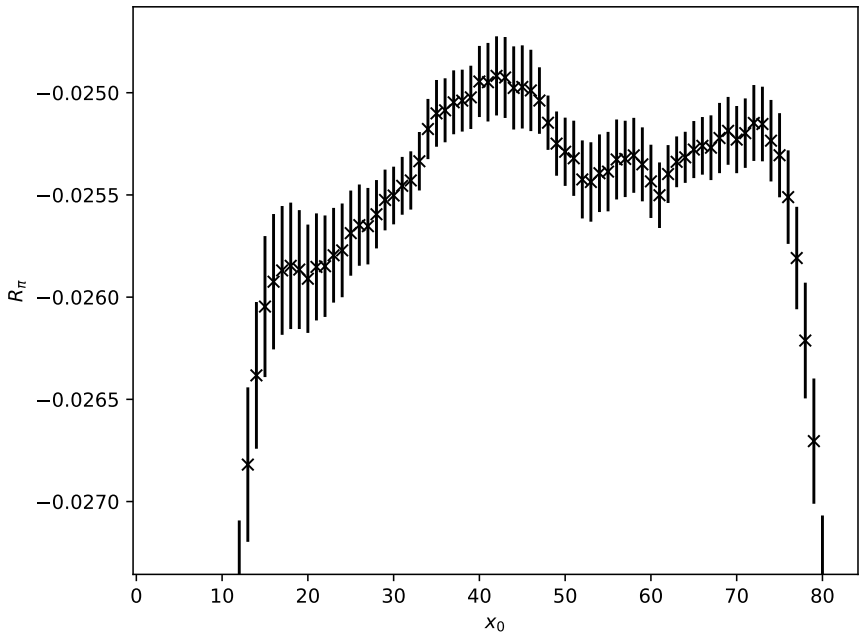

(a)

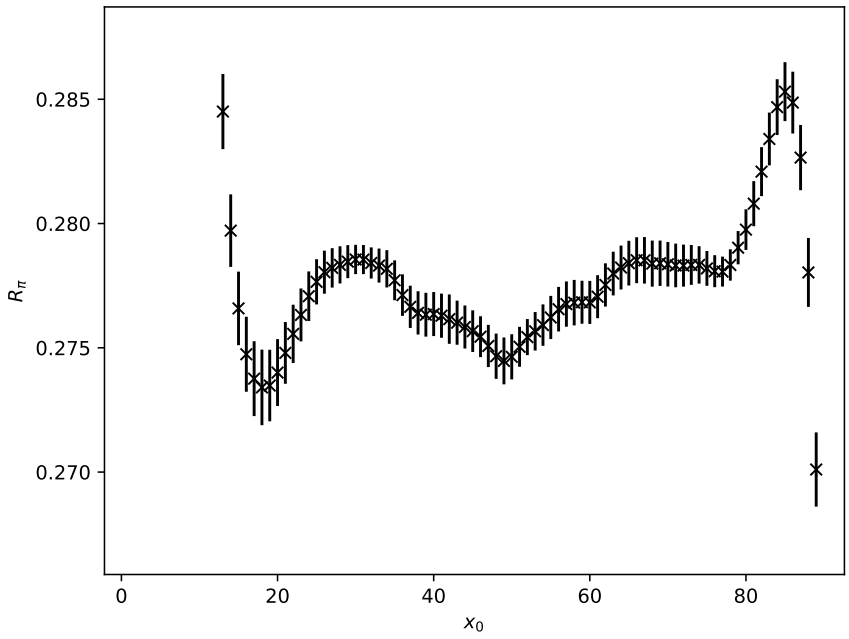

(b)

Figure 2.3: (a): vacuum-to-pion axial matrix element R_π from eq. (2.38) for ensemble H101 in the Wilson regularization. (b): the same but for the mixed action regularization for one point in our valence parameters grid, see Sec. 3.

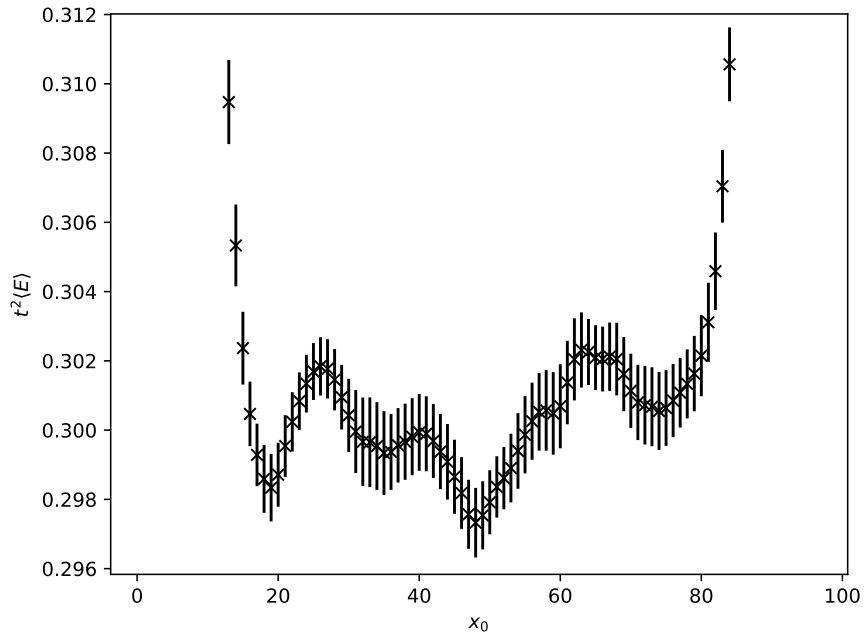

(a)

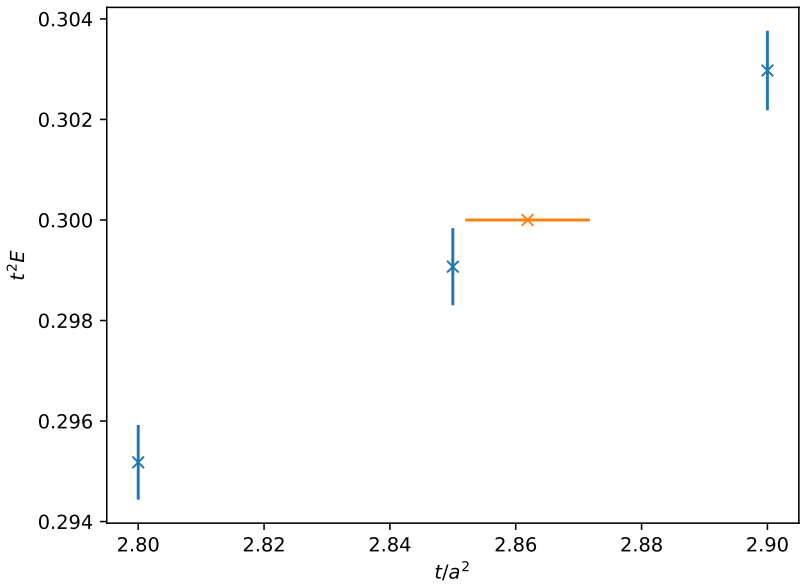

(b)

Figure 2.4: (a): $t^2E(t)$ for one value of the flow time t/a^2 near t_0/a^2 as a function of the euclidean time x_0/a. (b): euclidean-time averaged values of $t^2E(t)$ for several flow times t/a^2 near t_0/a^2 (blue points) and the interpolated result for t_0/a^2 (orange point)).

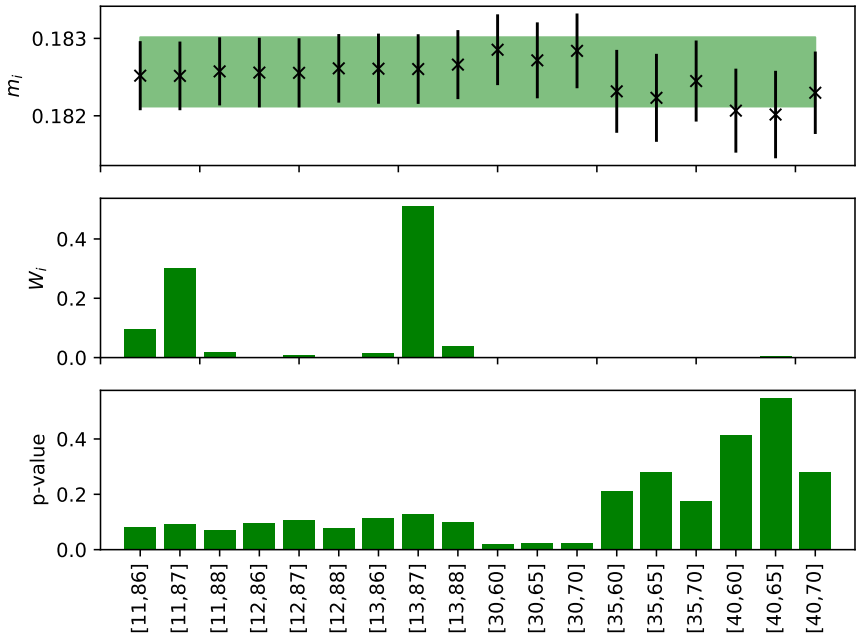

Figure 2.5: Model variation for the extraction of the ground state signal in the pion effective mass of ensemble H101 in the Wilson regularization, shown in Fig. **??**. From top to bottom we show the ground state signal result from a fit to eq. (2.64) for each fit interval choice, the weight associated to each choice according to eq. (2.59), and the goodness of fit measured through the p-values defined in []. We see that the highest weights are associated to a compromise between good fits (in terms of p-values) and fits with large number of points. The right-most models in the plot are heavily penalized even though they have the best p-values, since they cut a large number of points and models with not so severe cuts get also good p-values. The band in the top figure indicates the final weighted average result with the systematic uncertainty in eq. (2.61) included.

Part III

PRECISSION PHYSICS FROM A LATTICE QCD MIXED ACTION

3

MIXED ACTION SETUP

3.1 MOTIVATION

Our lattice setup is based on a mixed action with Wilson $\mathcal{O}(a)$ improved quarks in the sea and full twist Wilson tm quarks in the valence, the goal of which is to control cutoff effects associated with heavy quarks.

For the definition of the mixed action approach, we recall eq. (1.73)

$$\left\langle O^{ij}(x_1)O^{ji}(x_2)\right\rangle = -\frac{1}{\mathcal{Z}}\int \mathcal{D}[U]e^{-S_G[U]-S_{\text{eff}}[U]}\times \tag{3.1}$$

$$\text{tr}\left(\Gamma D_i^{-1}(x_1,x_2)\Gamma D_j^{-1}(x_2,x_1)\right), \tag{3.2}$$

$$S_{\text{eff}}[U] = -\sum_i^{N_f}\log\det(D_i). \tag{3.3}$$

We see that the Dirac operator D appears first in the Boltzmann factor $e^{-S_G[U]-S_{\text{eff}}[U]}$ with which the set of gauge ensembles is generated, and then in the fermionic observable whose expectation value we are interested in. In particular, it appears in two separate stages of the analysis: one the generation of gauge ensembles, the other the inversion of the Dirac operator on said gauge configurations. This in principle allows for the use of different regularizations of the Dirac operator in these two steps, which is referred to as a mixed action approach.

The two separate sectors in which the Dirac operator appear, S_{eff} and the observable whose expectation value one is interested in, are referred to as sea and valence sectors respectively. By using different lattice regularizations of the Dirac operator in both sectors, unitarity is violated, even in the continuum, if the physical quark masses in both sectors do not coincide. This means that our mixed action setup will require a tuning procedure in which the values of the Wilson tm parameters are chosen in order to reproduce the same physical quark masses in the valence as in the sea sectors. This process is called matching of the mixed action.

The flavor content of our setup is as follows. On the one hand, the sea sector has $N_f = 2+1$ flavors, i.e. two mass-degenerate light quarks (corresponding to the u and d flavors) with mass m_l and one strange quark with mass m_s. On the other hand, the valence sector is composed of $N_f = 2+1+1$ flavors, adding a charm quark. Since we have $N_f = 2+1$ in the sea and $N_f = 2+1+1$ in the valence, the flavors we need to match are the light and strange, treating the charm quark in the valence as a partially quenched flavor.

In order to perform the matching of the theory, we need to know beforehand what values the physical quark masses take in the sea sector. This means that we need lattice measurements in the fully Wilson unitary setup (using the Wilson regularization in the sea and valence) in addition to the mixed action regularization. We therefore have two sets of data for lattice observables: those coming from the Wilson unitary setup, which we refer to as sea or Wilson results, and those coming from the mixed action itself. Using the two sets of data helps increasing the statistics of the scale setting and light quark masses analysis, as we will see in Secs 4-5. In addition to the matching of the sea and valence sectors, we also need to tune the valence action parameters to enforce full twist and automatic $\mathcal{O}(a)$ improvement.

The Chapter is structured as follows. In Sec. 3.2 we discuss the sea sector details: ensembles under study, lattice actions and boundary conditions. In Sec. 3.3 we discuss the valence sector, which employs Wilson tm quarks. In Sec. 3.4 we discuss the line of constant physics along which the ensembles under study were generated. They follow a chiral trajectory that suffers small mistunings and that must be corrected in order to go through the physical point. We discuss the details of a mass shifting procedure to account for these effects. Finally, in Sec. 3.5 we deal with the challenges of working with a mixed action and the need to match both sea and valence sectors in order to recover unitarity in the continuum. We also explain the procedure to tune Wilson tm valence quarks to full twist.

3.2 SEA SECTOR

The gauge ensembles that we employ are CLS ensembles [**CLS**] with $N_f = 2 + 1$ non-perturbatively $\mathcal{O}(a)$ improved Wilson fermions (see eq. (1.95)). They use the Lüscher-Weisz gauge action [], which has reduced $\mathcal{O}(a^2)$ effects and is defined in eqs. (1.87-1.88).

For most of the ensembles, open boundary conditions (OBC) in time are used for the gauge fields, since it has been shown that with periodic boundary conditions (PBC) autocorrelations increase as one approaches the continuum limit, a problem known as critical slowing down. This is related to the existence of topological disconnected sectors in gauge field space, which avoids the algorithm to sample correctly different topological sectors. In contrast to this, OBC let the topological charge flow through the boundaries and topology freezing is thus avoided. All ensembles use PBC over the spatial volume.

The ensembles we consider have 5 different values of the lattice spacing, and for each of them there is one ensemble at the symmetric point, which is defined as $m_l = m_s$, or equivalently by the κ parameter (see eq. (1.44)) as $\kappa_l = \kappa_s$. All the ensembles, the complete list of which is shown in Table E.1, follow the chiral trajectory defined in eq. (3.7).

3.3 VALENCE SECTOR

In the valence sector, we employ a $N_f = 2+1+1$ fully-twisted Wilson tm fermion action (see Sec. 1.3.3), whose Dirac operator reads

$$D_{\mathrm{W}} + \boldsymbol{m}^{(\mathrm{v})} + i\boldsymbol{\mu}^{(\mathrm{v})}\gamma_5, \tag{3.4}$$

with

$$\boldsymbol{\mu}^{(\mathrm{v})} = \mathrm{diag}(\mu_l, -\mu_l, -\mu_s, \mu_c)^{(\mathrm{v})}, \quad \boldsymbol{m}^{(\mathrm{v})} = \mathrm{diag}(m_l, m_l, m_s, m_c)^{(\mathrm{v})}. \tag{3.5}$$

In particular, we use the same standard quark mass for all flavors $m_l^{(\mathrm{v})} = m_s^{(\mathrm{v})} = m_c^{(\mathrm{v})} \equiv m^{(\mathrm{v})}$.

As discussed in Sec. 1.3.3, to impose full twist means that the twist angles α_i fulfill

$$\cot \alpha_i = \frac{m_i^{\mathrm{R}}}{\mu_i^{\mathrm{R}}} = 0. \tag{3.6}$$

To do so, it is enough to impose that the PCAC quark masses in eq. (2.48) vanish. When this is the case, automatic $\mathcal{O}(a)$ improvement of valence observables is obtained, up to cutoff effects coming from the sea sector due to the mixed action. However, these effects are expected to be $\mathcal{O}(g_0^4)$ in perturbation theory.

Since we are dealing with a mixed action setup, not only the tuning to full twist is needed, but also a matching between the physical light and strange quark masses in the sea and valence sectors (see Sec. 3.5) to ensure unitarity of the theory in the continuum limit. This means that we have to find the valence parameters $(\kappa, \mu_l, \mu_s)^{(\mathrm{v})}$ that satisfy both conditions. To do this, we employ a grid of valence values around an estimate of the target point in order to perform small interpolations that allow us to find the said target point $(\kappa, \mu_l, \mu_s)^{(\mathrm{v})^*}$.

3.4 CHIRAL TRAJECTORY

The set of CLS ensembles that we use are generated along the trajectory in the quark mass plane defined by a constant trace of the bare sea "(s)" quark mass matrix

$$\mathrm{tr}\left(M_q^{(\mathrm{s})}\right) = 2m_l^{(\mathrm{s})} + m_s^{(\mathrm{s})} = \mathrm{cnst}. \tag{3.7}$$

This trajectory ensures that at fixed lattice spacing the improved bare coupling

$$\tilde{g}_0^2 = g_0^2\left(1 + b_g \mathrm{tr}\left(aM_q^{(\mathrm{s})}\right)\right), \tag{3.8}$$

is kept constant as we vary the sea quark masses to approach the physical point. Note that for the Wilson unitary setup, sea and valence

quark masses are the same, but not for the mixed action setup. To ensure that this trajectory goes through the physical point, we define the dimensionless quantities

$$\phi_2 = 8t_0 m_\pi^2, \tag{3.9}$$

$$\phi_4 = 8t_0 \left(m_K^2 + \frac{1}{2} m_\pi^2 \right), \tag{3.10}$$

which to LO ChPT are proportional to the renormalized quark masses

$$\phi_2 \propto m_l^{\mathrm{R}}, \tag{3.11}$$

$$\phi_4 \propto 2m_l^{\mathrm{R}} + m_s^{\mathrm{R}} = \mathrm{tr}\left(M_q^{\mathrm{R}} \right). \tag{3.12}$$

The trace of the renormalized quark mass matrix $\mathrm{tr}\left(M_q^{\mathrm{R}} \right)$ is in turn proportional to the bare quark mass matrix up to $\mathcal{O}(a)$ cutoff effects

$$\mathrm{tr}\left(M_q^{\mathrm{R}} \right) = Z_m r_m \left[\left(1 + a\bar{d}_m \mathrm{tr}\left(M_q \right) \right) \mathrm{tr}\left(M_q \right) + a d_m \mathrm{tr}\left(M_q^2 \right) \right]. \tag{3.13}$$

Thus, setting the sea value of ϕ_4 to its physical value for all ensembles ensure that eq. (3.7) holds and goes through the physical point, up to small mistunings due to higher terms in the chiral expansion and to cutoff effects.

To correct for these mistunings, we perform small mass shifts [**BKS**] in the bare sea quark masses by Taylor expanding lattice observables as

$$O\left(m_l^{(\mathrm{s})'}, m_s^{(\mathrm{s})'} \right) = O\left(m_l^{(\mathrm{s})}, m_s^{(\mathrm{s})} \right) + \sum_q \left(m_q^{(\mathrm{s})'} - m_q^{(\mathrm{s})} \right) \frac{dO}{dm_q^{(\mathrm{s})}}, \tag{3.14}$$

with the total derivative given by

$$\frac{dO}{dm_q^{(\mathrm{s})}} = \sum_i \frac{\partial O}{\partial \langle P_i \rangle} \left[\left\langle \frac{\partial P_i}{\partial m_q^{(\mathrm{s})}} \right\rangle - \left\langle P_i \frac{\partial S}{\partial m_q^{(\mathrm{s})}} \right\rangle + \langle P_i \rangle \left\langle \frac{\partial S}{\partial m_q^{(\mathrm{s})}} \right\rangle \right]. \tag{3.15}$$

Here O is an arbitrary lattice observable and $\{P_i\}_{i=1,2,\ldots}$ is the set of primary observables, in our case the corresponding two-point functions on which it depends. The first term in the r.h.s. of this equation corresponds to the valence contribution to the derivative, while the other terms correspond to the sea contributions. Note that for the Wilson unitary setup, all terms contribute, while for the mixed action setup, since the two-point functions $\{P_i\}$ do not depend explicitly on $m_q^{(\mathrm{s})}$, the first term in the r.h.s. of eq. (3.15) vanishes.

In particular the sum over q in eq. (3.14) can be done in any direction of the quark mass plane, and we choose to mass shift only the strange quark. For practical purposes, since we want to mass shift all relevant observables for each ensemble to satisfy that the sea value of ϕ_4 is equal to its physical value, $\phi_4^{(\mathrm{s})} = \phi_4^{\mathrm{ph}} = \text{const.}$, we rewrite the Taylor expansion as

$$O\left(\phi_4^{(\mathrm{s})'} = \phi_4^{\mathrm{ph}} \right) = O\left(\phi_4^{(\mathrm{s})} \right) + \left(\phi_4^{\mathrm{ph}} - \phi_4^{(\mathrm{s})} \right) \frac{dO}{d\phi_4^{(\mathrm{s})}}, \tag{3.16}$$

with

$$\frac{dO}{d\phi_4^{(s)}} = \frac{dO/dm_s^{(s)}}{d\phi_4^{(s)}/dm_s^{(s)}}. \tag{3.17}$$

Note that by sea value $\phi_4^{(s)}$ we refer to ϕ_4 computed in the Wilson unitary setup, and its derivative has both sea and valence contributions, while $dO/dm_s^{(s)}$ has valence and sea contributions when the observable O is computed in the Wilson unitary setup, and only sea contributions when O is computed in the mixed action regularization. In the Wilson unitary setup, imposing $\phi_4^{(s)} = \phi_4^{ph} = \text{const.}$ means that so does the valence value of ϕ_4, while for the mixed action regularization this is not true. In this case in addition to fixing $\phi_4^{(s)} = \phi_4^{ph} = \text{const.}$ with the mass shifting procedure we need later to impose $\phi_4^{(v)} = \phi_4^{(s)}$, which is done through the matching between sea and valence sectors.

The observables we will be interested for the scale setting (see Sec. 4) are $\sqrt{t_0}f_\pi$, $\sqrt{t_0}f_K$ and $\sqrt{t_0}f_{\pi K}$, the latter defined in eq. (4.1), while for the determination of the physical quark masses (see Sec. 5) we need $\sqrt{t_0}m_{12}^R$, $\sqrt{t_0}m_{13}^R$. All these quantities are physical and so are their derivatives w.r.t. ϕ_4. Thus, one can measure these derivatives for each ensemble and then fit them as a function of ϕ_2 and the lattice spacing. This allows to evaluate the result of these fits at the values of ϕ_2 and t_0/a^2 corresponding to each ensemble and perform the mass shift with that result instead of using the individual measurements of each ensemble. This has the advantage of improving the precision for observables whose mass derivatives are noisy (or even not computed), which is particularly relevant for the finest lattice spacing and the most chiral ensembles under study.

For fitting the derivatives we use

$$F = A + B\phi_2 + D\frac{a^2}{t_0}, \tag{3.18}$$

for all choices of O except for the PCAC quark masses, for which we use

$$F = A + B\phi_2 + C\phi_2^2 + (D + E\phi_2)\frac{a^2}{t_0}, \tag{3.19}$$

for empirical reasons.

In the case of ϕ_2 in the Wilson regularization, we exclude the symmetric point ensembles from the fit of its mass derivative, since $\phi_2^{sym} = \frac{2}{3}\phi_4$ by construction. Thus, for these ensembles we will use this relation directly to mass shift ϕ_2.

Results for the fit parameters are presented in Table 3.1, while plots are shown in Figs. 3.1-3.2.

We have assumed knowledge of the physical value of ϕ_4 to which we mass shift all ensembles. However, in order to determine it we need

the physical value of the intermediate scale t_0, which is the target of the analysis. Thus, we start the process with an educated guess of $t_0^{\rm ph}$, which provides with an initial guess for $\phi_4^{\rm ph}$. Once the scale setting has been done and a new determination of $t_0^{\rm ph}$ is obtained, the analysis is iterated, updating the value of $\phi_4^{\rm ph}$ to which the ensembles are shifted, until convergence is observed in this observable. The initial guess used for $t_0^{\rm ph,\ guess}$ is just a number with no error. After several iterative steps of the analysis, we obtain the new estimate

$$t_0^{\rm ph,\ guess} = 0.1445(6), \tag{3.20}$$

where the uncertainty keeps all the correlations with the lattice data entering the analysis. Eq. (3.20) determines the value of $\phi_4^{\rm ph}$ to which we perform the mass shifts in the subsequent sections, the input values for m_π and m_K given in eq. (4.3).

O	A	B	C	D	E
$\sqrt{t_0} f_{\pi K}^{\rm W}$	0.017(8)	-0.007(10)	-	0.024(26)	-
$\sqrt{t_0} f_{\pi}^{\rm W}$	0.006(8)	0.008(9)	-	0.020(26)	-
$\sqrt{t_0} f_{K}^{\rm W}$	0.024(10)	-0.016(11)	-	0.022(27)	-
$\sqrt{t_0} m_{12}^{\rm W,\ R}$	0.006(4)	-0.033(13)	0.090(12)	0.046(17)	-0.074(27)
$\sqrt{t_0} m_{13}^{\rm W,\ R}$	0.050(6)	0.030(17)	-0.066(18)	-0.069(33)	0.070(45)
$\phi_2^{\rm W}$	0.004(36)	0.131(92)	-	0.874(129)	-
t_0	-0.437(84)	0.214(101)	-	-0.264(274)	-
$\sqrt{t_0} f_{\pi K}^{\rm tm}$	-0.009(7)	0.011(8)	-	-0.014(18)	-
$\sqrt{t_0} f_{\pi}^{\rm tm}$	-0.007(6)	0.013(8)	-	-0.028(18)	-
$\sqrt{t_0} f_{K}^{\rm tm}$	-0.009(8)	0.010(10)	-	-0.006(18)	-
$\sqrt{t_0} m_{12}^{\rm tm,\ R}$	-0.004(3)	0.035(10)	-0.041(9)	0.020(16)	0.026(24)
$\phi_2^{\rm tm}$	0.031(17)	-0.032(23)	-	-0.102(73)	-
$\phi_4^{\rm tm}$	0.006(37)	0.050(47)	-	-0.298(126)	-

Table 3.1: Results for the fit parameters in eqs. (3.18-3.19) for the lattice observables that will be used in the analysis. The superscript "W" refers to the observable being computed in the Wilson unitary setup, while "tm" refers to the mixed action setup.

3.5 MATCHING AND TUNING AT FULL TWIST

As explained in Sec. 3.3, when working with a mixed action, after performing the mass shifts in section. 3.4, we need to match the physical quark masses of the sea and valence sectors. To do this, we use a grid of valence parameter values to find the target point

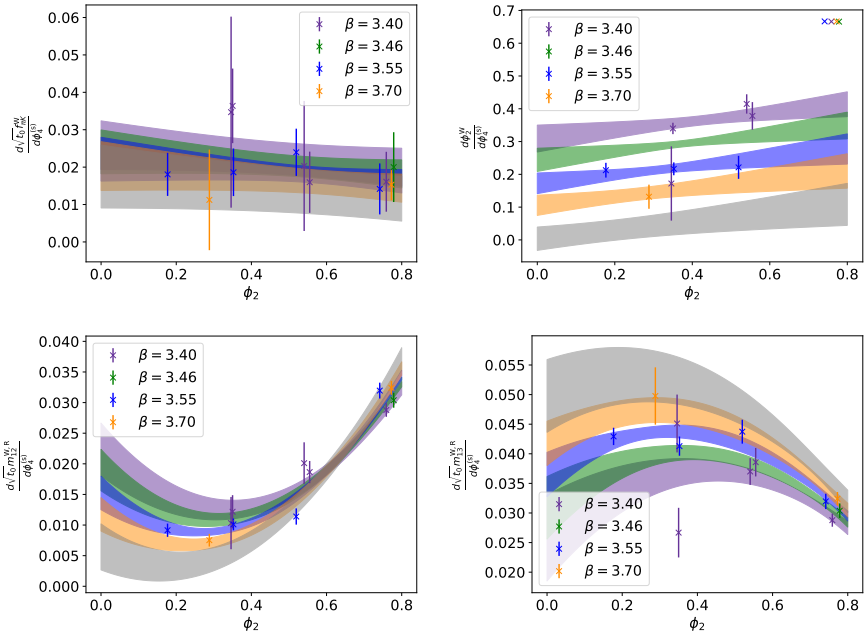

Figure 3.1: Derivatives $dO/d\phi_4^{(s)}$ for the Wilson unitary setup for $O = \sqrt{t_0} f_{\pi K}$, ϕ_2, $\sqrt{t_0} m_{12}^{\mathrm{R}}$, $\sqrt{t_0} m_{13}^{\mathrm{R}}$. For the fit eqs. (3.18-3.19) were used. Results for the fit parameters are presented in Table 3.1.

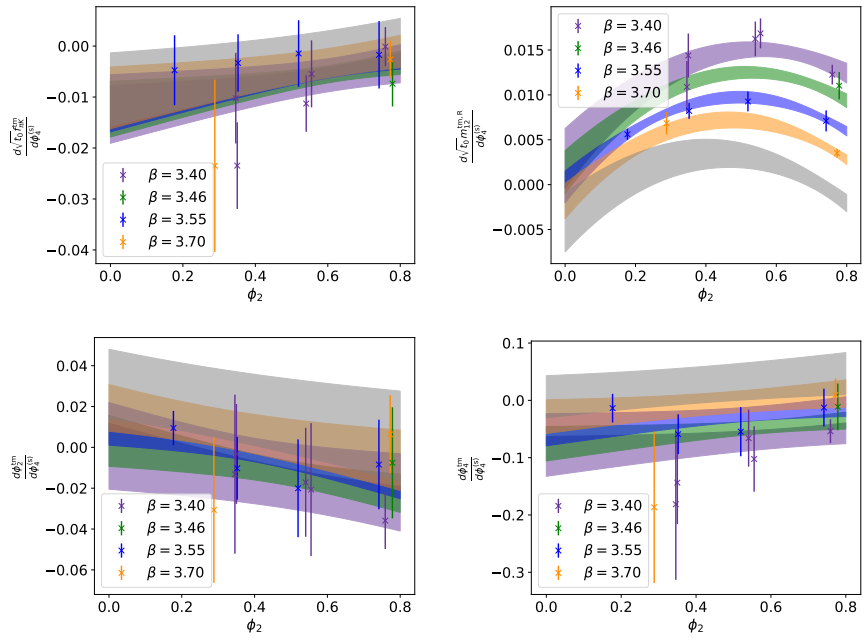

Figure 3.2: Derivatives $dO/d\phi_4^{(s)}$ for the mixed action setup for $O = \sqrt{t_0} f_{\pi K}$, ϕ_2, ϕ_4, $\sqrt{t_0} m_{12}^{\mathrm{R}}$. For the fit eqs. (3.18-3.19) were used. Results for the fit parameters are presented in Table 3.1.

with small interpolations. In order to know the values of the relevant observables in the sea, we need measurements in the fully Wilson unitary setup (with Wilson fermions in both sea and valence). These will be referred to as Wilson or sea data or results, while the mixed action measurements, once the matching is done, will be referred to as Wtm or mixed action data or results.

In practice, to compute the physical quark masses we need the relevant improvement coefficients. In order not to rely on these for the matching procedure, instead of matching the physical quark masses m_l^{R}, m_s^{R}, we choose to use the pion and kaon masses in units of the gradient flow scale t_0

$$\phi_2^{(\mathrm{s})} = \phi_2^{(\mathrm{v})}, \tag{3.21}$$

$$\phi_4^{(\mathrm{s})} = \phi_4^{(\mathrm{v})}. \tag{3.22}$$

since these quantities are proportional to the physical quark masses to LO ChPT.

In addition to this, we need to tune the Wilson tm action to full twist, which means setting the PCAC quark mass to zero

$$m_{ud}^{(\mathrm{v})} = m_{ll'}^{(\mathrm{v})} \equiv m_{12}^{(\mathrm{v})} = 0. \tag{3.23}$$

In principle, we should also send the strange PCAC quark mass to zero. However, since the $\kappa^{(\mathrm{v})}$ parameter we use is flavor degenerate, this condition is automatically satisfied (up to cutoff effects, see Fig. **??**) once eq. (3.23) is imposed.

To impose eqs. (3.21-3.23), we perform interpolations of the valence observables $m_{12}^{(\mathrm{v})}, \phi_2^{(\mathrm{v})}, \phi_4^{(\mathrm{v})}$ in the $(\kappa, \mu_l, \mu_s)^{(\mathrm{v})}$ hyperplane, using as fit functions the following expressions motivated by ChPT

$$m_{12}^{(\mathrm{v})} = p_1 \left(\frac{1}{\kappa^{(\mathrm{v})}} - \frac{1}{\kappa^{(\mathrm{v})*}} \right) + p_2 \left(\mu_l^{(\mathrm{v})} - \mu_l^{(\mathrm{v})*} \right), \tag{3.24}$$

$$\phi_2^{(\mathrm{v})} = \frac{p_3}{\mu_l^{(\mathrm{v})}} \left(\frac{1}{\kappa^{(\mathrm{v})}} - \frac{1}{\kappa^{(\mathrm{v})*}} \right)^2 + p_4 \left(\mu_l^{(\mathrm{v})} - \mu_l^{(\mathrm{v})*} \right) + \phi_2^{(\mathrm{s})}, \tag{3.25}$$

$$\phi_2^{(\mathrm{v})} = \frac{p_5}{\mu_l^{(\mathrm{v})}} \left(\frac{1}{\kappa^{(\mathrm{v})}} - \frac{1}{\kappa^{(\mathrm{v})*}} \right)^2 + \frac{p_6}{\mu_s^{(\mathrm{v})}} \left(\frac{1}{\kappa^{(\mathrm{v})}} - \frac{1}{\kappa^{(\mathrm{v})*}} \right)^2 \tag{3.26}$$

$$+ p_7 \left(\mu_l^{(\mathrm{v})} - \mu_l^{(\mathrm{v})*} \right) + p_8 \left(\mu_s^{(\mathrm{v})} - \mu_s^{(\mathrm{v})*} \right) + \phi_4^{(\mathrm{s})}. \tag{3.27}$$

This way, the target point values $(\kappa, \mu_l, \mu_s)^{(\mathrm{v})*}$ are found as fit parameters. The interpolation is shown in Fig. 3.3. A simultaneous fit of these three quantities is performed.

The mixed action results for the quark masses are given exactly by the target twist mass parameters $\mu_{l,s}^{(\mathrm{v})*}$, while the extraction of the pion and kaon decay constants in the mixed action setup requires a

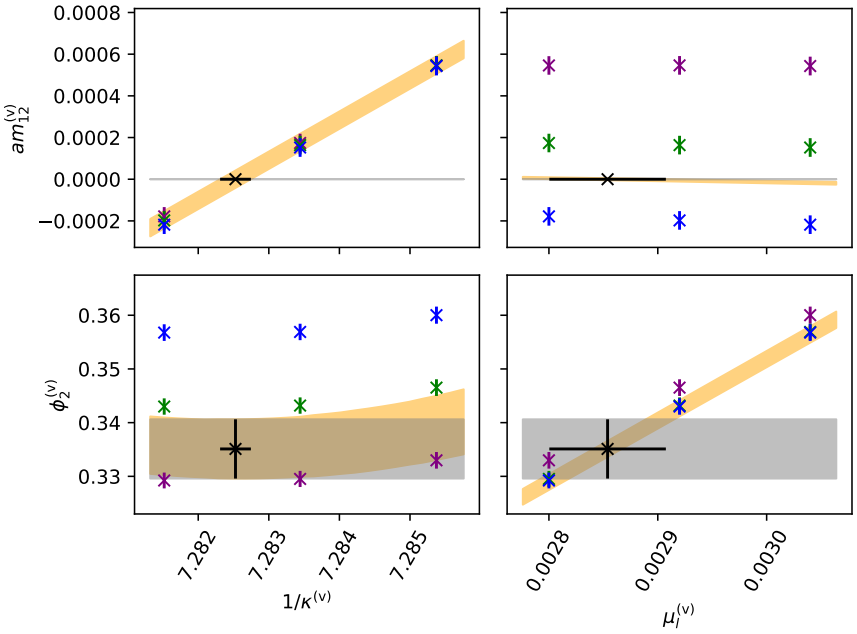

Figure 3.3: Plot of the matching of sea (gray band) and valence values of ϕ_2 and tune to full twist $am_{12}^{(v)} = 0$ along the grid of valence parameters values. Each point represents a different measurement of a lattice observables in the valence along the grid, and the orange band represents the interpolation. The black point is the target result $(\kappa, \mu_l, \mu_s)^{(v)*}$. Here we only show the matching of $\phi_2^{(v)}$ and $am_{12}^{(v)}$, though the matching of $\phi_4^{(v)}$ is done simultaneously. Ensemble is H105.

new interpolation along the valence grid to the target point. The fit functions for this interpolation are

$$f_\pi^{(v)} = q_1 \left(\frac{1}{\kappa^{(v)}} - \frac{1}{\kappa^{(v)*}} \right)^2 + q_2 \left(\frac{1}{\kappa^{(v)}} - \frac{1}{\kappa^{(v)*}} \right) + q_3 \mu_l^{(v)}, \tag{3.28}$$

$$f_K^{(v)} = r_1 \left(\frac{1}{\kappa^{(v)}} - \frac{1}{\kappa^{(v)*}} \right)^2 + r_2 \left(\frac{1}{\kappa^{(v)}} - \frac{1}{\kappa^{(v)*}} \right) + r_3 \mu_l^{(v)} + r_4 \mu_s^{(v)}. \tag{3.29}$$

The interpolation for the decay constants combination $f_{\pi K}$ defined in eq. (4.1) is shown in Fig. 3.4.

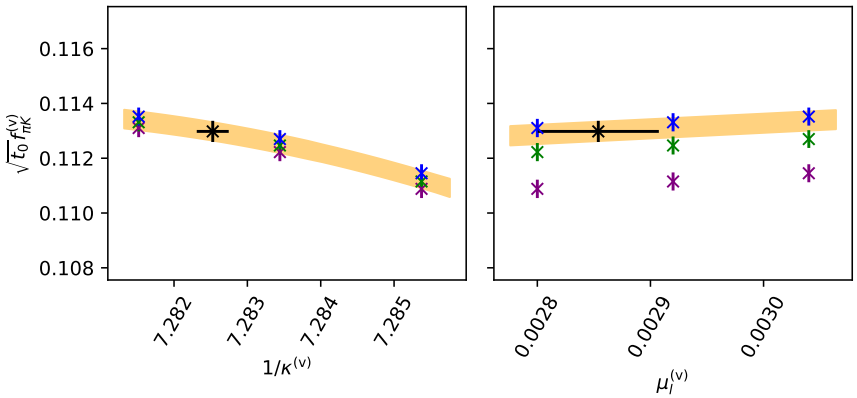

Figure 3.4: Interpolation of $\sqrt{t_0} f_{\pi K}$ (see eq. (4.1)) along the valence grid to the target point $(\kappa, \mu_l, \mu_s)^{(v)*}$. The points with different colors represent measurements at different values of the valence parameters. Ensemble is H105.

4

SCALE SETTING

4.1 MOTIVATION

The scale setting involves the precise determination of one reference observable, the scale, in physical units, to which any other observable is compared in order to extract the value of the latter in physical units.

We decide to use the gradient flow scale t_0 introduced in Sec. 2.6 as an intermediate reference scale since it can be computed in the lattice with high precision. Following the discussion in Sec. 1.7, we choose for the phenomenological input the decay constants of the pion and kaon

$$\Lambda \equiv f_{\pi K} = \frac{2}{3}\left(f_K + \frac{1}{2}f_\pi\right). \tag{4.1}$$

After measuring $\sqrt{t_0}f_{\pi K}$ for each ensemble, one must perform a chiral-continuum limit in order to extract its value at the physical point and in the continuum. To define the physical point we use the pion and kaon masses, or equivalently the dimensionless quantities ϕ_2 and ϕ_4. For the determination of the physical value of these quantities we need again the physical value of t_0, which is the target of the analysis. As in Sec. 3, we start with an initial guess in eq. (3.20) and iterate the analysis until convergence is observed. Thus, with each iterative step both the values of ϕ_2 to which we perform the chiral extrapolation and the value of ϕ_4 to which we shifted our observables are updated.

Since all lattice observables and the action that we use are $\mathcal{O}(a)$ improved, we expect lattice artifacts to start at $\mathcal{O}(a^2)$. In order to perform the chiral-continuum limit, we explore different ways of parameterizing the dependence on ϕ_2, ϕ_4 and on the lattice spacing a, and employ the same techniques of model averaging discussed in Sec. 2.7.

After performing the chiral-continuum limit, using as external physical input the values of the pion and kaon decay constants we can determine the value of the scale t_0 as

$$\sqrt{t_0^{\text{ph}}} = \frac{\left(\sqrt{t_0}f_{\pi K}\right)^{\text{latt}}\Big|_{a=0}}{f_{\pi K}^{\text{exp}}}. \tag{4.2}$$

In particular, we are studying ensembles which employ $N_f = 2+1$ fermions, and thus assume isospin symmetry for the light flavor. This means that the physical input for the masses and decay constants we need is not that of Nature, but that of isosymmetric QCD (isoQCD).

These values are given by the Flavor Lattice Average Group (FLAG) in [**FLAG21**]

$$m_\pi^{\text{isoQCD}} = 134.9768(5)\ \text{MeV}, \quad m_K^{\text{isoQCD}} = 497.611(13)\ \text{MeV}, \tag{4.3}$$

$$f_\pi^{\text{isoQCD}} = 130.56(2)_{\text{exp}}(13)_{\text{QED}}(2)_{|V_{ud}|}\ \text{MeV}, \tag{4.4}$$

$$f_K^{\text{isoQCD}} = 157.2(2)_{\text{exp}}(2)_{\text{QED}}(4)_{|V_{us}|}\ \text{MeV}. \tag{4.5}$$

As we see, the kaon decay constant receives a large contribution to its uncertainty from the determination of the $|V_{us}|$ CKM matrix element. Also, QED corrections are stronger in the kaon than in the pion. All these subtleties motivate a scale setting that uses only the pion decay constant as physical input. For this reason we also study this possibility when doing the model variation for the chiral-continuum extrapolation.

4.2 RESULTS: THE PHYSICAL POINT

The choice of the decay constants to set the scale, and in particular of the combination in eq. (4.1) is due to its chiral behavior, since at fixed value of ϕ_4 (as in our case thanks to the mass shifting procedure, see Sec. 3.4) to NLO SU(3) ChPT it only depends on ϕ_2 through chiral logarithms,

$$F^{\text{cont}}_{\chi,\pi K}(\phi_2) \equiv \left(\sqrt{8t_0} f_{\pi K}\right)^{\text{cont}} = \tag{4.6}$$

$$= \frac{A}{4\pi}\left[1 + \frac{7}{6}L\left(\frac{\phi_2}{A^2}\right) - \frac{4}{3}L\left(\frac{\phi_4 - \frac{1}{2}\phi_2}{A^2}\right) - \frac{1}{2}L\left(\frac{\frac{4}{3}\phi_4 - \phi_2}{A^2}\right) + B\phi_4\right], \tag{4.7}$$

with the chiral logarithms given by

$$L(x) = x\log(x), \tag{4.8}$$

and A, B related to chiral low energy constants (LEC). We use this expression to perform the chiral-continuum extrapolation of $\sqrt{t_0} f_{\pi K}$. We will use the label $[SU(3)\chi PT]$ for this continuum dependence.

Another possibility for the physical point extrapolation is to use Taylor expansions in ϕ_2 around the symmetric point. We can either go to second or fourth order in the Taylor expansion

$$F^{\text{cont}}_{\text{Tay},\pi K}(\phi_2) \equiv \sqrt{8t_0} f^{\text{cont}}_{\pi K} = A + B\left(\phi_2 - \phi_2^{\text{sym}}\right)^2, \tag{4.9}$$

or

$$F^{\text{cont}}_{\text{Tay},\pi K}(\phi_2) = A + B\left(\phi_2 - \phi_2^{\text{sym}}\right)^2 + C\left(\phi_2 - \phi_2^{\text{sym}}\right)^4, \tag{4.10}$$

labeling these models as $[Tay]$ and $[Tay4]$. Due to symmetry reasons, there are no terms with odd powers of ϕ_2 [].

Since the kaon decay constant is expected to receive more severe QED corrections than the pion, and the determination of its physical value for isosymmetric-QCD is affected by the uncertainty of the element of the CKM matrix $|V_{us}|$, we can also use the quantity $\sqrt{t_0} f_\pi$ to set the scale, and SU(2) ChPT to perform the physical point extrapolation. According to the latter,

$$F^{\text{cont}}_{\chi,\pi}(\phi_2) \equiv \sqrt{8t_0} f^{\text{cont}}_\pi = A\phi_2 + B\left(1 - 2L\left(\frac{\phi_2}{B^2}\right)\right), \tag{4.11}$$

$$F^{\text{cont}}_{\chi,K}(\phi_2) \equiv \sqrt{8t_0} f^{\text{cont}}_K = C\phi_2 + D\left(1 - \frac{3}{4}L\left(\frac{\phi_2}{B^2}\right)\right), \tag{4.12}$$

in which case we fit both f_π and f_K since they share a fit parameter, in order to help control the extrapolation in f_π. In the end, however, we set the scale only with external input for f_π.

In addition to the extrapolation in the pion mass, we need to supplement these fit functions with cutoff effects in order to describe our lattice data. For this we will explore two possibilities

$$F^{\text{latt}}(\phi_2) = F^{\text{cont}}(\phi_2) + W\frac{a^2}{8t_0}, \tag{4.13}$$

$$F^{\text{latt}}(\phi_2) = F^{\text{cont}}(\phi_2) + W\frac{a^2}{8t_0}\alpha_S^{\Gamma_1}, \tag{4.14}$$

$$F^{\text{latt}}(\phi_2) = F^{\text{cont}}(\phi_2) + (W + Z\phi_2)\frac{a^2}{8t_0}. \tag{4.15}$$

We assign the labels $[a^2]$, $[a^2\alpha_S^\Gamma]$ and $[a^2 + a^2\phi_2]$ to characterize the lattice artifacts of these models.

In order to assess the systematic uncertainty in the extraction of $\sqrt{t_0}$, we will explore all these continuum-chiral extrapolations and their different results. In the same direction we also explore the impact of performing data cuts from the fits. In particular, we consider the following cuts (in addition to the "no cut" choice)

$$\beta > 3.40, \quad \beta > 3.46, \quad \phi_2 < 0.6, \tag{4.16}$$

$$\phi_2 < 0.4, \quad \beta > 3.40 \;\&\; \phi_2 < 0.6, \tag{4.17}$$

$$m_\pi L > 4.1. \tag{4.18}$$

Finally, to perform all of these fits, we have two data sets: the Wilson unitary setup and the mixed action. Both must share the same continuum limit, but different cutoff effects. We can thus perform the continuum-chiral extrapolations for the Wilson data, for the mixed action, or for a combined data set, parameterizing the data with the same continuum limit behavior $F^{\text{cont}}(\phi_2)$ but different cutoff effects (different W, Z fit parameters for Wilson and mixed action data). This third choice allows to further constrain the continuum extrapolation and keep it well under control, while increasing the statistics and getting better precision for $\sqrt{t_0}$. As a universality check, we perform

the continuum limit of only symmetric point ensembles of both the Wilson and mixed action data, without imposing a common value in the continuum. Since all these points have the same ϕ_2 they follow a line of constant physics as we approach the continuum. This extrapolation is shown in Fig. 4.1 and indeed it shows that both data sets agree perfectly well in the continuum, with the mixed action data having much milder cutoff effects.

Once the various models to extrapolate to the continuum and physical point have been explored, we use the model averaging technique in Sec. 2.7 to assign a weight to each model

$$W \propto \exp\left(-\frac{1}{2}\left(\chi^2 - 2\left\langle\chi^2\right\rangle\right)\right), \tag{4.19}$$

that allows us to compute a weighted average for $\sqrt{t_0}$, as well as the associated systematic uncertainty

$$\left\langle\sqrt{t_0}\right\rangle = \sum_i \sqrt{t_0^{(i)}} W^{(i)}, \tag{4.20}$$

$$\sigma^2_{\text{syst}} = \left\langle\sqrt{t_0}^2\right\rangle - \left\langle\sqrt{t_0}\right\rangle^2. \tag{4.21}$$

In Figs. 4.3-4.5 we show the model average results for the Wilson unitary setup, for the mixed action and for the combined analysis. In Appendix H we show the numerical results of $\sqrt{t_0}$ for each model considered, together with their weights and p-values, for the Wilson, mixed action and combined analysis. In Fig. 4.2 we show the pion mass dependence of the continuum-chiral extrapolation for one of the best models explored in terms of the TIC for the combined data sets, together with the lattice spacing dependence for the same model, projecting all points to the physical pion mass ϕ_2^{ph} using the fit result for the continuum piece $F^{\text{cont}}(\phi_2)$.

The final results for $\sqrt{t_0}$ in physical units as computed from the model average for the different data sets are

$$\sqrt{t_0} = 0.1439(7)_{\text{stat}}(3)_{\text{syst}} \text{ fm, Wilson,} \tag{4.22}$$

$$\sqrt{t_0} = 0.1433(8)_{\text{stat}}(8)_{\text{syst}} \text{ fm, Mixed action,} \tag{4.23}$$

$$\sqrt{t_0} = 0.1437(6)_{\text{stat}}(3)_{\text{syst}} \text{ fm, Combined.} \tag{4.24}$$

4.3 RESULTS: THE SYMMETRIC POINT

The symmetric point is defined as the point in the quark mass plane such that

$$m_{ud} \equiv m_l = m_s. \tag{4.25}$$

In terms of our usual quantities ϕ_2, ϕ_4 this means

$$\phi_2 = \frac{2}{3}\phi_4, \tag{4.26}$$

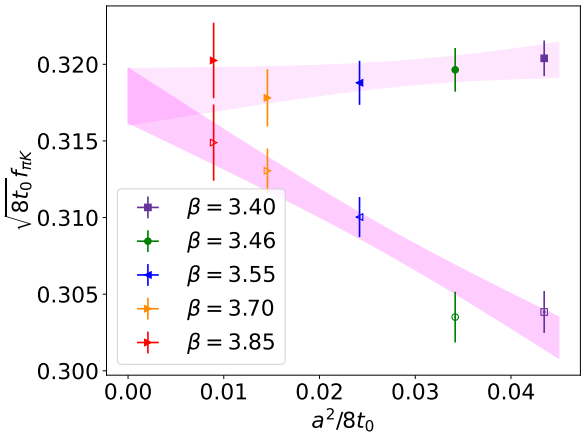

Figure 4.1: Continuum limit of symmetric point ensembles for the Wilson unitary results or sea data set (empty points) and for the mixed action results (filled points). A common continuum limit is not imposed. Cutoff effects are parameterized as pure $\mathcal{O}(a^2)$ artifacts.

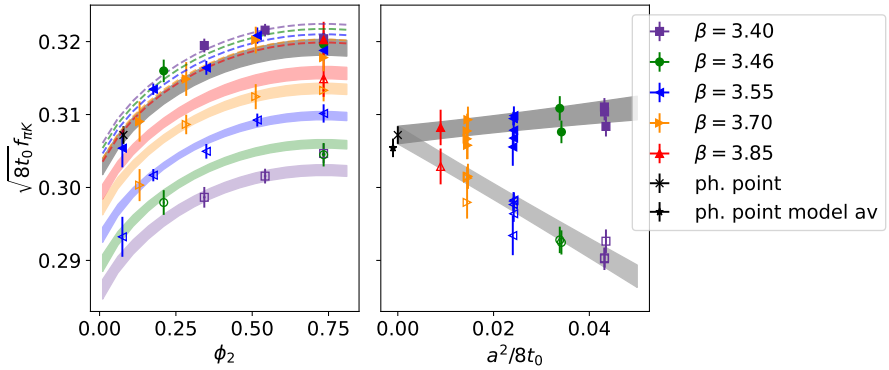

Figure 4.2: *Left*: Pion mass dependence of $\sqrt{8t_0}f_{\pi K}$ for the SU(3) ChPT model with pure $\mathcal{O}(a^2)$ cutoff effects: $[SU(3)\chi PT][a^2][-]$. We show the result of the combined fit of both Wilson (empty) and mixed action (filled) results. The colored bands represent the pion mass dependence for each lattice spacing for the Wilson results, while the dashed lines represent the dependence for the mixed action results. In the latter case we only plot the central value of the corresponding bands for visualization purposes. *Right*: the same model, with point projected to the physical pion mass ϕ_2^{ph} using the fit result for the continuum mass dependence $F(\phi_2)^{\text{cont}}$. In this plot we show the lattice spacing dependence of our ensembles. We show two physical point results: the rightmost in the plot corresponds to the result coming from the fit model itself, while the leftmost is the result obtained from the model average.

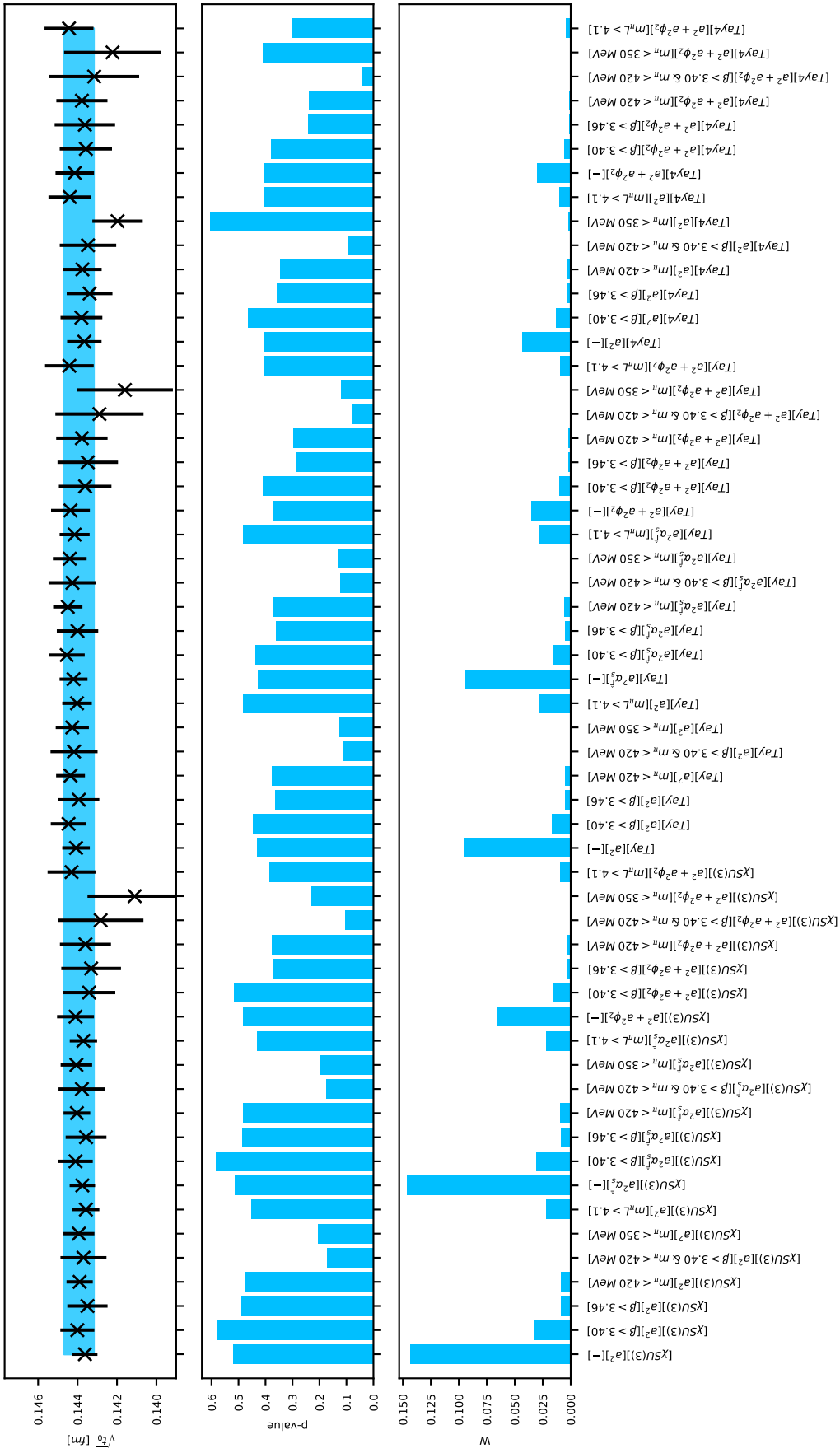

Figure 4.3: Model average results for the determination of $\sqrt{t_0}$ at the physical point using the Wilson results. In the top figure we show the results coming from each fit model together with the final averaged result with the systematic uncertainty coming from the model variation added (blue band). In the middle plot we show the quality of fits as measured by the p-value **[chi_exp]**. In the bottom figure we show the assigned weight to each model according to eq. (4.19). We provide a Table connecting each label to the

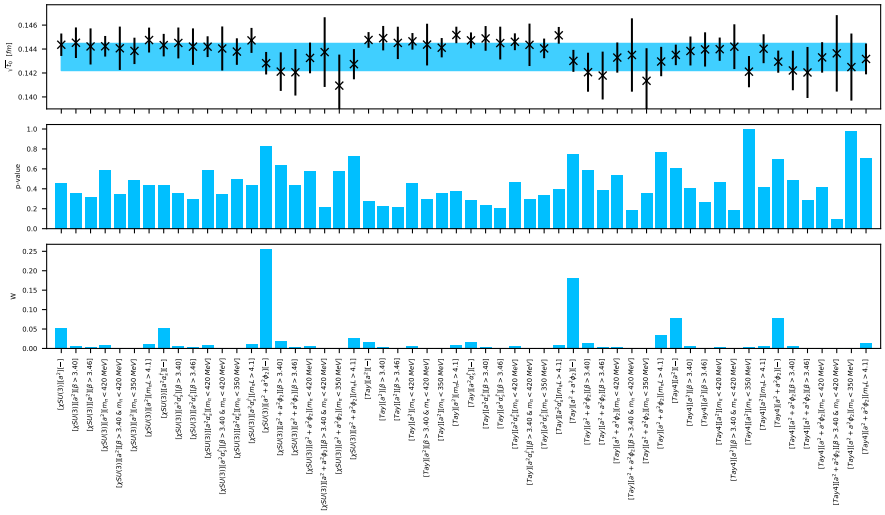

Figure 4.4: Model average results for the determination of $\sqrt{t_0}$ at the physical point using the mixed action results. In the top figure we show the results coming from each fit model together with the final averaged result with the systematic uncertainty coming from the model variation added (blue band). In the middle plot we show the quality of fits as measured by the p-value [**chi_exp**]. In the bottom figure we show the assigned weight to each model according to eq. (4.19). We provide a Table connecting each label to the corresponding fit models in Appendix H.

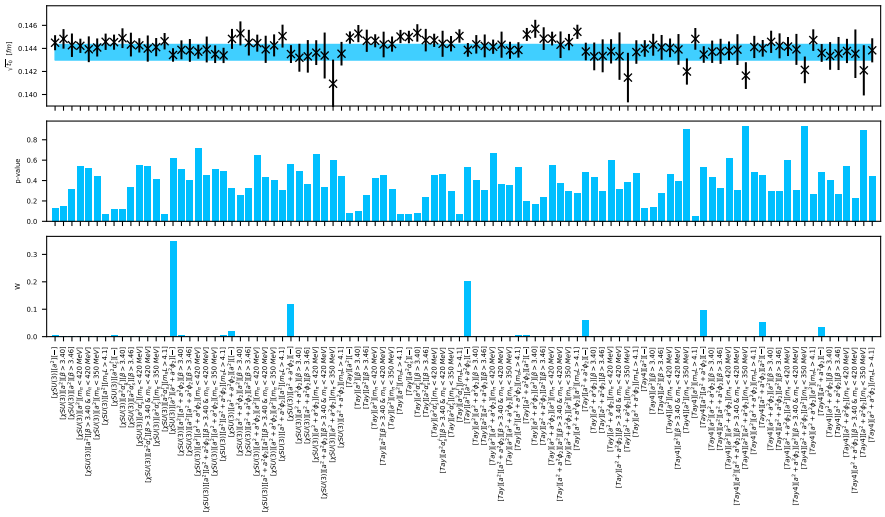

Figure 4.5: Model average results for the determination of $\sqrt{t_0}$ at the physical point using the combined analysis of both Wilson and mixed action results. In the top figure we show the results coming from each fit model together with the final averaged result with the systematic uncertainty coming from the model variation added (blue band). In the middle plot we show the quality of fits as measured by the p-value [**chi_exp**]. In the bottom figure we show the assigned weight to each model according to eq. (4.19). We provide a Table connecting each label to the corresponding fit models in Appendix H.

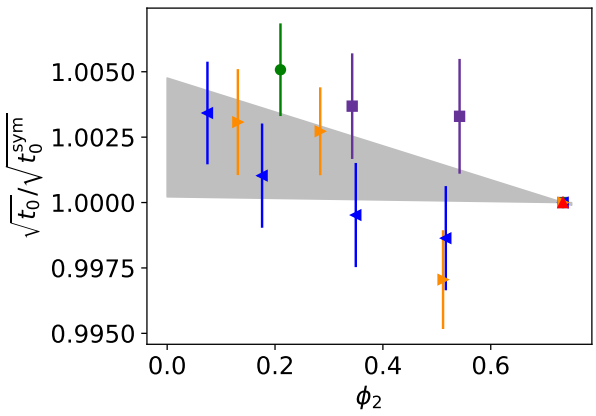

Figure 4.6: Fit to eq. (4.28) in order to extract t_0 at the symmetric point. The color and symbol code is the same as in Fig. 4.2.

where ϕ_4 again is given by its physical value after the iterative procedure to find $t_0^{\rm ph}$ and after mass shifting (see Sec. 3.4). In order to extract $t_0(\phi_2^{\rm sym}, \phi_4^{\rm ph})$, following [**âĂć**] we build the ratio

$$\frac{\sqrt{t_0/a^2}}{\sqrt{t_0^{\rm sym}/a^2}}, \tag{4.27}$$

where $\sqrt{t_0/a^2}$ is the measurement of the gradient flow scale in each ensemble and $\sqrt{t_0^{\rm sym}/a^2}$ is said quantity for the symmetric point at the corresponding value of the inverse coupling β. We now fit this ratio to

$$F(\phi_2) = \sqrt{1 + p(\phi_2 - \phi_2^{\rm sym})}. \tag{4.28}$$

Once the data is fitted, we extract $t_0^{\rm sym}$ in physical units as

$$\sqrt{t_0^{\rm sym}} = \frac{\sqrt{t_0^{\rm ph}}}{F(\phi_2^{\rm ph})}. \tag{4.29}$$

For $t_0^{\rm ph}$ and $\phi_2^{\rm ph}$ we can use our determination for the Wilson, mixed action or combined data sets. The result of this fit is shown in Fig. 4.6. Our result for the scale at the symmetric point is

$$\sqrt{t_0^{\rm sym}} = 0.1436()_{\rm stat}()_{\rm syst}\ \text{fm, Wilson,} \tag{4.30}$$

$$\sqrt{t_0^{\rm sym}} = 0.1430()_{\rm stat}()_{\rm syst}\ \text{fm, Mixed action,} \tag{4.31}$$

$$\sqrt{t_0^{\rm sym}} = 0.1433()_{\rm stat}()_{\rm syst}\ \text{fm, Combined.} \tag{4.32}$$

4.4 RESULTS: LATTICE SPACING

Just as in the previous section, we can use the fit to $\frac{\sqrt{t_0/a^2}}{\sqrt{t_0^{\text{sym}}/a^2}}$ to compute

$$\left(\sqrt{\frac{t_0}{a^2}}\right)^{\text{ph}} = \sqrt{\frac{t_0^{\text{sym}}}{a^2}} F(\phi_2^{\text{ph}}). \tag{4.33}$$

Then, the lattice spacing is extracted as

$$a = \frac{\sqrt{t_0^{\text{ph}}}}{\left(\sqrt{\frac{t_0}{a^2}}\right)^{\text{ph}}}. \tag{4.34}$$

Again, for ϕ_2^{ph} we can use either our determination of t_0^{ph} for the Wilson, mixed action or combined data sets. These results are shown in Table 4.1.

β	a [fm] Wilson	a [fm] mixed action	a [fm] combined
3.40	$0.0847()_{\text{stat}}()_{\text{syst}}$	$0.0843()_{\text{stat}}()_{\text{syst}}$	$0.0847()_{\text{stat}}()_{\text{syst}}$
3.46	$0.0751()_{\text{stat}}()_{\text{syst}}$	$0.0748()_{\text{stat}}()_{\text{syst}}$	$0.0751()_{\text{stat}}()_{\text{syst}}$
3.55	$0.0632()_{\text{stat}}()_{\text{syst}}$	$0.0629()_{\text{stat}}()_{\text{syst}}$	$0.0632()_{\text{stat}}()_{\text{syst}}$
3.70	$0.0490()_{\text{stat}}()_{\text{syst}}$	$0.0488()_{\text{stat}}()_{\text{syst}}$	$0.0490()_{\text{stat}}()_{\text{syst}}$
3.85	$0.0384()_{\text{stat}}()_{\text{syst}}$	$0.0382()_{\text{stat}}()_{\text{syst}}$	$0.0384()_{\text{stat}}()_{\text{syst}}$

Table 4.1: Values of the lattice spacing a in physical units extracted from the deterimation of the gradient flow scale t_0 with the Wilson, mixed action and combined analysis. The lattice spacing is extracted from measures of both t_0 at the physical and symmetric points using eq. (4.34).

4.5 RESULTS: t_0^*

Following [**âĂć**], we define the gradient flow scale t_0 at the point

$$\phi_4 = 1.11, \quad \phi_2 = \frac{2}{3}\phi_4 \equiv \phi_2^{\text{sym}}. \tag{4.35}$$

This defines t_0^*

$$t_0^* = t_0 \left(\phi_2^{\text{sym}},\ \phi_4 = 1.11\right). \tag{4.36}$$

This quantity is of importance for... [**âĂć**] To compute it, we need to repeat the analysis above, this time mass shifting our ensembles to the value $\phi_4 = 1.11$ without errors and compute the gradient flow scale at the symmetric point as explained in the sections above.

The values we find for $\sqrt{t_0^*}$ in physical units for the Wilson, mixed action and combined cases are

$$\sqrt{t_0^*} = 0.1439()_{\text{stat}}()_{\text{syst}} \text{ fm, Wilson,} \tag{4.37}$$

$$\sqrt{t_0^*} = 0.1440()_{\text{stat}}()_{\text{syst}} \text{ fm, Mixed action,} \tag{4.38}$$

$$\sqrt{t_0^*} = 0.1438()_{\text{stat}}()_{\text{syst}} \text{ fm, Combined.} \tag{4.39}$$

5 LIGHT QUARK MASSES

5.1 MOTIVATION

Blabla

5.2 RESULTS

Part IV

CONCLUSIONS

CONCLUSIONS AND OUTLOOK

Blabla, semileptonics

CONCLUSIONES Y PERSPECTIVAS

Blabla, semileptónicas

Part V

APPENDIX

A

CONVENTIONS

In this appendix we set some useful notation used throughout this work. We begin with the Dirac or Gamma matrices γ_μ, which are 4×4 complex matrices defined by the anticommutator relation

$$\{\gamma_\mu, \gamma_\nu\} = 2g_{\mu\nu}1_{4\times4}, \tag{A.1}$$

with $g_{\mu\nu}$ the metric tensor of 4-dimensional space-time. We will work in the Euclidean and flat space, so

$$g_{\mu\nu} = \text{diag}(+1, +1, +1, +1). \tag{A.2}$$

Some useful properties of the Gamma matrices are

- Hermiticity: $\gamma_\mu^\dagger = \gamma_\mu$.
- They are traceless: $\text{tr}(\gamma_\mu) = 0$.
- Involutory: $\gamma_\mu^{-1} = \gamma_\mu$.

A fifth Gamma matrix can be defined as

$$\gamma_5 = \gamma_0\gamma_1\gamma_2\gamma_3, \tag{A.3}$$

which fullfils the same properties as above, and anticommutes with all other Gamma matrices

$$\{\gamma_5, \gamma_\mu\} = 0. \tag{A.4}$$

These matrices control the flavor content of hadrons, and as such appear in the definition of the lattice hadron interpolators. The relevant quark bilinears needed for this work are

- Scalar density: $S^{ij} = \bar{\psi}^i\psi^j$.
- Pseudoscalar density: $P^{ij} = \bar{\psi}^i\gamma_5\psi^j$.
- Axial current: $A_\mu^{ij} = \bar{\psi}^i\gamma_\mu\gamma_5\psi^j$.
- Vector current: $V_\mu^{ij} = \bar{\psi}^i\gamma_\mu\psi^j$.

These bilinears are defined in the physical basis $\{\psi, \bar{\psi}\}$. By the change of variables

$$\psi \to e^{i\frac{\pi}{2}\gamma_5 T/2}\psi, \quad \bar{\psi} \to \bar{\psi}e^{i\frac{\pi}{2}\gamma_5 T/2}, \tag{A.5}$$

we define the twisted basis, with T a diagonal matrix in flavor space. With this change of variables and at full twist with $N_f = 2 + 1 + 1$

$$T = \text{diag}(+1, -1, -1, +1), \tag{A.6}$$

the bilinears are rotated as

$$S^{ij} \to S^{ij}, \tag{A.7}$$
$$P^{ij} \to P^{ij}, \tag{A.8}$$
$$A^{ij}_{\mu} \to iV^{ij}_{\mu}, \tag{A.9}$$
$$V^{ij}_{\mu} \to -iA^{ij}_{\mu}, \tag{A.10}$$

for $(i,j) = (u,d),(u,s),(c,d),(c,s)$, and

$$S^{ij} \to -iP^{ij}, \tag{A.11}$$
$$P^{ij} \to iS^{ij}, \tag{A.12}$$
$$A^{ij}_{\mu} \to A^{ij}_{\mu}, \tag{A.13}$$
$$V^{ij}_{\mu} \to V^{ij}_{\mu}, \tag{A.14}$$

for $(i,j) = (u,u),(u,c),(d,d),(d,s),(s,s),(c,c)$.

B

SIMULATION DETAILS

In this Appendix we discuss the details of the generation of gauge field configurations with dynamical quarks for the study of Lattice QCD.

All ensembles studied in this thesis were generated using the openQCD software, and hence the details we review here are those of the alorithms implemented for this software [**âĂć**].

Tipically simulations of lattice QCD with dynamical quarks require a large amount of computer resources due to the large number of degrees of freedom, the need for big volumes and small lattice spacings. The constant efforts by the community paved the way for simulations with up to four dynamical quarks.

As outlined in Sec. 1, the expectation value of a composite operator O can be computed in the lattice as

$$\langle O \rangle = \frac{1}{\mathcal{Z}} \int \mathcal{D}[U] e^{-S_G[U]-S_{\text{eff}}[U]} O[U] \approx \frac{1}{N_{\text{cnfg}}} \sum_{i=1}^{N_{\text{cnfg}}} O[U_i] + \mathcal{O}\left(\frac{1}{\sqrt{N_{\text{cnfg}}}}\right), \tag{B.1}$$

where the gauge fields U_i are sampled from the probability density

$$dP[U] = \frac{e^{-S_G[U]-S_{\text{eff}}[U]}}{\int \mathcal{D}[U] e^{-S_G[U]-S_{\text{eff}}[U]}}. \tag{B.2}$$

The central idea is to perform an importance sampling of the distribution eq. (B.2), such that regions of field space with high probability are highly populated with gauge configurations U_i. To achieve this, typically gauge configurations are generated following a Markov chain. This is defined as a sequence $\{U_k\}_{k=1}^{N_{\text{cnfg}}}$ such that the k-th element is generated from the previous one, with k labelling the Monte Carlo (MC) time. This way, the Markov Chain is generated from the initial state U_1 and the transition probability $T(U_{k-1} \to U_k)$. This way, gauge configurations in one same Markov Chain are highly correlated, issue which we deal with in Appendix D. The transition probabilities must obey the following conditions:

- Ergodicity: given a subset of states S from the Markov Chain, there are always at least two states $s \in S$ and $s' \notin S$ with $T(s \to s') > 0$. This is of particular importance in the context of Lattice QCD and Lattice Yang-Mills theories in order to ensure that the simulation algorithm is sampling correctly all topological sectors of the theory, which may not always be the case for different algorithms.

- Equilibrium: normalizing the transition probability as

$$\sum_s T(s \to s') = 1 \ \forall s, \tag{B.3}$$

then it must hold that

$$\sum_s P(s)T(s \to s') = P(s') \ \forall s', \tag{B.4}$$

where $P(s)$ is the equilibrium distribution in eq. (B.2). This ensures that starting from a random configuration, after applying iteratively the transition probability, we asymptotically reach the target equilibrium distribution eq. (B.2).

Different choices for the transition probability $T(s \to s')$ satisfying the above conditions define the different sampling algorithms which we go on to review.

B.1 METROPOLIS ALGORITHM

The Metropolis algorithm **[âĂć]** is one of the most popular choices for generating a Markov Chain of gauge field configurations for pure gauge theories, for which the target distribution is

$$dP[U] = \frac{e^{-S_G[U]}}{\int \mathcal{D}[U] e^{-S_G[U]}}. \tag{B.5}$$

The idea is to define an a priori selection probability $T_0(U_i \to U_j)$ to update a single gauge link. One such choice is to take a random element g of the SU(N) group close to the identity and update the gauge link $U_\mu(n)$ as $U_\mu(n)' = gU_\mu(n)$ such that the new gauge configuration U_j is close to the original one U_i. In order for the transition to be symmetric, group elements g and g^{-1} have to be selected with equal probability. After updating with this a priori transition probability, one supplements the updating process with an accept-reject step, such that the new proposed gauge link is accepted with probability

$$P_{\text{acc}}(i,j) = \min\left(1, e^{-\Delta S}\right), \quad \Delta S = S[U_j] - S[U_i]. \tag{B.6}$$

Then the total transition probability is given by

$$T(U_i \to U_j) = T_0(U_i \to U_j) P_{\text{acc}}(i,j) + \delta_{ij} \sum_k T_0(U_i \to U_j)(1 - P_{\text{acc}}(i,j)). \tag{B.7}$$

This T satisfies all the desired properties for a transition probability and asymptotically reaches the target distribution probability for pure gauge theories.

The drawback of this algorithm is that it only updates a single gauge link at each step and as such is highly inefficient, particularly for large volume simulations. Over the years new alternatives for pure gauge simulations have been proposed, such as the heat bath **[âĂć]** and overrelaxation **[âĂć]** algorithms.

B.2 HYBRID MONTE CARLO

Having as target distribution that of pure gauge theory is equivalent as treating quarks in the sea as static sources (infinitely heavy). In order to simulate full QCD, one needs to have dynamical quarks in the sea, meaning having target distribution eq. (B.2), where S_{eff} introduces non-local dependencies in the gauge links due to the quark determinant. Therefore algorithms like Metropolis, which updates the gauge configurations link by link experiences a significant computational cost that increases with the lattice volume squared, which makes the algorithm unpractical for dynamical simulations purposes. The Hybrid Monte Carlo (HMC) algorithm [**âĂć**] significantly improves efficiency by doing global updates of the gauge configurations.

The HMC uses the classical equations of motion to propose new gauge configurations. To this purpose, the field space is extended with the introduction of su(3)-valued conjugate momenta $\pi_\mu(x)$ of the link variables $U_\mu(x)$. The Hamiltonian of the system is

$$H[\pi, U] = \frac{1}{2}\sum_{x,\mu} \pi^a_\mu(x)\pi^a_\mu(x) + S_{\text{G}}[U] + S_{\text{eff}}[U]. \tag{B.8}$$

This way expectation values can be computed as

$$\langle O \rangle = \frac{\int \mathcal{D}[\pi, U] e^{-H[\pi,U]} O[U]}{\int \mathcal{D}[\pi, U] e^{-H[\pi,U]}}. \tag{B.9}$$

Now the classical equations of motion read

$$\dot{\pi}_\mu(x) = -F_\mu(x), \quad F_\mu(x) = \frac{\partial S[e^\omega U]}{\partial \omega}|_{\omega=0}, \quad \omega \in su(N), \tag{B.10}$$

$$\dot{U}_\mu(x) = \pi_\mu(x) U_\mu(x), \tag{B.11}$$

where the dot notation "$\dot{a}$" means derivation w.r.t. MC time. This way, starting from an initial configuration at zero MC time, integrating the equations of motion provides with a global new gauge configuration to be used as proposal for the update of the gauge links. This new global proposal is subject to an accept-reject step like the one in the Metropolis algorithm with

$$P_{\text{acc}} = \min\left(1, e^{-\Delta H}\right), \quad \Delta H = H[\pi', U'] - H[\pi, U]. \tag{B.12}$$

We have presented the basic formulation of the HMC algorithm but further refinements and improvements, specially in terms of the integration of the classical equations of motion have taken place over the years [**âĂć**].

This far we have not given details on how to compute the effective fermion action

$$S_{\text{eff}}[U] = -\sum_{i=1}^{N_f} \log \det(D_i). \tag{B.13}$$

This is a typically challenging task, since it involves dealing with Grassmann variables. A usual solution is to use pseudofermion fields $\Phi(x)$ **[âĂć]**, which are auxiliary fields that carry color and spinor indices c, α but that are complex instead of Grassmann numbers. Restricting to the mass-degenerate doublet of light quarks, where the effective action becomes

$$e^{-S_{\text{eff}}} = \det(D_l)\det(D_l) = \det(D_l^\dagger D_l), \tag{B.14}$$

in the pseudo-fermion representation this becomes

$$\det(D_l^\dagger D_l) = \frac{1}{\mathcal{Z}_\Phi} \int \mathcal{D}[\Phi] e^{-S_{\text{pf}}[U,\Phi]}, \tag{B.15}$$

with $\mathcal{Z}_\Phi$ the pseudo-fermion partition function, and the pseudo-fermion action given by

$$S_{\text{pf}}[U,\Phi] = \Phi^\dagger \left(D_l^\dagger D_l\right)^{-1} \Phi \tag{B.16}$$

Finally the integration measure for these auxiliary fields reads

$$\mathcal{D}[\Phi] = \Pi_{x,\alpha,c} d\Phi_{\alpha c}(x) d\Phi^*_{\alpha c}(x). \tag{B.17}$$

Now we have all ingredients needed for HMC sampling with dynamical fermions. First one samples randomly a set of conjugate momenta π_μ and pseudo-fermion fields Φ with gaussian distribution $\propto \exp\left(-\frac{1}{2}\pi_\mu \pi_\mu - S_{\text{pf}}\right)$. Together with an initial gauge field configuration U_i, the classical equations of motion are integrated up to some later time. At this point one implements the accept-reject step and updates the gauge configuration to U_{i+1}.

This far we assumed two degenerate flavors of quarks to compute the effective fermion action. The inclusion of a strange quark, as in the case of the CLS ensembles we use in this work, complicates things since it does not belong to a mass-degenerate doublet, and thus one needs to compute $\det(D_s)$ and not $\det(D_l^\dagger D_l)$. When this happens the quark determinant is not ensured to be positive anymore due to explicit chiral symmetry breaking by the Wilson term in Wilson quarks. In CLS ensembles this difficulty is tackled by the Rational Hybrid Monte Carlo algorithm **[âĂć]**. However, it was found that some configurations still suffered from a negative strange quark determinant. In this case we introduce a reweighting factor with minus sign to account for the effect. Reweighting is discussed in the next section.

B.3 REWEIGHTING

The idea of reweighting was first proposed **[âĂć]** in order to deal with exceptional gauge configurations in the HMC algorithm. These are gauge configurations with near to zero eigenvalues for the Dirac operator, which can appear due to the explicit chiral symmetry breaking induced by the Wilson term in the Wilson fermion action.

In the context of CLS ensembles, a small twisted mass term μ_0 is included in the light quark determinant as [**1206.2809**]

$$\det\left(Q^\dagger Q\right) \to \det\left(\left(Q^\dagger Q+\mu_0^2\right)^2\left(Q^\dagger Q+2\mu_0^2\right)^{-1}\right), \tag{B.18}$$

with the Hermitian Dirac operator given by $Q=\gamma_5 D$. This provides an infrared cutoff to cancel low-mode eigenvalues. Using the Hasenbusch's mass factorization []

$$\det\left(\left(Q^\dagger Q+\mu_0^2\right)^2\left(Q^\dagger Q+2\mu_0^2\right)^{-1}\right) \tag{B.19}$$

$$=\det\left(Q^\dagger Q+\mu_n^2\right)\det\left(\frac{Q^\dagger Q+\mu_0^2}{Q^\dagger Q+2\mu_0^2}\right)\times\Pi_{i=1}^{n}\det\left(\frac{Q^\dagger Q+\mu_{i-1}^2}{Q^\dagger Q+\mu_i^2}\right), \tag{B.20}$$

where the twisted mass factors are ordered as $\mu_0<\mu_1<...<\mu_n$. We used γ_5-hermiticity of the Dirac operator D so that

$$Q^\dagger Q=\gamma_5 D^\dagger \gamma_5 D=D^\dagger D. \tag{B.21}$$

The values of the twisted mass factors have to be properly chosen as large values might lead to large fluctuations and poor efficiency of the algorithm. After introducing such twisted masses, in order to account for their effect and recover the target desired distribution $dP[U]$ of QCD (un which this twisted mass is not present) a reweighting of expectation values over gauge configurations is needed

$$\langle O\rangle_{\mathrm{rw}}=\frac{\langle OW\rangle}{\langle W\rangle}, \tag{B.22}$$

where W is the reweighting factor and in this case reads

$$W=\det\left(Q^\dagger Q\left(Q^\dagger Q+2\mu_0^2\right)\left(Q^\dagger Q+\mu_0^2\right)^{-2}\right). \tag{B.23}$$

In addition to twisted mass reweighting, reweighting is also needed due to the use of the RHMC algorithm to simulate the strange quark determinant []. This algorithm uses the rational approximation to the strange quark determinant, which is expected to make it positive. However, as mentioned in the previous section, , it was found that some configurations still got a negative sign for the strange quark determinant. This is solved by a reweighting factor of $W_s=-1$ for said configurations (see Table B.1).

id	cnfg
H105r001	3
H105r002	1

H105r005	254, 255, 256, 257, 259, 260, 261, 264, 265, 266, 269, 280, 282, 283, 284, 285, 286, 287, 288, 289, 291, 299, 301, 313, 314, 315, 316, 331, 332, 333, 334, 335, 336, 337, 338, 339, 340, 341, 342
E250	???
J303r003	324, 325, 326

Table B.1: List of configurations with negative sign of the strange quark determinant for each ensemble. A reweighting factor $W_s = -1$ is introduced in said configuration in order to account for the effect.

C

SOLVERS

For the computation of correlation functions of fermions in the lattice (e.g. a two-point function, see eq. (1.73)) the inversion of the Dirac operator is required. In particular it is needed to compute the inverse of $D(x,y)$ for all spatial positions $\vec{x},\vec{y}$. This is referred to as inverting the all-to-all Dirac operator. This is computationally very expensive, and stochastic methods can be employed to reduce the computational cost. A set of stochastic noise sources η are introduced such that

$$\langle \eta_i(x) \rangle_\eta = 0, \quad \left\langle \eta_i^\dagger(x)\eta_j(y) \right\rangle_\eta = \delta_{x,y}\delta_{i,j}, \tag{C.1}$$

with $\langle . \rangle_\eta$ meaning average over the N_η samples of some noise distribution. Some common choices are gaussian, Z_2 or $U(1)$. From these we define

$$\xi_i^q(x) = \sum_y D_q^{-1}(x,y)\eta_i(y), \quad \zeta_i^r(x) = \sum_y D_r^{-1}(x,y)\gamma_5\Gamma_B^\dagger\eta_i(y), \tag{C.2}$$

with Γ_B some Gamma matrix. Now, two-point functions like the one in eq. (1.73)) can be expressed as

$$\langle O_A^{rq} O_B^{qr} \rangle - \frac{a^6}{L^3}\sum_{\vec{y}} \left\langle \left\langle (\Gamma_A\gamma_5\zeta_i^r(y))^\dagger \xi_i^q(y) \right\rangle_\eta \right\rangle \tag{C.3}$$

$$\approx -\frac{a^6}{L^3}\frac{1}{N_\eta}\sum_{i=1}^{N_\eta}\sum_{\vec{y}} \left\langle (\Gamma_A\gamma_5\zeta_i^r(y))^\dagger \xi_i^q(y) \right\rangle, \tag{C.4}$$

without the need to compute the all-to-all inverted Dirac operator, therefore reducing significantly the computational effort.

In order to invert the Dirac operator with flavor q, the solution to the Dirac equation

$$D_q(x,y)\psi_r(y) = \delta_{x,y}\delta_{q,r} \equiv \eta_{x,y,q,r}, \tag{C.5}$$

must be found. This is usually done by an iterative procedure. The basic idea is to start from an initial approximate solution ψ_0 and define the residue ρ (we supress indices for simplicity)

$$\rho = D\psi_0 - \eta. \tag{C.6}$$

Then, one solves

$$D\psi_1 = \rho, \tag{C.7}$$

finding the new residue and iterates the process, with the final approximate solution given by

$$\psi = \psi_0 + \psi_1 + ... \tag{C.8}$$

The algorithm stops when some convergence criterion is met

$$|\rho| < \epsilon. \tag{C.9}$$

The difference between the true and approximate solutions is

$$|\psi - \psi_{\text{true}}| < \epsilon\kappa(D), \tag{C.10}$$

with $\kappa(D)$ the condition number of matrix D

$$\kappa(D) = |D||D^{-1}|. \tag{C.11}$$

The smaller the condition number of the Dirac operator, the less iterative steps one needs to perform in order to find the solution to the Dirac equation. Thus convergence can be improved by suitably transforming the system into one with a smaller $\kappa(D)$. This can be done by finding some similarity transformations easily invertible such that one can write

$$LDR\psi' = L\eta, \quad \psi = R^{-1}\psi'. \tag{C.12}$$

This is called preconditioning, and there are many different variations. Some of the most used are even-odd preconditioning [**âĂć**] and distance preconditioning [**âĂć**].

There are also more sophisticated algorithms to solve the Dirac equation based on conjugate gradient solvers [**âĂć**] and the Krylov subspace solvers [**âĂć**].

D

ERROR ANALYSIS

In this appendix we discuss how to perform the data analysis of correlation functions and the different lattice observables extracted from lattice simulations.

Lattice data is measured from Monte Carlo (MC) sampling, and estimates of expectation values of physical observables are extracted from means over the MC time. A crucial step is to assign a proper statistical and systematic uncertainties to these mean values, for which it is needed to take into account the autocorrelated nature of MC measurements. This autocorrelation arises form the fact that each gauge configuration is proposed from the previous one (Markov chain). Some popular methods to deal with these correlations are binning, bootstrap and the jack-knife methods [].

A recent technique which we will use in this work was proposed by the ALPHA collaboration [**Gamma-method**] and is known as Γ-method, which explicitely computes the autocorrelation function to estimate the statistical uncertainty.

In lattice simulations tipically one measures a primary observable p_i over several ensembles (defined by the simulation parameters like e.g. the inverse coupling β and κ parameter)

$$p_i^\alpha(k), k = 1, ..., N_\alpha, \tag{D.1}$$

where α labels the ensemble and k is the MC time running over the total number of gauge configurations N_α of the given ensemble. In our context, primary observable means a correlation function for some given euclidean time. An estimate for the true value P_i^α is given by the mean value

$$\bar{p}_i^\alpha = \frac{1}{N_\alpha} \sum_{k=1}^{N_\alpha} p_i^\alpha(k) \rightarrow_{N_\alpha \rightarrow \infty} P_i^\alpha. \tag{D.2}$$

This is an unbiased estimator. Fluctuations over the MC time can be computed as

$$\delta_i^\alpha(k) = p_i^\alpha(k) - \bar{p}_i^\alpha. \tag{D.3}$$

Due to the Central Limit theorem, we are ensured that $\bar{p}_i^\alpha$ behaves as a Gaussian distribution independently of the distribution of $p_i^\alpha(k)$, and so the statistical uncertainty associated to $\bar{p}_i^\alpha$ is simply given by the standard deviation σ_i^α,

$$P_i^\alpha \approx \bar{p}_i^\alpha \pm \sigma_i^\alpha. \tag{D.4}$$

This standard deviation can be computed from the autocorrelation Γ function

$$(\sigma_i^\alpha)^2 = \frac{1}{N_\alpha} \sum_{k=-\infty}^{\infty} \Gamma_{ii}^{\alpha\alpha}(k), \tag{D.5}$$

where the Γ function is defined as

$$\Gamma_{ij}^{\alpha\beta} = \frac{\delta_{\alpha\beta}}{N_\alpha - k} \sum_{k'=1}^{N_\alpha - k} \delta_i^\alpha(k + k')\delta_j^\alpha(k'). \tag{D.6}$$

From the primary observable p_i^α we can compute derived observables $F = f(p_i^\alpha)$, such as meson masses coming from pseudoscalar two point functions. As in the primary observable case, we can estimate this derived observable as

$$\bar{F} = f(\bar{p}_i^\alpha). \tag{D.7}$$

To compute the statistical uncertainty, we can expand f around the true value P_i^α

$$f(P_i^\alpha + \epsilon_i^\alpha) = f(P_i^\alpha) + \bar{f}_i^\alpha \epsilon_i^\alpha + \mathcal{O}((\epsilon_i^\alpha)^2), \tag{D.8}$$

with

$$\bar{f}_i^\alpha = \frac{\partial f(x)}{\partial x}|_{x=P_i^\alpha}. \tag{D.9}$$

Now the autocorrelation function of the derived observable F for ensemble α can be defined as

$$\Gamma_F^\alpha(k) = \sum_{ij} \bar{f}_i^\alpha \bar{f}_j^\alpha \Gamma_{ij}^{\alpha\alpha}(k), \tag{D.10}$$

from which the standard deviation of F can be derived

$$\sigma_F^2 = \sum_\alpha \frac{\Gamma_F^\alpha(0)}{N_\alpha} 2\tau_{\text{int}}^\alpha(F), \tag{D.11}$$

where we assumed that several ensembles contribute to F, and hence the sum $\sum_\alpha$ over the subset of them which contribute. The integrated autocorrelation time $\tau_{\text{int}}^\alpha(F)$ is defined as

$$\tau_{\text{int}}^\alpha(F) = \frac{1}{2} + \sum_{k=1}^{\infty} \frac{\Gamma_F^\alpha(k)}{\Gamma_F^\alpha(k)}. \tag{D.12}$$

To estimate it, a truncation in MC time k is needed. The autocorrelation function admits the following expansion [**âĂć**]

$$\Gamma(k) \approx \sum_{n=0}^{\infty} e^{-k/\tau_n}. \tag{D.13}$$

The slowest mode $\tau_0 \equiv \tau_{\text{exp}}$ is called the exponential autocorrelation time and it gives the decay rate of $\Gamma(k)$. Truncating eq. (D.12) at MC

time $k = W_F^\alpha$ introduces a systematic uncertainty of $\mathcal{O}(\exp(-W_F^\alpha/\tau_{\text{exp}}^\alpha))$. The Γ-method proposes as optimal window that which minimizes the sum of statistical (estimated in [**J.Stat.Phys.50(1988)109**]) and systematic contributions

$$W_F^\alpha = \min_W \left(\sqrt{\frac{2(2W+1)}{N_\alpha}} + e^{-W/\tau_{\text{exp}}^\alpha} \right). \tag{D.14}$$

In [**âĂć**] it was proposed to set $\tau_{\text{exp}} = S_\tau \tau_{\text{int}}$, with S_τ some value between 2 and 5. One can also vary W_F^α until saturation in τ_{int}^α is reached. In [**âĂć**] it was also proposed to add an exponential tail

$$\tau_{\text{exp}}^\alpha \frac{\Gamma_F^\alpha(W_F^\alpha+1)}{\Gamma_F^\alpha(0)}, \tag{D.15}$$

to eq. (D.12) to account for the systematic effect of truncating the sum over MC time. For this an estimate of τ_{exp}^α is needed for each ensemble. In the case of CLS ensembles an estimation is given in []

$$\tau_{\text{exp}}^\alpha = 14(3)\frac{t_0}{a^2}. \tag{D.16}$$

In this thesis we use the Γ-method explained above as it is implemented by the ADerrors.jl julia package [**âĂć**].

E

LATTICE ENSEMBLES

id	β	m_π [MeV]	m_K [MeV]	T/a	L/a	$m_\pi L$	cnfg
H101	3.40	421	421	96	32	5.8	1001,1009
H102r001	3.40	355	442	96	32	4.9	997
H102r002	3.40	360	445	96	32	5.0	1008
H105	3.40	284	471	96	32	3.9	947,1042
H105r005	3.40	286	467	96	32	3.9	837
H400	3.46	426	426	96	32	5.2	505,540
D450	3.46	222	480	128	64	5.4	1000
N202	3.55	416	416	128	48	6.4	899
N203	3.55	348	446	128	48	5.4	756,787
N200	3.55	287	468	128	48	4.4	856,856
D200	3.55	203	486	128	64	4.2	2001
E250	3.55	130	497	192	96	4.0	1009
N300r002	3.70	424	424	128	48	5.1	1521
N302	3.70	348	453	128	48	4.2	2201
J303	3.70	259	480	192	64	4.1	1073
E300	3.70	176	496	192	96	4.2	1139
J500	3.85	417	417	192	64	5.2	789,655,431
J501	3.85	340	453	192	64	4.3	1635,1142,1150

Table E.1: List of CLS ensembles [] under study. They use the Lüscher-Weisz gauge action defined in eq. (1.88) and non-perturbatively $\mathcal{O}(a)$ improved $N_f = 2 + 1$ Wilson fermions. All ensembles use open boundary conditions in time except for E250, and periodic boundary conditions for all spatial directions.

F

LEAST-SQUARES FITTING

We employ a least-squares method to fit our data to some fit function. This method is based on finding the minimum of the χ^2 function

$$\chi^2 = \sum_{i,j=1}^{N_{\text{dat}}} \left(y_i - f(x_i;\vec{p})\right) C_{ij}^{-1} \left(y_j - f(x_j;\vec{p})\right), \tag{F.1}$$

where $\{x_i, y_i\}_{i=1,\dots,N_{\text{dat}}}$ are the data points we want to fit, x being the independent variable and y the abscissa. C^{-1} is the inverse of the covariance matrix of the y-data, and $f(x;\vec{p})$ is the fit function with fit parameters $\vec{p} = (p_1, \dots, p_{N_{\text{param}}})$. For a given fit function $f(x;\vec{p})$, the method finds the parameters values that minimize eq. (F.1) for given data points $\{x_i, y_i\}_{i=1,\dots,N_{\text{dat}}}$.

In our case we perform fits to extract the ground state signal of lattice observables, fitting e.g. an effective mass to a constant plus some exponential signals along the lattice time extent. In this case, euclidean time plays the role of the x. This means fitting $\sim 96 - 192$ points, which in practice makes it very difficult to computate an invertible covariance matrix. In this scenario it is common to use not the full covariance matrix in eq. (F.1) but only its diagonal part. This is referred to as uncorrelated fit, as opposed to a fully correlated fit, which uses the full covariance matrix. However, after minimizing the χ^2 using only the diagonal part of C, uncertainties are propagated taking into account all the correlations between the data.

We also perform fits for the chiral-continuum extrapolation of $\sqrt{8t_0} f_{\pi K}$ to set the scale. In this case, the y variable is $\sqrt{8t_0} f_{\pi K}$ while the x is ϕ_2, and thus the latter has its own uncertainty. In this situation, a generalized χ^2 function can be defined to include uncertainties in x as

$$\chi^2 = \sum_{i,j=1}^{2N_{\text{dat}}} \left(Y_i - F(X_i;\vec{p},\vec{q})\right) \mathcal{C}_{ij}^{-1} \left(Y_j - F(X_j;\vec{p},\vec{q})\right), \tag{F.2}$$

$$Y = (x_1, \dots, x_{N_{\text{dat}}}, y_1, \dots, y_{N_{\text{dat}}}), \quad X = (x_1, \dots, x_{N_{\text{dat}}}, x_1, \dots, x_{N_{\text{dat}}}), \tag{F.3}$$

$$F(X_i;\vec{p},\vec{q}) = \begin{cases} q_i & \text{if } 1 \le i \le N_{\text{dat}} \\ f(x_i;\vec{p}) & \text{if } N_{\text{dat}} + 1 \le i \le 2N_{\text{dat}} \end{cases}, \tag{F.4}$$

where $\mathcal{C}$ is now the covariance matrix of the generalized data vector Y. Again, since we have 16 different ensembles, a fully correlated fit means that we have $\sim 32 \times 32$ covariance matrices which are hard to invert. For this reason, we use the χ^2 definition in eq. (F.1) for the chiral-continuum extrapolation, i.e. we neglect the correlation

between ϕ_2 and $\sqrt{8t_0}f_{\pi K}$ in the definition of the χ^2, but we use the full covariance matrix of the $\sqrt{8t_0}f_{\pi K}$ data. Again, to propagate errors we take into account all the correlations between the data, and in particular between ϕ_2 and $\sqrt{8t_0}f_{\pi K}$.

In **[chi_exp]** a method to measure the quality of the fit for uncorrelated fits is defined, in terms of a p-value. It is also defined a method to compute the expected value of the minimum of χ^2, $\langle\chi^2\rangle$. In the case of a fully correlated fit $\langle\chi^2\rangle = \text{dof}$. For the chiral-continuum fits, even though we neglect the uncertainties of ϕ_2 and the correlation of it with $\sqrt{8t_0}f_{\pi K}$ in the definition of the χ^2, we observe

$$\frac{\langle\chi^2\rangle}{\text{dof}} \sim 0.98. \tag{F.5}$$

G

FINITE VOLUME EFFECTS

Simulating QCD in a finite box introduces finite volume effects which can be a source for systematic uncertainties. In Table E.1 we show the volume of each ensemble in terms of $m_\pi L$. It is conventional to consider finite volume effects under control if $m_\pi L \geq 4$.

ChPT provides us with formulae to account for these finite volume effects. In particular, to NLO the pion mass and decay constant, as well as the kaon decay constant, receive the following corrections

$$X^{(\infty)} = X^{(L)} \frac{1}{1 + R_X}, \tag{G.1}$$

where $X^{(\infty)}$ is observable X at infinite volume and $X^{(L)}$ is said observable at a finite volume L^3, with $X = m_\pi, m_K, f_\pi, f_K$,

$$R_{m_\pi} = \frac{1}{4}\xi_\pi \tilde{g}_1(\lambda_\pi) - \frac{1}{12}\xi_\eta \tilde{g}_1(\lambda_\eta), \tag{G.2}$$

$$R_{m_K} = \frac{1}{6}\xi_\eta \tilde{g}_1(\lambda_\eta), \tag{G.3}$$

$$R_{f_K} = -\xi_\pi \tilde{g}_1(\lambda_\pi) - \frac{1}{2}\xi_K \tilde{g}_1(\lambda_K), \tag{G.4}$$

$$R_{f_\pi} = -\frac{3}{8}\xi_\pi \tilde{g}_1(\lambda_\pi) - \frac{3}{4}\xi_K \tilde{g}_1(\lambda_K) - \frac{3}{8}\xi_\eta \tilde{g}_1(\lambda_\eta), \tag{G.5}$$

$$\xi_{PS} = \frac{m_{PS}^2}{(4\pi f_\pi)^2}, \tag{G.6}$$

$$\lambda_{PS} = m_{PS} L, \tag{G.7}$$

$$\tilde{g}_1(x) = \sum_{n=1}^{\infty} \frac{4m(n)}{\sqrt{n}x} K_1(\sqrt{n}x), \tag{G.8}$$

$$m_\eta^2 = \frac{4}{3}m_K^2 - \frac{1}{3}m_\pi^2, \tag{G.9}$$

where $K_1(x)$ is a Bessel function of the second kind, and the multiplicities $m(n)$ [] are listed in Table G.1. It is manifest that the lighter the pion mass and the smaller the volume, the stronger the volume corrections. We find these corrections to be less than half a standard deviation for the ensembles with the smallest volumes and lightest pion masses. We nonetheless apply the corrections to all the ensembles.

PCAC quark masses are short distance observables and as such do not receive any infinite volume correction.

n	1	2	3	4	5	6	7	8	9	10	11	12	13	14	15	16	17	18	19	20

n	1	2	3	4	5	6	7	8	9	10	11	12	13	14	15	16	17	18	19	20
$m(n)$	6	12	8	6	24	24	0	12	30	24	24	8	24	48	0	6	48	36		

Table G.1: Multiplicities $m(n)$ calculated in [] for $n \leq 20$.

H

$\sqrt{t_0}$: MODEL VARIATION

Wilson analysis	
$[SU(3)\chi PT]$	Eq. (4.6)
$[Tay]$	Eq. (4.9)
$[Tay4]$	Eq. (4.10)
$[a^2]$	Eq. (4.13)
$[a^2\alpha_S^\Gamma]$	Eq. (4.13)
$[a^2 + a^2\phi_2]$	Eq. (4.13)
$[-]$	No cut in data
$[\beta > 3.40]$	Remove $\beta = 3.40$ ensembles
$[\beta > 3.46]$	Remove $\beta = 3.40$ and $\beta = 3.46$ ensembles
$[m_\pi < 420\ MeV]$	Remove symmetric point ensembles
$[m_\pi < 350\ MeV]$	Remove $\phi_2 > 0.4$ ensembles
$[\beta > 3.40\ \&\ m_\pi < 420\ MeV]$	Remove symmetric point and $\beta = 3.40$ ensembles
$[m_\pi L > 4.1]$	Remove ensembles with volumes $m_\pi L \leq 4.1$

Table H.1: Correspondence between each fit model for the chiral-continuum extrapolation of $\sqrt{8t_0}f_{\pi K}$ and the labels used in the corresponding tables and figures. For the combined analysis, we are dealing with two independent cutoff effects, those of the Wilson results and those of the mixed action. In this case we will use two labels for these effects, the first referring to the lattice artifacts explored for the Wilson results, the second one for the mixed action results. If only one label is used it means the same lattice artifacts were explored for both regularizations.

Wilson analysis			
Model	p-value	W	$\sqrt{t_0}$ [fm]
$[\chi SU(3)][a^2][-]$	0.4538	0.0536	0.1444(9)
$[\chi SU(3)][a^2][\beta > 3.40]$	0.347	0.0072	0.1445(13)
$[\chi SU(3)][a^2][\beta > 3.46]$	0.3016	0.0024	0.1442(15)
$[\chi SU(3)][a^2][m_\pi < 420\ MeV]$	0.5992	0.0092	0.1442(9)
$[\chi SU(3)][a^2][\beta > 3.40\ \&\ m_\pi < 420\ MeV]$	0.3458	0.0008	0.1441(18)
$[\chi SU(3)][a^2][m_\pi < 350\ MeV]$	0.4922	0.0015	0.1438(11)

$[\chi SU(3)][a^2][m_\pi L > 4.1]$	0.4482	0.0125	0.1448(10)
$[\chi SU(3)][a^2\alpha_s^{\hat{\Gamma}}][-]$	0.4406	0.0534	0.1443(9)
$[\chi SU(3)][a^2\alpha_s^{\hat{\Gamma}}][\beta > 3.40]$	0.3506	0.0072	0.1445(13)
$[\chi SU(3)][a^2\alpha_s^{\hat{\Gamma}}][\beta > 3.46]$	0.3092	0.0024	0.1442(15)
$[\chi SU(3)][a^2\alpha_s^{\hat{\Gamma}}][m_\pi < 420\ MeV]$	0.5754	0.0093	0.1442(9)
$[\chi SU(3)][a^2\alpha_s^{\hat{\Gamma}}][\beta > 3.40\ \&\ m_\pi < 420\ MeV]$	0.3456	0.0008	0.144(18)
$[\chi SU(3)][a^2\alpha_s^{\hat{\Gamma}}][m_\pi < 350\ MeV]$	0.4968	0.0015	0.1438(11)
$[\chi SU(3)][a^2\alpha_s^{\hat{\Gamma}}][m_\pi L > 4.1]$	0.4316	0.0123	0.1447(10)
$[\chi SU(3)][a^2 + a^2\phi_2][-]$	0.7856	0.2553	0.1428(9)
$[\chi SU(3)][a^2 + a^2\phi_2][\beta > 3.40]$	0.6454	0.0192	0.1421(16)
$[\chi SU(3)][a^2 + a^2\phi_2][\beta > 3.46]$	0.4416	0.0029	0.1421(19)
$[\chi SU(3)][a^2 + a^2\phi_2][m_\pi < 420\ MeV]$	0.5718	0.0055	0.1433(13)
$[\chi SU(3)][a^2 + a^2\phi_2][\beta > 3.40\ \&\ m_\pi < 420\ MeV]$	0.2188	0.0003	0.1437(29)
$[\chi SU(3)][a^2 + a^2\phi_2][m_\pi < 350\ MeV]$	0.5694	0.0011	0.1409(26)
$[\chi SU(3)][a^2 + a^2\phi_2][m_\pi L > 4.1]$	0.7036	0.0268	0.1427(13)
$[Tay][a^2][-]$	0.2988	0.0176	0.1448(7)
$[Tay][a^2][\beta > 3.40]$	0.2422	0.0033	0.1449(10)
$[Tay][a^2][\beta > 3.46]$	0.2042	0.0012	0.1445(14)
$[Tay][a^2][m_\pi < 420\ MeV]$	0.4568	0.0056	0.1446(7)
$[Tay][a^2][\beta > 3.40\ \&\ m_\pi < 420\ MeV]$	0.295	0.0007	0.1444(17)
$[Tay][a^2][m_\pi < 350\ MeV]$	0.3514	0.0009	0.1441(8)
$[Tay][a^2][m_\pi L > 4.1]$	0.3886	0.0092	0.1452(7)
$[Tay][a^2\alpha_s^{\hat{\Gamma}}][-]$	0.2848	0.0174	0.1447(7)
$[Tay][a^2\alpha_s^{\hat{\Gamma}}][\beta > 3.40]$	0.2378	0.0033	0.1449(10)
$[Tay][a^2\alpha_s^{\hat{\Gamma}}][\beta > 3.46]$	0.2034	0.0012	0.1445(14)
$[Tay][a^2\alpha_s^{\hat{\Gamma}}][m_\pi < 420\ MeV]$	0.4832	0.0055	0.1446(7)
$[Tay][a^2\alpha_s^{\hat{\Gamma}}][\beta > 3.40\ \&\ m_\pi < 420\ MeV]$	0.2886	0.0007	0.1444(18)
$[Tay][a^2\alpha_s^{\hat{\Gamma}}][m_\pi < 350\ MeV]$	0.365	0.0009	0.1441(8)
$[Tay][a^2\alpha_s^{\hat{\Gamma}}][m_\pi L > 4.1]$	0.389	0.0091	0.1451(7)
$[Tay][a^2 + a^2\phi_2][-]$	0.7542	0.1824	0.143(9)
$[Tay][a^2 + a^2\phi_2][\beta > 3.40]$	0.5864	0.0148	0.1421(16)
$[Tay][a^2 + a^2\phi_2][\beta > 3.46]$	0.3882	0.0025	0.1418(20)
$[Tay][a^2 + a^2\phi_2][m_\pi < 420\ MeV]$	0.5502	0.0048	0.1433(13)
$[Tay][a^2 + a^2\phi_2][\beta > 3.40\ \&\ m_\pi < 420\ MeV]$	0.193	0.0003	0.1435(31)
$[Tay][a^2 + a^2\phi_2][m_\pi < 350\ MeV]$	0.361	0.0006	0.1413(27)
$[Tay][a^2 + a^2\phi_2][m_\pi L > 4.1]$	0.7688	0.0332	0.143(12)
$[Tay4][a^2][-]$	0.601	0.0775	0.1435(9)
$[Tay4][a^2][\beta > 3.40]$	0.4034	0.0059	0.1438(12)

$[Tay4][a^2][\beta > 3.46]$	0.2634	0.0013	0.144(14)
$[Tay4][a^2][m_\pi < 420\ MeV]$	0.4524	0.0034	0.144(10)
$[Tay4][a^2][\beta > 3.40\ \&\ m_\pi < 420\ MeV]$	0.1862	0.0003	0.1442(19)
$[Tay4][a^2][m_\pi < 350\ MeV]$	0.9954	0.0028	0.1421(13)
$[Tay4][a^2][m_\pi L > 4.1]$	0.4256	0.0066	0.144(12)
$[Tay4][a^2 + a^2\phi_2][-]$	0.7002	0.0781	0.1429(9)
$[Tay4][a^2 + a^2\phi_2][\beta > 3.40]$	0.4956	0.006	0.1422(17)
$[Tay4][a^2 + a^2\phi_2][\beta > 3.46]$	0.2932	0.001	0.142(21)
$[Tay4][a^2 + a^2\phi_2][m_\pi < 420\ MeV]$	0.4126	0.0018	0.1433(13)
$[Tay4][a^2 + a^2\phi_2][\beta > 3.40\ \&\ m_\pi < 420\ MeV]$	0.0954	0.0001	0.1436(32)
$[Tay4][a^2 + a^2\phi_2][m_\pi < 350\ MeV]$	0.9816	0.001	0.1425(28)
$[Tay4][a^2 + a^2\phi_2][m_\pi L > 4.1]$	0.711	0.014	0.1432(13)

Table H.2: Model average results for the determination of $\sqrt{t_0}$ at the physical point using the Wilson results. In the first column we label the fit model and data cuts considered. In the second and third columns we show the quality of fits as measured by the p-value **[chi_exp]** and the assigned weight to each model according to eq. (4.19), respectively. Finally, in the fourth column we show the results coming from each fit model.

Mixed action analysis			
Model	p-value	W	$\sqrt{t_0}$ [fm]
$[\chi SU(3)][a^2][-]$	0.5122	0.1434	0.1436(6)
$[\chi SU(3)][a^2][\beta > 3.40]$	0.5808	0.0317	0.144(9)
$[\chi SU(3)][a^2][\beta > 3.46]$	0.4858	0.0082	0.1435(10)
$[\chi SU(3)][a^2][m_\pi < 420\ MeV]$	0.4852	0.0087	0.1439(7)
$[\chi SU(3)][a^2][\beta > 3.40\ \&\ m_\pi < 420\ MeV]$	0.1792	0.0005	0.1437(12)
$[\chi SU(3)][a^2][m_\pi < 350\ MeV]$	0.2008	0.0005	0.1439(8)
$[\chi SU(3)][a^2][m_\pi L > 4.1]$	0.4458	0.0217	0.1436(7)
$[\chi SU(3)][a^2\hat{\alpha_s^\Gamma}][-]$	0.5176	0.146	0.1438(6)
$[\chi SU(3)][a^2\hat{\alpha_s^\Gamma}][\beta > 3.40]$	0.5752	0.0306	0.1441(9)
$[\chi SU(3)][a^2\hat{\alpha_s^\Gamma}][\beta > 3.46]$	0.5038	0.0082	0.1436(10)
$[\chi SU(3)][a^2\hat{\alpha_s^\Gamma}][m_\pi < 420\ MeV]$	0.477	0.009	0.144(7)
$[\chi SU(3)][a^2\hat{\alpha_s^\Gamma}][\beta > 3.40\ \&\ m_\pi < 420\ MeV]$	0.178	0.0005	0.1438(12)
$[\chi SU(3)][a^2\hat{\alpha_s^\Gamma}][m_\pi < 350\ MeV]$	0.2	0.0005	0.1441(8)
$[\chi SU(3)][a^2\hat{\alpha_s^\Gamma}][m_\pi L > 4.1]$	0.4344	0.0216	0.1437(7)
$[\chi SU(3)][a^2 + a^2\phi_2][-]$	0.4856	0.0657	0.1441(9)
$[\chi SU(3)][a^2 + a^2\phi_2][\beta > 3.40]$	0.495	0.0162	0.1434(13)

$[\chi SU(3)][a^2 + a^2\phi_2][\beta > 3.46]$	0.3948	0.0031	0.1433(15)
$[\chi SU(3)][a^2 + a^2\phi_2][m_\pi < 420\ MeV]$	0.3896	0.0032	0.1436(13)
$[\chi SU(3)][a^2 + a^2\phi_2][\beta > 3.40\ \&\ m_\pi < 420\ MeV]$	0.1118	0.0002	0.1428(22)
$[\chi SU(3)][a^2 + a^2\phi_2][m_\pi < 350\ MeV]$	0.228	0.0005	0.1411(24)
$[\chi SU(3)][a^2 + a^2\phi_2][m_\pi L > 4.1]$	0.3848	0.0092	0.1443(12)
$[Tay][a^2][-]$	0.4352	0.0949	0.1441(7)
$[Tay][a^2][\beta > 3.40]$	0.4458	0.0163	0.1445(9)
$[Tay][a^2][\beta > 3.46]$	0.3664	0.0045	0.1439(10)
$[Tay][a^2][m_\pi < 420\ MeV]$	0.378	0.0051	0.1444(7)
$[Tay][a^2][\beta > 3.40\ \&\ m_\pi < 420\ MeV]$	0.1156	0.0003	0.1442(12)
$[Tay][a^2][m_\pi < 350\ MeV]$	0.1184	0.0003	0.1443(8)
$[Tay][a^2][m_\pi L > 4.1]$	0.489	0.028	0.144(7)
$[Tay][a^2\hat{\alpha_s^\Gamma}][-]$	0.4562	0.0942	0.1442(7)
$[Tay][a^2\hat{\alpha_s^\Gamma}][\beta > 3.40]$	0.4456	0.0161	0.1446(9)
$[Tay][a^2\hat{\alpha_s^\Gamma}][\beta > 3.46]$	0.3532	0.0045	0.144(11)
$[Tay][a^2\hat{\alpha_s^\Gamma}][m_\pi < 420\ MeV]$	0.3748	0.0052	0.1445(7)
$[Tay][a^2\hat{\alpha_s^\Gamma}][\beta > 3.40\ \&\ m_\pi < 420\ MeV]$	0.118	0.0003	0.1443(12)
$[Tay][a^2\hat{\alpha_s^\Gamma}][m_\pi < 350\ MeV]$	0.1262	0.0003	0.1444(9)
$[Tay][a^2\hat{\alpha_s^\Gamma}][m_\pi L > 4.1]$	0.4916	0.0277	0.1441(8)
$[Tay][a^2 + a^2\phi_2][-]$	0.3618	0.0346	0.1444(10)
$[Tay][a^2 + a^2\phi_2][\beta > 3.40]$	0.4062	0.01	0.1436(13)
$[Tay][a^2 + a^2\phi_2][\beta > 3.46]$	0.277	0.0019	0.1435(15)
$[Tay][a^2 + a^2\phi_2][m_\pi < 420\ MeV]$	0.2902	0.002	0.1438(13)
$[Tay][a^2 + a^2\phi_2][\beta > 3.40\ \&\ m_\pi < 420\ MeV]$	0.0774	0.0001	0.1429(22)
$[Tay][a^2 + a^2\phi_2][m_\pi < 350\ MeV]$	0.1214	0.0002	0.1416(24)
$[Tay][a^2 + a^2\phi_2][m_\pi L > 4.1]$	0.4122	0.0095	0.1444(12)
$[Tay4][a^2][-]$	0.4128	0.043	0.1437(9)
$[Tay4][a^2][\beta > 3.40]$	0.4722	0.0132	0.1438(11)
$[Tay4][a^2][\beta > 3.46]$	0.3622	0.0028	0.1434(12)
$[Tay4][a^2][m_\pi < 420\ MeV]$	0.3458	0.0026	0.1438(10)
$[Tay4][a^2][\beta > 3.40\ \&\ m_\pi < 420\ MeV]$	0.0884	0.0002	0.1435(14)
$[Tay4][a^2][m_\pi < 350\ MeV]$	0.6182	0.0016	0.142(13)
$[Tay4][a^2][m_\pi L > 4.1]$	0.4106	0.0098	0.1444(11)
$[Tay4][a^2 + a^2\phi_2][-]$	0.4188	0.0298	0.1441(10)
$[Tay4][a^2 + a^2\phi_2][\beta > 3.40]$	0.3806	0.0052	0.1436(13)
$[Tay4][a^2 + a^2\phi_2][\beta > 3.46]$	0.258	0.0011	0.1436(15)
$[Tay4][a^2 + a^2\phi_2][m_\pi < 420\ MeV]$	0.2338	0.0011	0.1438(13)
$[Tay4][a^2 + a^2\phi_2][\beta > 3.40\ \&\ m_\pi < 420\ MeV]$	0.0384	0.0001	0.1432(23)

$[Tay4][a^2 + a^2\phi_2][m_\pi < 350\ MeV]$	0.4078	0.0006	0.1422(25)
$[Tay4][a^2 + a^2\phi_2][m_\pi L > 4.1]$	0.319	0.0039	0.1444(12)

Table H.3: Model average results for the determination of $\sqrt{t_0}$ at the physical point using the mixed actions results. In the first column we label the fit model and data cuts considered. In the second and third columns we show the quality of fits as measured by the p-value **[chi_exp]** and the assigned weight to each model according to eq. (4.19), respectively. Finally, in the fourth column we show the results coming from each fit model.

Combined analysis			
Model	p-value	W	$\sqrt{t_0}$ [fm]
$[\chi SU(3)][a^2][-]$	0.1358	0.0048	0.1445(7)
$[\chi SU(3)][a^2][\beta > 3.40]$	0.1574	0.0003	0.1448(8)
$[\chi SU(3)][a^2][\beta > 3.46]$	0.3434	0.0002	0.1443(10)
$[\chi SU(3)][a^2][m_\pi < 420\ MeV]$	0.543	0.0019	0.1442(6)
$[\chi SU(3)][a^2][\beta > 3.40\ \&\ m_\pi < 420\ MeV]$	0.5304	0.0	0.1439(11)
$[\chi SU(3)][a^2][m_\pi < 350\ MeV]$	0.4242	0.0	0.1441(8)
$[\chi SU(3)][a^2][m_\pi L > 4.1]$	0.0712	0.0001	0.1446(7)
$[\chi SU(3)][a^2\hat{\alpha_s^\Gamma}][-]$	0.1244	0.0039	0.1445(7)
$[\chi SU(3)][a^2\hat{\alpha_s^\Gamma}][\beta > 3.40]$	0.1382	0.0002	0.1449(9)
$[\chi SU(3)][a^2\hat{\alpha_s^\Gamma}][\beta > 3.46]$	0.3442	0.0002	0.1443(10)
$[\chi SU(3)][a^2\hat{\alpha_s^\Gamma}][m_\pi < 420\ MeV]$	0.5526	0.0018	0.1443(6)
$[\chi SU(3)][a^2\hat{\alpha_s^\Gamma}][\beta > 3.40\ \&\ m_\pi < 420\ MeV]$	0.5466	0.0	0.144(11)
$[\chi SU(3)][a^2\hat{\alpha_s^\Gamma}][m_\pi < 350\ MeV]$	0.4258	0.0	0.1441(8)
$[\chi SU(3)][a^2\hat{\alpha_s^\Gamma}][m_\pi L > 4.1]$	0.0722	0.0001	0.1446(7)
$[\chi SU(3)][a^2][a^2 + a^2\phi_2][-]$	0.609	0.3484	0.1434(6)
$[\chi SU(3)][a^2][a^2 + a^2\phi_2][\beta > 3.40]$	0.5194	0.0053	0.1439(8)
$[\chi SU(3)][a^2][a^2 + a^2\phi_2][\beta > 3.46]$	0.415	0.0002	0.1438(10)
$[\chi SU(3)][a^2][a^2 + a^2\phi_2][m_\pi < 420\ MeV]$	0.7278	0.0027	0.1437(6)
$[\chi SU(3)][a^2][a^2 + a^2\phi_2][\beta > 3.40\ \&\ m_\pi < 420\ MeV]$	0.4466	0.0	0.1439(11)
$[\chi SU(3)][a^2][a^2 + a^2\phi_2][m_\pi < 350\ MeV]$	0.5134	0.0	0.1435(8)
$[\chi SU(3)][a^2][a^2 + a^2\phi_2][m_\pi L > 4.1]$	0.4782	0.0038	0.1434(7)
$[\chi SU(3)][a^2 + a^2\phi_2][a^2][[-]$	0.3258	0.0211	0.1448(9)
$[\chi SU(3)][a^2 + a^2\phi_2][a^2][\beta > 3.40]$	0.2534	0.0006	0.1453(10)
$[\chi SU(3)][a^2 + a^2\phi_2][a^2][\beta > 3.46]$	0.3392	0.0001	0.1445(11)
$[\chi SU(3)][a^2 + a^2\phi_2][a^2][m_\pi < 420\ MeV]$	0.6576	0.0014	0.1445(7)
$[\chi SU(3)][a^2 + a^2\phi_2][a^2][\beta > 3.40\ \&\ m_\pi < 420\ MeV]$	0.4318	0.0	0.1439(12)

$[\chi SU(3)][a^2 + a^2\phi_2][a^2][m_\pi < 350\ MeV]$	0.3924	0.0	0.1443(10)
$[\chi SU(3)][a^2 + a^2\phi_2][a^2][m_\pi L > 4.1]$	0.301	0.0008	0.1451(10)
$[\chi SU(3)][a^2 + a^2\phi_2][-]$	0.551	0.1182	0.1435(8)
$[\chi SU(3)][a^2 + a^2\phi_2][\beta > 3.40]$	0.4834	0.0022	0.1432(12)
$[\chi SU(3)][a^2 + a^2\phi_2][\beta > 3.46]$	0.3552	0.0001	0.1433(14)
$[\chi SU(3)][a^2 + a^2\phi_2][m_\pi < 420\ MeV]$	0.653	0.0007	0.1436(11)
$[\chi SU(3)][a^2 + a^2\phi_2][\beta > 3.40\ \&\ m_\pi < 420\ MeV]$	0.3546	0.0	0.1434(20)
$[\chi SU(3)][a^2 + a^2\phi_2][m_\pi < 350\ MeV]$	0.6044	0.0	0.1409(21)
$[\chi SU(3)][a^2 + a^2\phi_2][m_\pi L > 4.1]$	0.4386	0.0013	0.1435(10)
$[Tay][a^2][-]$	0.0778	0.0014	0.1449(5)
$[Tay][a^2][\beta > 3.40]$	0.1006	0.0001	0.1453(7)
$[Tay][a^2][\beta > 3.46]$	0.2476	0.0001	0.1447(10)
$[Tay][a^2][m_\pi < 420\ MeV]$	0.4376	0.0009	0.1447(6)
$[Tay][a^2][\beta > 3.40\ \&\ m_\pi < 420\ MeV]$	0.4476	0.0	0.1443(11)
$[Tay][a^2][m_\pi < 350\ MeV]$	0.3122	0.0	0.1444(7)
$[Tay][a^2][m_\pi L > 4.1]$	0.0738	0.0001	0.145(6)
$[Tay][a^2\alpha_s^{\hat{\Gamma}}][-]$	0.0684	0.0011	0.145(5)
$[Tay][a^2\alpha_s^{\hat{\Gamma}}][\beta > 3.40]$	0.08	0.0001	0.1453(8)
$[Tay][a^2\alpha_s^{\hat{\Gamma}}][\beta > 3.46]$	0.246	0.0001	0.1447(10)
$[Tay][a^2\alpha_s^{\hat{\Gamma}}][m_\pi < 420\ MeV]$	0.4526	0.0009	0.1447(6)
$[Tay][a^2\alpha_s^{\hat{\Gamma}}][\beta > 3.40\ \&\ m_\pi < 420\ MeV]$	0.459	0.0	0.1444(11)
$[Tay][a^2\alpha_s^{\hat{\Gamma}}][m_\pi < 350\ MeV]$	0.3022	0.0	0.1444(7)
$[Tay][a^2\alpha_s^{\hat{\Gamma}}][m_\pi L > 4.1]$	0.066	0.0001	0.1451(6)
$[Tay][a^2][a^2 + a^2\phi_2][-]$	0.537	0.2037	0.1439(6)
$[Tay][a^2][a^2 + a^2\phi_2][\beta > 3.40]$	0.4162	0.0023	0.1444(8)
$[Tay][a^2][a^2 + a^2\phi_2][\beta > 3.46]$	0.3158	0.0001	0.1442(10)
$[Tay][a^2][a^2 + a^2\phi_2][m_\pi < 420\ MeV]$	0.6588	0.0014	0.1441(6)
$[Tay][a^2][a^2 + a^2\phi_2][\beta > 3.40\ \&\ m_\pi < 420\ MeV]$	0.3542	0.0	0.1443(11)
$[Tay][a^2][a^2 + a^2\phi_2][m_\pi < 350\ MeV]$	0.3642	0.0	0.1438(7)
$[Tay][a^2][a^2 + a^2\phi_2][m_\pi L > 4.1]$	0.5224	0.0049	0.1439(7)
$[Tay][a^2 + a^2\phi_2][a^2][-]$	0.202	0.005	0.1452(6)
$[Tay][a^2 + a^2\phi_2][a^2][\beta > 3.40]$	0.1702	0.0002	0.1457(8)
$[Tay][a^2 + a^2\phi_2][a^2][\beta > 3.46]$	0.242	0.0	0.1448(10)
$[Tay][a^2 + a^2\phi_2][a^2][m_\pi < 420\ MeV]$	0.5562	0.0006	0.1449(6)
$[Tay][a^2 + a^2\phi_2][a^2][\beta > 3.40\ \&\ m_\pi < 420\ MeV]$	0.3556	0.0	0.1443(12)
$[Tay][a^2 + a^2\phi_2][a^2][m_\pi < 350\ MeV]$	0.2928	0.0	0.1445(7)
$[Tay][a^2 + a^2\phi_2][a^2][m_\pi L > 4.1]$	0.2708	0.0005	0.1454(6)
$[Tay][a^2 + a^2\phi_2][-]$	0.4792	0.0599	0.1437(8)

$[Tay][a^2 + a^2\phi_2][\beta > 3.40]$	0.4258	0.0014	0.1433(12)
$[Tay][a^2 + a^2\phi_2][\beta > 3.46]$	0.307	0.0	0.1434(14)
$[Tay][a^2 + a^2\phi_2][m_\pi < 420\ MeV]$	0.6018	0.0005	0.1437(11)
$[Tay][a^2 + a^2\phi_2][\beta > 3.40\ \&\ m_\pi < 420\ MeV]$	0.3	0.0	0.1433(21)
$[Tay][a^2 + a^2\phi_2][m_\pi < 350\ MeV]$	0.3786	0.0	0.1415(21)
$[Tay][a^2 + a^2\phi_2][m_\pi L > 4.1]$	0.468	0.0018	0.1437(10)
$[Tay4][a^2][-]$	0.1282	0.0021	0.144(7)
$[Tay4][a^2][\beta > 3.40]$	0.1448	0.0002	0.1443(10)
$[Tay4][a^2][\beta > 3.46]$	0.268	0.0001	0.1441(11)
$[Tay4][a^2][m_\pi < 420\ MeV]$	0.452	0.0006	0.144(8)
$[Tay4][a^2][\beta > 3.40\ \&\ m_\pi < 420\ MeV]$	0.4054	0.0	0.1439(13)
$[Tay4][a^2][m_\pi < 350\ MeV]$	0.9132	0.0001	0.142(11)
$[Tay4][a^2][m_\pi L > 4.1]$	0.0532	0.0	0.1448(9)
$[Tay4][a^2][a^2 + a^2\phi_2][-]$	0.533	0.0966	0.1435(7)
$[Tay4][a^2][a^2 + a^2\phi_2][\beta > 3.40]$	0.4422	0.0016	0.1437(10)
$[Tay4][a^2][a^2 + a^2\phi_2][\beta > 3.46]$	0.3306	0.0001	0.1437(11)
$[Tay4][a^2][a^2 + a^2\phi_2][m_\pi < 420\ MeV]$	0.623	0.0007	0.1438(8)
$[Tay4][a^2][a^2 + a^2\phi_2][\beta > 3.40\ \&\ m_\pi < 420\ MeV]$	0.3042	0.0	0.1439(13)
$[Tay4][a^2][a^2 + a^2\phi_2][m_\pi < 350\ MeV]$	0.9366	0.0001	0.1416(12)
$[Tay4][a^2][a^2 + a^2\phi_2][m_\pi L > 4.1]$	0.468	0.0019	0.1441(10)
$[Tay4][a^2 + a^2\phi_2][a^2][-]$	0.4446	0.0518	0.144(7)
$[Tay4][a^2 + a^2\phi_2][a^2][\beta > 3.40]$	0.3054	0.0006	0.1446(10)
$[Tay4][a^2 + a^2\phi_2][a^2][\beta > 3.46]$	0.3146	0.0	0.1442(11)
$[Tay4][a^2 + a^2\phi_2][a^2][m_\pi < 420\ MeV]$	0.604	0.0005	0.1442(8)
$[Tay4][a^2 + a^2\phi_2][a^2][\beta > 3.40\ \&\ m_\pi < 420\ MeV]$	0.3132	0.0	0.1439(13)
$[Tay4][a^2 + a^2\phi_2][a^2][m_\pi < 350\ MeV]$	0.9356	0.0001	0.1421(12)
$[Tay4][a^2 + a^2\phi_2][a^2][m_\pi L > 4.1]$	0.2658	0.0003	0.1447(9)
$[Tay4][a^2 + a^2\phi_2][-]$	0.4814	0.0337	0.1436(8)
$[Tay4][a^2 + a^2\phi_2][\beta > 3.40]$	0.3934	0.0007	0.1433(12)
$[Tay4][a^2 + a^2\phi_2][\beta > 3.46]$	0.2618	0.0	0.1436(14)
$[Tay4][a^2 + a^2\phi_2][m_\pi < 420\ MeV]$	0.537	0.0002	0.1438(11)
$[Tay4][a^2 + a^2\phi_2][\beta > 3.40\ \&\ m_\pi < 420\ MeV]$	0.2242	0.0	0.1435(21)
$[Tay4][a^2 + a^2\phi_2][m_\pi < 350\ MeV]$	0.8916	0.0	0.1421(22)
$[Tay4][a^2 + a^2\phi_2][m_\pi L > 4.1]$	0.4466	0.0007	0.1438(10)

Table H.4: Model average results for the determination of $\sqrt{t_0}$ at the physical point using the combined analysis of both Wilson and mixed action results. In the first column we label the fit model and data cuts considered. In the second and third columns we show the quality of fits as measured by the p-value [**chi_exp**] and the assigned weight to each model according to eq. (4.19), respectively. Finally, in the fourth column we show the results coming from each fit model.

DECLARATION

Put your declaration here.

Saarbrücken, June 2018

André Miede & Ivo Pletikosić

COLOPHON

This document was typeset using the typographical look-and-feel `classicthesis` developed by André Miede and Ivo Pletikosić. The style was inspired by Robert Bringhurst's seminal book on typography "*The Elements of Typographic Style*". `classicthesis` is available for both LaTeX and LyX:

https://bitbucket.org/amiede/classicthesis/

Happy users of `classicthesis` usually send a real postcard to the author, a collection of postcards received so far is featured here:

http://postcards.miede.de/

Thank you very much for your feedback and contribution.